

# UC Irvine

## UC Irvine Electronic Theses and Dissertations

### Title

Coloring outside the lines: how crossing traditional boundaries in barrel cortex creates an emergent substrate for whisker coding

### Permalink

<https://escholarship.org/uc/item/6dp280cm>

### Author

Jacobs, Nathan Simpson

### Publication Date

2015

### Copyright Information

This work is made available under the terms of a Creative Commons Attribution License, available at <https://creativecommons.org/licenses/by/4.0/>

Peer reviewed|Thesis/dissertation

UNIVERSITY OF CALIFORNIA, IRVINE

Coloring outside the lines: how crossing traditional boundaries in barrel cortex creates  
an emergent substrate for whisker coding

DISSERTATION

submitted in partial satisfaction of the requirements  
for the degree of

DOCTOR OF PHILOSOPHY

in Biological Sciences

by

Nathan S. Jacobs

Dissertation committee:  
Professor Ron Frostig, Chair  
Professor Craig Stark  
Professor Raju Metherate

2015

Chapter 2 © Frontiers Media  
All other materials © 2015 Nathan S Jacobs

## **Dedication**

To my friends, family, colleagues, mentors, taxpayers, and research subjects that made this work possible.

## TABLE OF CONTENTS

	Page
LIST OF FIGURES	v
LIST OF TABLES	vi
ACKNOWLEDGEMENTS	vii
CURRICULUM VITAE	viii
ABSTRACT OF THE DISSERTATION	ix
CHAPTER 1: INTRODUCTION	1
CHAPTER 2: Whisker array functional representation in rat barrel cortex: transcendence of one-to-one topography and its underlying mechanism	
Summary & Key Points	15
Introduction	17
Methods	19
Results	27
Discussion	39
CHAPTER 3: Emergence of spatiotemporal invariance in large neuronal ensembles in rat barrel cortex	
Summary & Key Points	50
Introduction	52
Methods	53
Results	59
Discussion	80
CHAPTER 4: Blocking the spread of evoked activity constrains pattern of sensory induced protection from ischemic attack	
Summary & Key Points	88
Introduction	90
Methods	91
Results	99
Discussion	104
CHAPTER 5: Experimental summary and discussion	110

REFERENCES	115
APPENDIX A: Coincident spike waveforms confound interpretation of spike counts	123
APPENDIX B: Spatially organized ensembles required for single trial sensory coding	124
APPENDIX C: Lateral versus vertical functional connectivity in barrel cortex	133

---

Abbreviations:

ISOI - intrinsic signal optical imaging

LFP - local field potential

MUP - multi-unit potential

S1 - primary somatosensory cortex

A1 - primary auditory cortex

## LIST OF FIGURES

	Page	
Figure 1.1	Topography and columns in barrel cortex	3
Figure 1.2	Horizontal organization of barrel cortex	7
Figure 1.3	Most single whisker evoked activity occurs outside of appropriate whisker barrel	8
Figure 1.4	Spatial overlap of single whisker point spreads peaks at single, central location	10
Figure 2.1	Rat whisker-to-barrel system	20
Figure 2.2	Representative cases of rat barrel cortex response to stimulating an array of 24 whiskers	27
Figure 2.3	Average <i>in vivo</i> data for the 24-whiskers array	30
Figure 2.4	Predicting the <i>in vivo</i> multi-whisker functional representation (MWFR) for the 24-whiskers array based on linear summation of single whisker functional representations (SWFRs)	33
Figure 2.5	Multi-whisker functional representation (MWFR) for the 24-whiskers array dependent on single whisker functional representation (SWFR) interactions occurring at the cortical level	36
Figure 2.6	Subset of 4 whiskers also evokes an activity mountain with a single central peak that can be predicted by modeling	41
Figure 2.7	Reduction in variability of response properties for multi-whisker functional representations (MWFRs) compared to single whisker functional representation (SWFR)	46
Figure 3.1	Whisker stimuli and spatial profile of whisker evoked ensemble activity in barrel cortex	56
Figure 3.2	Recording movies of continuous ensemble activity in barrel cortex	57
Figure 3.3	Single whisker evoked LFP for the first deflection	61

Figure 3.4	Single whisker evoked MUP for the first deflection	62
Figure 3.5	Whisker array evoked LFP for the first deflection	68
Figure 3.6	Whisker array evoked MUP for the first deflection	69
Figure 3.7	PCA visualizes differences between single whisker and whisker array evoked activity	71
Figure 3.8	Continuous quantification of evoked LFP and MUP for repeated whisker deflections	74
Figure 3.9	Peak frames of activity for repeated whisker deflections	75
Figure 3.10	Whisker stimulation engages entire mesoscopic field of view for each stimulus amplitude	79
Figure 4.1	Auditory stimulation protects MCA territory from impending stroke damage	94
Figure 4.2	Gray matter transection blocks spread of auditory evoked activity but leaves collateral blood flow intact	101
Figure 4.3	Gray matter transection by itself produces no tissue infarction, but blocks sensory induced protection from ischemic stroke	103
Figure 4.4	Beyond transection, somatosensory cortex suffers loss of function	106
Figure A1	Coincident spike waveforms near peak responses	124
Figure B1	Relationship between single neuron tuning curves and single whisker evoked point spreads	125
Figure B2	Spatial profile of activity resolves ambiguity of whisker stimulus identity on single trials	129
Figure B3	Funneling of multi-whisker responses occurs on single trials	132
Figure C1	Cortical activity more correlated within layers than columns	145

## LIST OF TABLES

		Page
Table 2.1	Statistics summaries of multi-whisker functional representation (MWFR) and single whisker functional representation (SWFR) data	47
Table 3.1	Onset and peak latencies for whisker evoked LFP and MUP	87

## **ACKNOWLEDGEMENTS**

I'd like to thank all members of the Frostig lab who were directly involved in each of the projects of this dissertation. In particular my mentor Ron Frostig who was involved in every aspect of each project and provided a constant source of motivation and constructive criticism. I would also like to specifically thank Cynthia Chen-Bee who was the primary author on the work discussed in Chapter 2 and was a general mentor for the entire lab. I'd like to thank Chris Lay who is co-first author of the work discussed in Chapter 3.

In addition to the co-authors of this research I'd also like to thank the other members of the Frostig lab for all their help, guidance, and lively conversations about all aspects of this work. Brett-Johnson, Ellen Wann, and Aneeka Hancock were especially helpful. Outside the Frostig lab I'd like to thank the continued support and constructive criticism from Timothy Allen at Florida International University formerly a postdoc at UCI, as well as the members of my thesis committee Raju Metharate and Craig Stark. Raju Metharate was particularly helpful in key aspects of interpreting the data in Chapter 2.

I'd also like to thank financial support from the NIH, the GAANN grants, and the department of Neurobiology and Behavior through teaching assistantships.

Last and most important I'd like to thank my wife for all of her unconditional support, encouragement, and discussions throughout this work. I'd also like to thank my family and friends for their support and encouragement.

# CURRICULUM VITAE

## Nathan Simpson Jacobs

University of California, Irvine  
Dept of Neurobiology & Behavior  
nathanj@uci.edu

---

### Education

University of California, Los Angeles  
Bachelor of Science, Neuroscience (2008)

University of California, Irvine  
Doctor of Philosophy in the Biological Sciences (2015)  
Department of Neurobiology and Behavior

### Research Experience

*Doctoral Research* : University of California, Irvine, 2009-present  
(adviser: **Ron Frostig**)

- Role of large cortical activity spreads in sensory coding, intracortical interactions, and protection from impending ischemic stroke.
- Neuronal invariance of sensory evoked activity in large cortical ensembles
- Contributions of the hippocampus to memory for elapsed time (rotation project with Norbert Fortin)

*Undergraduate / Research Technician* : University of California, Los Angeles, 2008-2009  
(adviser: **Michael Fanselow**)

- Contributions of gap-junctions to auditory fear learning
- Effect of ethanol and estrus cycle phase during contextual fear learning
- Calcium-permeable NMDARs (NR1 deletion) and context discrimination
- Baseline anxiety interactions with acquisition of auditory fear memory

*Undergraduate Field Research Quarter* : University of California, Los Angeles, in Moorea, French Polynesia, 2006 (research advisors: William Hamner, Peggy Fong)

- Bleaching and recovery of the tropical hard-coral species *Porites rus* during a simulated warming event

## Publications

*Manuscript in review, Frontiers in Neural Circuits.* **NS Jacobs**, CH Chen-Bee, RD Frostig. "Emergence of invariance in large neuronal ensembles in the rat barrel cortex."

*Manuscript in preparation, Stroke.* **NS Jacobs** (co-first author), C Lay, M Davis, C Chen-Bee, RD Frostig. "Reperfusion without evoked cortical activity fails to protect somatosensory cortex following permanent middle-cerebral artery occlusion in rats."

**NS Jacobs**, TA Allen, N Nguyen, NJ Fortin. (2013) "Critical Role of the Hippocampus in Memory for Elapsed Time." *Journal of Neuroscience*.

CC Lay, **NS Jacobs**, AM Hancock, Y Zhou, RD Frostig. (2013) "Early stimulation treatment provides complete sensory-induced protection from ischemic stroke under isoflurane anesthesia." *European Journal of Neuroscience* e1460-9568.

C Chen-Bee, Y Zhou, **NS Jacobs**, B Lim, RD Frostig. (2012) "Whisker Array Functional Representation in Rat Barrel Cortex: Transcendence of One-to-One Topography and its Underlying Mechanism." *Frontiers in Neural Circuits* 6 (93).

S Bissiere, M Zelikowsky, R Ponnusamy, **NS Jacobs**, HT Blair, MS Fanselow. (2011) "Electrical synapses control hippocampal contributions to fear learning and memory." *Science* 331 (6013), 87.

JD Cushman, MD Moore, **NS Jacobs**, RW Olsen, MS Fanselow. (2011) "Behavioral Pharmacogenetic Analysis on the Role of the  $\alpha 4$  GABAA Receptor Subunit in the Ethanol-Mediated Impairment of Hippocampus-Dependent Contextual Learning." *Alcoholism: Clinical and Experimental Research* 35 (11), 1948–1959.

**NS Jacobs**, JD Cushman, MS Fanselow. (2010) "The accurate measurement of fear memory in Pavlovian conditioning: resolving the baseline issue." *Journal of neuroscience methods* 190 (2), 235-239.

BJ Wiltgen, GA Royle, EE Gray, A Abdipranoto, N Thangthaeng, **NS Jacobs**, F Saab, S Tonegawa, SF Heinemann, TJ O'Dell, MS Fanselow, B Vissel. (2010) "A role for calcium-permeable AMPA receptors in synaptic plasticity and learning." *PLoS one* 5 (9).

## Awards and Honors

GAANN Fellowship, UCI, 2013.

Invitation to speak at ReMIND conference, UCI, 2011.

NSF graduate fellowship research program, *honorable mention*, 2010 & 2011.

Cum Laude Latin Honors & Departmental Highest Honors, UCLA, 2004.

## **ABSTRACT OF THE DISSERTATION**

Large cortical activity spreads and their functional consequences in rat barrel cortex

By

Nathan S Jacobs

Doctor of Philosophy in Biological Sciences  
University of California, Irvine, 2015  
Professor Ron D Frostig, Chair

A distinguishing feature of animals is their ability to detect, internalize, and respond to their surrounding environment. Despite the seeming simplicity of our basic sensory functions, the ability to sense requires a surprisingly complex neural architecture. Mammalian sensory systems follow several organizing principles including topography and cortical columns. The two organizing principles of topography and columns are exquisitely demonstrated in the somatosensory (touch) system of rodents. Unlike humans, rats spend most of their time in dark tunnels underground and rely on the rich tactile information provided by their whiskers. The array of whiskers on the snout project to a discrete, barrel-shaped regions in the primary somatosensory cortex that match the pattern and orientation of the facial whiskers. This remarkable region is referred to as the rodent barrel cortex, and is perhaps one of the best-studied sensory cortices in the mammalian brain. However, our understanding of the rodent barrel cortex comes mostly from the anatomy and function of individual neurons, despite a general agreement that sensory function arises from large populations of neurons not single neurons.

This dissertation focuses on the functional organization of barrel cortex from a

mesoscopic perspective that encompasses large populations of neurons. A primary focus is the functional consequence of large, intracortical activity spreads which are ubiquitous in sensory cortex but are still poorly understood. Experimental evidence focusing on the rodent barrel cortex is presented demonstrating how large, intracortical activity spreads (point spreads) underlie sensory coding and integration, provide a robust substrate for invariant sensory coding, and establish a large area of protection from ischemic attack.

## **CHAPTER 1: Introduction**

### *Organizing principles of mammalian sensory systems*

A distinguishing feature of animals is their ability to detect, internalize, and respond to their environment. These relatively basic functions are easily taken for granted. Unless something goes wrong, as in the case of blindness, we simply assume that when we open our eyes we will effortlessly be able to see what is in front of us. If it is dark, we simply reach out until we feel what we're looking for and grab it. Yet even these basic sensory functions require a surprisingly complex neural architecture.

In the mammalian brain, each sensory system has a dedicated hierarchy of brain structures that extend from primary sensory neurons in the periphery to sensory regions of the neocortex. Each sensory system translates a particular disturbance in the environment (mechanical pressure, electromagnetic radiation, rapid oscillations in air pressure, or chemical concentrations) into neuronal activity that underlies each of our senses (touch, sight, hearing, and taste/smell, respectively). While each sensory system has a unique set of neural circuits and functions, there are clear organizing principles that occur in all sensory systems (Merzenich et al., 1980).

First, sensory systems are separated by modality. Each sense has a dedicated set of brain structures that are primarily responsible for processing sensory information for that modality. For example, the neocortex can be parcellated into primary sensory regions for each sense such as primary somatosensory cortex for the somatosensory system, and so on. Later stages of sensory processing may involve integration of information from multiple sensory systems, but at least initially sensory processing is separated based on modality. Separating the neural architecture into distinct systems for each modality is therefore one important organizing principle of sensory systems.

A second important organizing principle of sensory systems is topography. Axonal projections from neighboring primary sensory neurons in the periphery often project to neighboring regions in the brain, and these neighboring regions in the brain often project to neighboring regions in other brain structures. This concept of topographic organization was pioneered by the neurosurgeon and scientist Penfield who, while performing brain surgery on patients with intractable epilepsy, electrically stimulated different parts of the cortex in humans and was surprised to find topographic maps of sensory and motor functions (Penfield and Jasper, 1954). While not all sensory regions are spatially organized, all primary sensory cortices exhibit topography.

A third and final important organizing principle of sensory systems is cortical columns. In the neocortex, vertical extensions of axons and dendrites connect cortical layers into a single “column” (Feldmeyer, 2012) of cortical neurons that are all preferentially tuned to the same stimulus parameter. Cortical columns were first proposed by Mountcastle in 1957 and first observed in visual cortices by Hubel and Wiesel (1962). Since then, cortical columns have been found in other primary sensory cortices and provide an important theoretical framework for understanding sensory functions in the brain (for review, see Merzenich et al., 1980).

The neural architecture supporting our basic sensory functions is organized based on these three general principles- separation by modality, topography, and cortical columns. Perhaps one of the best studied sensory structures is the rodent barrel cortex, which exquisitely demonstrates these organizing principles (**Fig. 1.1**).

### *The rodent barrel cortex*

The rodent barrel cortex is a subdivision of primary somatosensory cortex associated

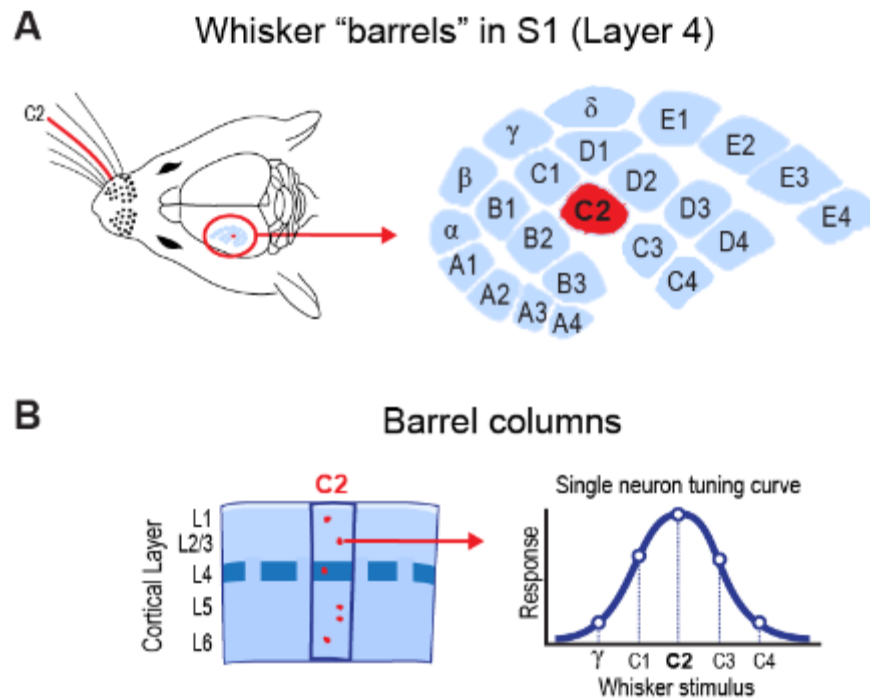


**Figure 1.1. Topography and columns in barrel cortex. (A)** Anatomical representations (barrels) of each whisker on the snout are found in layer 4 of primary somatosensory cortex. **(B)** Neurons within each barrel as well as neurons in the column of tissue extending above and below each whisker barrel (barrel column) preferentially respond to the same whisker. Fight, schematic of a tuning curve for a single neuron.

with the many motile facial vibrissae (whiskers) on the snout of rodents. All mammals share the same sensory modalities, but different species rely more on certain sensory systems. For example, humans rely heavily on vision and have enormous eyes with retinas that are packed with light sensitive neurons. Many types of rodents such as rats, on the other hand, spend most of their time in dark tunnels underground and therefore rely much more on somatosensory (touch) information.

To explore their underground environment, rats use an array of highly sensitive, motile vibrissae (whiskers) on their snout which they whisk back and forth at 5-10 Hz to palpitate nearby objects and surfaces. This array of whisker collects a wealth of tactile information that is

processed by the somatosensory system. Large portions of the somatosensory system of rats and other rodents are dedicated just to the whiskers. Interestingly, these somatosensory regions tend to be parcellated into distinct regions for each individual whisker on the snout (for comprehensive review see, see Fox, 2008).

Sensory neurons in whisker follicles on the snout project to distinct, barrel-shaped regions in the principal nucleus of the brainstem called “barrelettes.” Neurons in each barrelette of the principal nucleus project to distinct regions in the dorsomedial nucleus of the thalamus called “barreloids.” Finally, each barreloid in the thalamus projects to distinct regions in primary somatosensory cortex (S1) called “barrels.” In S1, the collection of barrel shaped cytoarchitectural units associated with each of the facial whiskers is referred to as the barrel cortex (for main excitatory pathways, see Feldmeyer, 2012). The topography of barrels in barrel cortex perfectly matches the spatial arrangement of whiskers on the snout (see schematic in **Fig. 1.1**, top panels). Whisker specific topography in rodent S1 was first discovered in the mouse by Woolsey and Van der Loose (1970) and shortly thereafter found in the rat (Killakey et al., 1975). Thus, barrel cortex adheres to the important organizing principle of topography.

The rodent barrel cortex also adheres to columnar organization. Cortical columns of neurons above and below each whisker barrel, sometimes referred to as “barrel columns,” are connected with vertically oriented axonal and dendritic processes (Feldmeyer, 2012). This vertical connectivity establishes a ‘column’ of cortical neurons that with few exceptions respond preferentially to the same whisker (see schematic in **Fig. 1.1**, bottom panel). In addition to this vertical connectivity, a robust horizontal connectivity in barrel cortex has also been described more recently (Frostig et al., 2008; Stheberge et al., 2014; Narayanan et al., 2015).

Barrel cortex provides a compelling demonstration of topography and columns, two important organizing principles of mammalian sensory systems. Together, the topography and

columnar organization of barrel cortex suggests anatomical and functional parcellation by whisker. In this parcellated view of barrel cortex, distinct barrel columns of similarly tuned neurons form the functional units of barrel cortex (Fox, 2008). This parcellated view of barrel cortex, however, only tells half of the story.

Evidence for a parcellated view of barrel cortex comes largely from a reductionist approach to studying sensory coding in the brain. Reductionist or bottom-up approaches provide important information about the constituents and underlying mechanics of a complex system like the barrel cortex. Yet understanding the properties and functions of individual neurons provides only a partial view of barrel cortex. Individual neurons in barrel cortex do not function as isolated units, they are part of a much larger, mesoscopic network of neurons stretching across barrel cortex that collectively respond to whisker stimuli. To fully understand the function of barrel cortex, the emergent properties of its spatially organized networks must also be studied. A complete understanding of barrel cortex therefore requires both a reductionist and an emergentist perspective.

#### *Reductionist and emergentist views of barrel cortex*

The barrel cortex can be viewed from both a reductionist perspective (focusing on peak responses in single neurons) or from the perspective of emergence (focusing on emergent patterns of activity across populations of neurons). These complementary perspectives rely on different methodologies, make different assumptions about sensory coding, and provide strikingly different information about the function and organization of barrel cortex.

A reductionist perspective of barrel cortex emphasizes understanding of the constituents of the system (ie, the individual neurons). To understand how a system works, it is important to understand how the parts of that system work. Likewise, to understand barrel cortex, it is

important to understand the properties of the neurons in barrel cortex.

Individual neurons in barrel cortex are primarily described by their tuning properties. Single neuron tuning curves are derived by a series of reductive steps that starts with long traces of ongoing activity and ends with the preferred stimulus for that neuron. First, responses in single neurons are measured with microelectrodes or intracellular calcium imaging. These measures provide a continuous readout of complex, ongoing patterns of activity in individual neurons. This continuous stream of activity in individual neurons can be reduced to a simple tuning curve indicating their preferred whisker stimulus, the whisker that evokes the most vigorous response (see **Fig. 1.1B**, right). In this way long traces of ongoing activity for each neuron can be reduced to just a single data point, its preferred whisker stimulus. Plotting the preferred stimuli of individual neurons across the cortical surface produces an intricate map of barrel cortex parcellated into distinct regions for each whisker (matching the anatomical parcellation by whisker seen in whisker barrels in cortical layer 4). By simplifying complex activity patterns to the main response features in individual neurons (their preferred whisker stimulus), a reductionist approach provides a clear theoretical framework of barrel cortex function based on parcellation by whisker.

An emergentist perspective provides a complementary view of whisker coding in barrel cortex. Emergence is the concept that some properties of a system arise from complex interactions *between* constituents of a system rather than from properties of the constituents themselves (Camazine, 2003; Van Regenmortel, 2004; Hazen et al., 2007, 2009). A simple example of emergence is the complex patterns formed by sand grains in a turbulent environment. As more and more grains of sand are added to the system, unexpected patterns emerge. First, sand grains begin clumping into small groups as they hit into each other, followed by the emergence of small ripples, and, with enough sand grains, large structures such as sand

dunes. Importantly, it is hard to predict the behavior the system (creation of sand dunes) from the properties of its constituents (the individual grains of sand).

Finding similar emergent features in the brain requires simultaneously recording the activity of many neurons using multi-site recordings or functional imaging methods. Such methods provide a “big picture” view of emergent patterns of activity across large populations of neurons. Such emergent patterns could arise in specific, sparse cortical networks where there is little or no spatial structure to the network. Another possibility is for emergent *spatiotemporal* patterns of activity to arise in large networks of adjacent neuronal populations with a clear spatial organization. It is possible that large global signals produced by such a “non-specific” network could occur without major interference with activities in smaller, sparser, or more specific cortical networks mentioned earlier. For example, local circuits might negate larger, slower

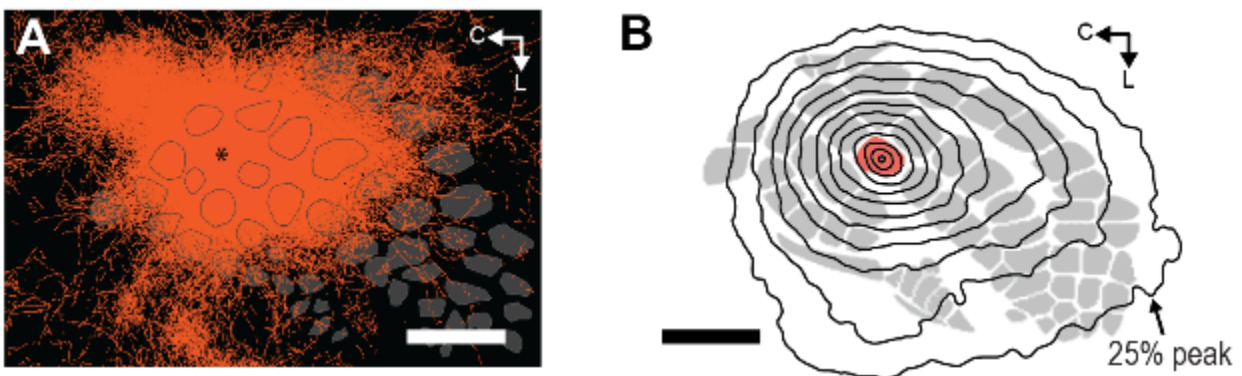


**Figure 1.2. Horizontal organization of barrel cortex. (A)** A dense plexus of intracortical, horizontal projection fibers radiate out from individual whisker barrels. Asterisk indicates location of injection of anterograde tracer (AAV1.1-aCaMKII-GFP, secondary labeling with GFP antibody and visualized with DABP). **(B)** Single whisker (C2) evoked activity as assessed by ISOI has a large spatial profile extending well beyond the boundaries of the whisker barrel column. Iso-activity lines are drawn for average “initial dip” ISOI signal ( $n=37$ ) at steps equivalent to 5% of peak response. The furthest iso level, clearly beyond the boundaries of barrel cortex, is at 25% of the peak response (1/4 max). *Data in (A) reproduced with permission from Johnson, 2015 (unpublished). Scale bars = 1 mm.*

global signals by normalizing their activity to some reference point. However, no consistent or characteristic sparse, specific network has been established in barrel cortex. In contrast, it is abundantly clear that large, spatially organized population responses are a ubiquitous feature not just in barrel cortex but generally in sensory cortex (for examples in primary somatosensory, auditory, and visual cortex, see: Grinvald et al., 1994; Barth et al., 1995; Das and Gilbert, 1995; Bakin et al., 1996; Bringuier et al., 1999; Brett-Green et al., 2001; Kaur et al., 2005; Roland et al., 2006; Ferezou et al., 2006, 2007; Sharon et al., 2007; Frostig et al., 2008; Chen-Bee et al., 2012; Mohajerani et al., 2013) and thus will be the focus of this dissertation.

An entirely different view of barrel cortex emerges from the vantage point of mesoscopic (several mm in rat cortex), spatially organized neuronal populations. In addition to the local, vertically oriented microcircuits in barrel columns there is also a horizontally oriented mesoscopic network in barrel cortex (Frostig et al., 2008; Stehberg et al., 2014; Narayanan et

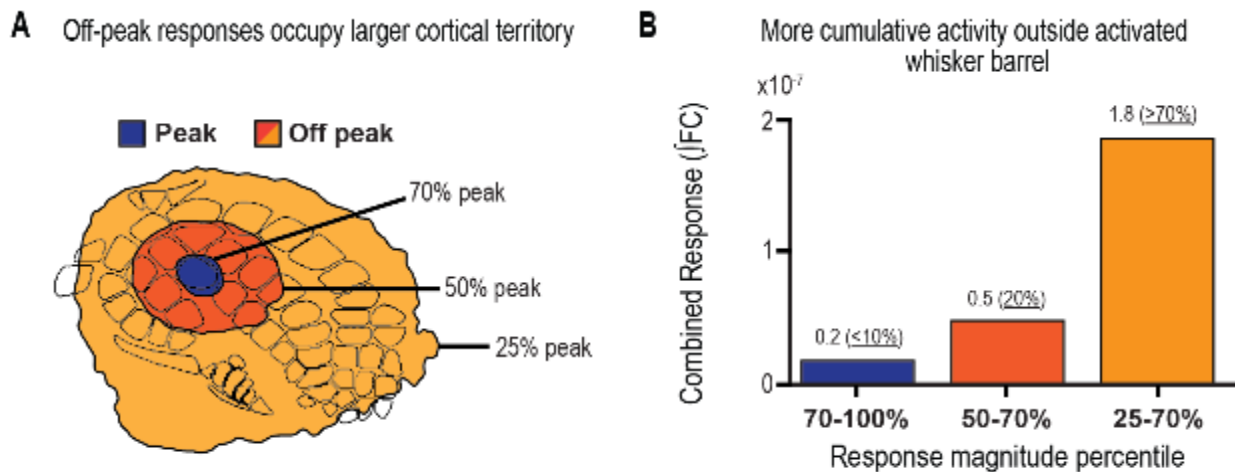


**Figure 1.3. Most single whisker evoked activity occurs outside whisker barrel column. (A)** Single whisker (C2) evoked point spread measured with ISOI (n=37). Iso levels are drawn at 70%, 50%, and 25% of peak value. The 70% iso level roughly corresponds to the expected boundary for the C2 whisker barrel. Note the much larger cortical territory occupied by weaker off-peak responses (orange) surrounding peak responses within the whisker barrel (blue). **(B)** Integrating responses over space reveals that over 70% of all evoked ISOI activity occurs outside the appropriate whisker barrel (sum of all response magnitudes between 25% and 70% of peak value).

al., 2015; see also **Appendix C**). A dense plexus of horizontal, intracortical projection fibers extend throughout and even beyond barrel cortex (**Fig. 1.2A**). This extensive horizontal connectivity supports a robust “point spread” of single whisker evoked activity that doesn’t stop at the edge of the barrel column but extends laterally for several mm and often continues beyond even the boundaries of barrel cortex (Frostig et al., 2008; Mohajerani et al., 2013; Ferezou et al., 2006; **Fig. 1.2B**). Single whisker evoked point spreads are characterized by a central peak of evoked activity that gradually tapers with increasing cortical distance. Using intrinsic signal optical imaging (ISOI), response in superficial cortical layers can be imaged across large cortical territories. Interestingly, integrating ISOI activity levels across the spatial domain reveals that the combined response *outside* the whisker barrel column may be much greater than the combined response *within* the whisker barrel column (**Fig. 1.3**).

Large point spreads of evoked activity are a ubiquitous feature of primary sensory cortex. Yet the function of point spreads in barrel cortex and other sensory cortices is still unclear. The relatively large spatial profile of sensory evoked point spreads is especially puzzling given the presumably high metabolic cost. One potential function that is discussed in **Chapter 2** and is illustrated in **Figure 1.4** is to allow for integration across large cortical areas. A complete understanding of barrel cortex will require understanding both its constituent neurons as well as its emergent response features and emergent functions at a mesoscopic level.

Comparing whisker evoked responses in single neurons (reductionist approach) and across large populations of neurons distributed across barrel cortex (emergentist approach) raises important questions about whisker coding in barrel cortex. Are the preferred stimuli of single neurons more important than large point spreads of evoked activity? Most likely both are

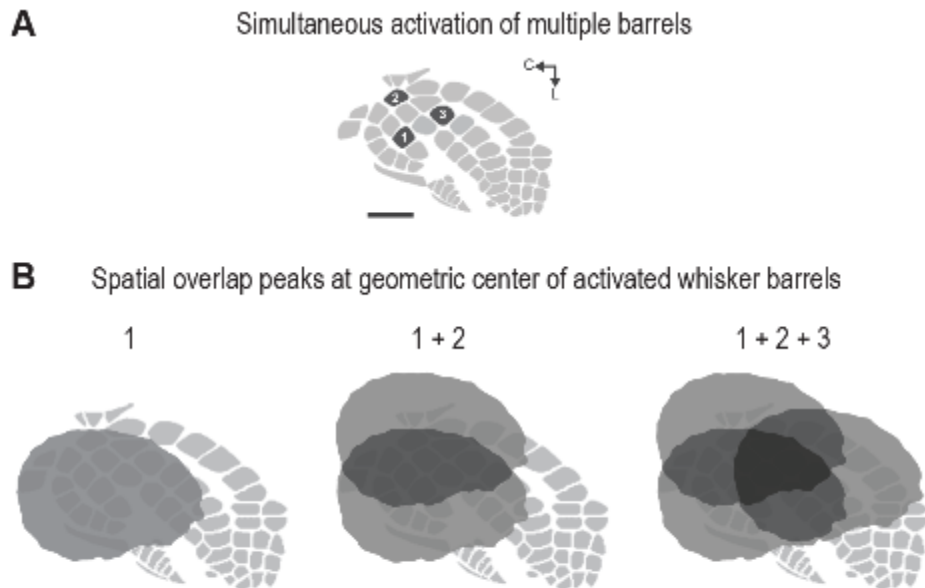


**Figure 1.4. Spatial overlap of single whisker point spreads peak at single, central location.** Schematic of simultaneous activation of three whisker barrels resulting in peak responses over each barrel (A). Spatial overlap between point spreads peaks at the geometric center of initial activation points (B). *Point spreads in (B) based on ISOI data thresholded at 35% of peak response. In (B), scale bar = 1 mm.*

important. However, most research on barrel cortex has focused on sensory coding in single neurons. As a result, very little is known about the potential functions of the large, whisker evoked point spreads and their possible interactions in barrel cortex.

Thus, our understanding of barrel cortex may be missing an important piece of the puzzle without its emergent response features. Novel substrates for whisker coding and integration may emerge within the large, spatially organized networks that make up barrel cortex. This dissertation attempts to take several important steps in filling this critical gap in our understanding of barrel cortex. The following experiments demonstrate that emergent response features such as large cortical activity spreads (ie point spreads) make fundamental

contributions to the nature and function of the rodent barrel cortex.

### *Summary of results*

This dissertation focuses on the functional organization of barrel cortex from a mesoscopic perspective. The following experiments focus on large, emergent patterns of cortical activity that extend across large cortical territories and involve coordinated activities across large populations of neurons. A primary focus is the functional consequences of large, intracortical activity spreads (point spreads) in barrel cortex.

**Chapter 2** of the dissertation discusses how overlapping spatial profiles of evoked cortical activity are important for establishing integrated multi-whisker responses. Stimulation of a single whisker evokes a “point spread” of cortical activity that starts at the appropriate whisker barrel but then spreads, with diminishing strength, across the rest of the whisker barrel map. Thus, each whisker evokes activity across a large cortical territory that overlaps with the area activated by other whiskers.

What happens when you stimulate multiple whiskers simultaneously? One possibility is that the overlapping point spreads simply add up. To test this possibility, we modelled multi-whisker responses using a spatial summation model that summated “overlapping” single whisker point spreads at each spatial location. This simple model made a very specific prediction: it predicted that multiple point spreads if evoked simultaneously would result in a single, central peak of activity at the geometric center of the overlapping point spreads. This prediction was tested with actual multi-whisker responses (by simultaneously stimulating a small group of 4-whiskers and separately the entire 24-whiskers array) and found to be accurate in all cases. Importantly, the point spreads and their presumed interaction was found to depend on an intracortical mechanism of summation. Interestingly, the single central peaks in rat

somatosensory cortex seem to be consistent with perceptual studies in humans showing that some multi-point tactile stimuli are perceived as a single, central stimulus (Bekesy, 1957, 1958, 1959).

**Chapter 3** of the dissertation provides evidence that large whisker evoked point spreads and integrated profiles of multi-whisker activity are not limited to superficial cortical layers but extend across many cortical layers. Furthermore, we found that both of these emergent features of barrel cortex are robust against major changes in whisker stimulus amplitude (> 200 fold change from 0.035° to 7° angular whisker displacement).

We found that while the amount of evoked activity decreased predictably with decreasing stimulus amplitude, what did not change was the broad spatial profile of activity. Even the weakest responses evoked activity that extended all the way beyond even the boundaries of barrel cortex. As generally predicted by the summation model presented in the previous chapter, invariance in the integrated profile of simultaneous multi-whisker stimulation was also found. Even the weakest whisker deflection amplitude produced an integrated profile of activity with a single, central peak. These results demonstrate that large scale spatial profiles of evoked activity provide a robust substrate for whisker coding and integration in barrel cortex across major changes in whisker deflection amplitude. These invariance results also prompted an additional observation that spatial profiles of evoked activity may be required to resolved fundamental ambiguities about sensory coding on single trials (**Appendix B**).

**Chapter 4** of the dissertation discusses how the same large spatial profile of evoked activity discussed in previous chapters is also critical for establishing a large area of sensory induced protection from ischemia. Previous work in the lab found that sensory stimulation within 2 hours of permanent middle cerebral artery occlusion (pMCAO) in rats increases collateral blood flow and prevents tissue infarction. An unresolved question in these studies was how a

discrete sensory stimulation such as deflection of a single whisker could protect the much larger ischemic territory including motor and other sensory cortices. One possibility raised by the large whisker evoked point spreads in naive rats is that the large profile of evoked activity is responsible for the large regions of sensory induced protection. This hypothesis was tested by dissociating increases in collateral blood flow (which also have a large spatial profile) from intracortical activation spread using gray matter transection. The resulting pattern of functional loss on either side of the transection indicate that evoked cortical activity may be directly involved in sensory induced protection from ischemic rather than indirectly through increases in collateral blood flow.

**Chapter 5** summarizes experimental results and discusses their potential broader implications. Much of what we know about brain function comes from a detailed understanding of individual neurons at the microscopic level and on the macroscopic level the general functions of larger brain structures. This leaves a large gap in our understanding of neuronal activity at a mesoscopic (intermediate) scale. At a mesoscopic scale, emergent patterns of activity can be observed across large populations of neurons. Many questions persist about how large, spatially organized networks of neurons may contribute to the creation of robust sensory representations required for high level functions such as stimulus abstraction and learning and memory.

The rodent barrel cortex exquisitely demonstrates topography, cortical columns, and parcellation by whisker in the tuning of individual neurons. Yet this traditional, reductionist view of barrel cortex lacks important details about emergent patterns of whisker evoked activity. Large intracortical activity spreads (point spreads) are ubiquitous in sensory cortex, yet very little is known about their role in sensory coding and integration. The likely enormous metabolic cost of creating, maintaining, and using the neural infrastructure underlying such large spatial profiles of neuronal activity suggests that they are not just artifacts of a sloppy design. This dissertation

attempts to fill a critical gap in our understanding of barrel cortex at the level of large, spatially organized populations of neurons.

## **CHAPTER 2: Whisker array functional representation in rat barrel cortex: transcendence of one-to-one topography and its underlying mechanism**

### *Summary*

The one-to-one relationship between whiskers, barrels, and barrel columns described for rat barrel cortex demonstrates that the organization of cortical function adheres to topographical and columnar principles. Supporting evidence is typically based on a single or few whiskers being stimulated, although behaving rats rely on the use of all their whiskers. Less is known about the cortical response when many whiskers are stimulated. Here, we use intrinsic signal optical imaging and supra- and sub-threshold electrophysiology recordings to map and characterize the cortical response to an array of all large whiskers. The cortical response was found to possess a single peak located centrally within a large activation spread, thereby no longer conveying information about the individual identities of the stimulated whiskers (e.g., many local peaks). Using modeling and pharmacological manipulations, we determined that this single central peak, plus other salient properties, can be predicted by and depends on large cortical activation spreads evoked by individual whisker stimulation. Compared to single whisker stimulation, the peak magnitude was comparable in strength and the response area was only 2.6-fold larger, with both exhibiting a reduction in variability that was particularly pronounced (3.8x) for the peak magnitude. Findings extended to a different collection (subset) of whiskers. Our results indicate the rat barrel cortex response to multi-site stimulation transcends one-to-one topography to culminate in a large activation spread with a single central peak, and offer a potential neurobiological mechanism for the psychophysical phenomenon of multi-site stimulation being perceived as though a single, central site has been stimulated.

### *Key points*

1. Single whisker 'point' stimuli evoke large, overlapping profiles of cortical activity.
2. Spatial summation of large single whisker representations predicts 'funneled' single, central peak of activity following simultaneous stimulation of multiple adjacent whiskers.
3. Predictions of 'funneled' activity confirmed by *in vivo* multi-whisker responses.
4. Pharmacological manipulation confirms intracortical spread mechanism for funneling.
5. One-to-one topography of whiskers breaks down for simultaneous multi-whisker stimuli.

### *Reference:*

Chen-Bee CH, Zhou Y, Jacobs NS, Lim B, Frostig RD (2012) Whisker array functional representation in rat barrel cortex: transcendence of one-to-one topography and its underlying mechanism. *Frontiers in Neural Circuits* doi: 10.3389/fncir.2012.00093.

## Introduction

The rat barrel cortex subdivision of the primary somatosensory system (for review see Fox, 2008) exquisitely demonstrates two fundamental principles of cortical functional organization. Each large whisker found on the snout (**Fig. 2.1A**) is individually represented anatomically in layer IV barrel cortex in a topographical manner (**Fig. 2.1B**), which adheres to the topographical principle of cortical organization. Each whisker is also individually represented functionally in a columnar manner in which neurons above, below, and within a barrel respond preferentially to the same whisker (**Fig. 2.1C**). Thus, barrel cortex also adheres to columnar principles of cortical organization. For barrel cortex, note both principles of organization strongly convey a one-to-one mapping of the whiskers onto the cortex. What is known about the function of barrel cortex is largely based on stimulating a single or few whiskers. Less is known about the barrel cortex response when an entire whisker array (>20 + whiskers) is stimulated. Such characterization should be of interest as rats rely on all their whiskers (vibrissae), typically “whisking” them together (repetitive back-and-forth movements in the rostral-caudal axis at ~5–10 Hz rate) during tactile exploration (Carvell and Simons, 1990). In other words, rats are routinely subjected to stimulation of many whiskers rather than just one or few. As remarked upon by Petersen et al. (2009), the relevant parameter space for the ability of whiskers to influence each other's cortical response is rather large. Therefore, the cortex's response to the entire whisker array is likely not a simple extrapolation of previous findings based on stimulating two or several whiskers.

Thus far, the cortical response to whisker array stimulation has been explicitly investigated in only a couple of studies. Single unit response preference to a particular direction of global motion across the whisker array (Jacob et al., 2008) or spatiotemporal patterns of evoked potentials as a metal wire swept sequentially across the whisker array (Benison et al.,

2006) have been characterized. To date, the total cortical activation spread responsive to whisker array stimulation [referred to as multi-whisker functional representation (MWFR)] has yet to be mapped and characterized in detail. In the present study, we studied MWFRs using intrinsic signal optical imaging and supra- and sub-threshold neuronal recordings from an array of eight independently moving electrodes as employed in previous studies of single whisker stimulation (Brett-Green et al., 2001; Frostig et al., 2008). The MWFR evoked by stimulating an array of 24 whiskers was found to possess only a single peak. This single peak was situated centrally within a large activation spread and located centrally within barrel cortex. Thus, the MWFR of 24 whiskers no longer conveyed one-to-one topographical information about the individual identities of the stimulated whiskers (e.g., 24 local peaks co-registering with the 24 appropriate whisker barrels). This main finding indicates that the rat barrel cortex response to multi-site stimulation transcends one-to-one topography, culminating in a large activation spread with a single central peak. An MWFR with a single central peak would offer a potential neurobiological mechanism for the well-known phenomenon of perceptual funneling reported across different sensory modalities and species including humans in which multi-site stimulation is perceived as though only a single, central site has been stimulated (Bekesy, 1967; Gardner and Spencer, 1972a; Gardner and Tast, 1981).

We also studied MWFRs in more detail with additional experiments, modeling, pharmacological manipulations, and comprehensive quantification. The interaction between large cortical activation spreads of individual whiskers (for review see Frostig, 2006 and Fox, 2008; for spread observed specifically beyond barrel cortex see Brett-Green et al., 2001; Ferezou et al., 2006, 2007; Frostig et al., 2008; Lim et al., 2012) was found to predict and directly contribute to the salient properties of the obtained cortical response including the single central activity peak, indicating an underlying mechanism for our MWFR findings. Compared to single whisker

stimulation, the 24-whiskers MWFR peak magnitude was comparable in strength and the response area was modestly larger. Both of these response properties exhibited a reduction in variability that was particularly pronounced for the peak magnitude. Last, findings were generalized to a different set of whiskers (subgroup of 4 neighboring whiskers within the array of 24 whiskers).

## **Materials and Methods**

Intrinsic signal optical imaging and electrophysiology recordings were performed as in previous studies and most details can be found elsewhere (Chen-Bee et al., 2000, 2007; Frostig et al., 2008). Summary and additional details are provided here.

### *Subjects*

All *in vivo* procedures were in compliance with the National Institutes of Health guidelines and reviewed and approved by the University of California Irvine Animal Care and Use Committee. Subjects were adult male Sprague–Dawley rats. Rats were induced with a bolus intraperitoneal injection of sodium pentobarbital (55 mg/kg b.w.) and maintained with supplemental injections as needed throughout the day. An 8 × 8 mm region of the exposed skull centered above barrel cortex was thinned with a dental drill and kept moist with saline. Rats were then slated for one of several types of experiments differing according to method of cortical activity assessment (imaging; electrophysiology) and multi-whisker stimulation condition being studied (24- and 4-whiskers), and whether lidocaine was locally injected into the cortex.

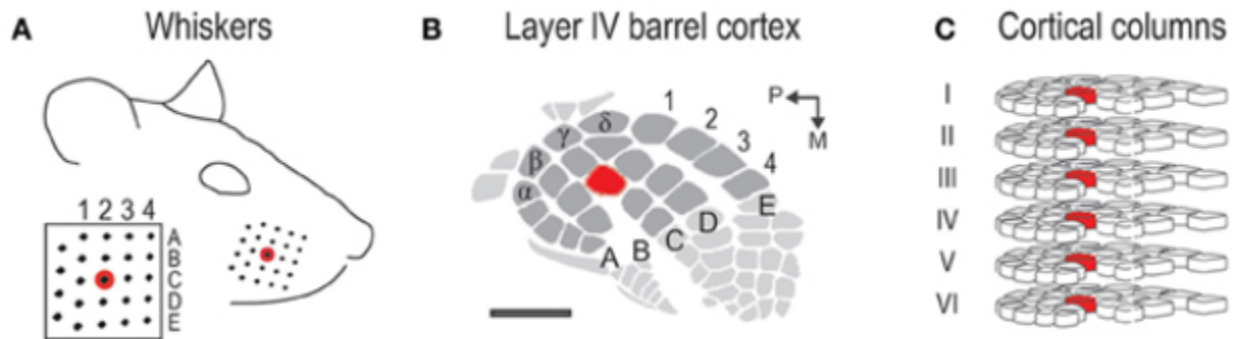


**Figure 2.1. Rat whisker-to-barrel system. (A)** The 24 largest whiskers located in rows A–E and arcs 1–4 plus the 4 Greek whiskers. Red = central whisker C2. **(B)** Barrel cortex subregion of layer IV primary somatosensory cortex. Anatomical representations (barrels) for the 24 whiskers are shaded in dark gray; C2 barrel shaded in red. Scale bar = 1 mm. **(C)** Cortical columns for the 24 whiskers. Each column contains neurons responding preferentially to a particular whisker. C2 column shaded in red.

### Whisker Stimulation

Whisker stimulation was restricted to only the right snout side (**Fig. 2.1A**). Besides single whisker C2 stimulation, two types of multi-whisker stimulation were employed: 24- and 4-whiskers. The whiskers slated for multi-whisker stimulation were of sufficient length to allow a probe to simultaneously deflect all of them while still avoiding contact of any mystacial fur by the probe. At the start of each experiment, the presence of all 24 large whiskers in rows A–E and arcs 1–4 plus all four Greek whiskers (**Fig. 2.1A**) were explicitly confirmed. All remaining (smaller) whiskers were trimmed off. As in previously established protocols, the stimulation of only whisker C2 was achieved with a copper wire probe attached to a computer-controlled stepping motor. Five deflections were delivered at 5 Hz rate for total time span of 1 s. Each deflection displaced whisker C2 approximately 1 mm along the rostra-caudal direction at a distance of approximately 5 mm from the skin. The parameters of single whisker stimulation

were replicated for multi-whisker stimulation. To stimulate all 24 whiskers, a computer-controlled stepping motor was still used, except a 5-prong probe constructed by mounting five parallel copper wires spaced 2 mm apart onto a base steel rod (**Fig. 2.2A**) was used instead of a single copper wire. In order for all 24 whiskers to be deflected at the same distance from the skin, the parallel copper wires were molded to follow the contour of the right snout. Also, for all 24 whiskers to be similarly displaced along the rostral-caudal direction, the resting position of the 5-prong probe was set such that all 24 whiskers were in contact with one of the five wires. The 4-whiskers stimulation was achieved in the same manner, except all but D3, D4, E3, and E4 whiskers were trimmed off prior to positioning of the 5-prong probe.

### *Intrinsic Signal Optical Imaging*

Intrinsic signal optical imaging was used for high-spatial resolution, wide field-of-view mapping of the total cortical activation spread evoked by whisker stimulation; the activation spread can be referred to as a MWFR or SWFR (single whisker functional representation) depending on the number of whiskers being stimulated. Two groups of rats underwent imaging, differing according to the type of MWFR being studied, 24-whiskers ( $n = 10$ ) or 4-whiskers ( $n = 7$ ). In every rat, the SWFR for whisker C2 was also imaged for reference and landmark purposes. Imaging was conducted with a 16-bit CCD camera (Cascade 512B II; Photometrics, Tucson, AZ) combined with an inverted 50 mm lens plus extenders. The camera's field-of-view (**Fig. 2.2B**) was a  $7.42 \times 7.42$  mm cortical region, mapped onto a  $256 \times 256$  pixel array. For future alignment of data files collected within the same rats as well as across rats, the field-of-view neuroaxis was oriented the same in every rat, plus the field-of-view remained constant across data files within each rat. The CCD camera was focused  $600 \mu\text{m}$  below the cortical surface before the start of data collection to minimize contributions from surface blood

vessels and maximize contributions integrated across the upper cortical layers. The imaged cortical region was continuously illuminated with a red LED (635 nm max, 15 nm full width at half-height). Imaging frames were captured at 10 Hz rate (i.e., 1 frame = 100 ms exposure time), and each imaging trial lasted 15 s. Onset of whisker stimulation occurred 1.5 s into the trial. A block of 64 trials was collected per whisker stimulation condition, with an intertrial interval averaging 6 s and ranging randomly between 1–11 s and thus an average of 21 s between the onset of consecutive stimulus deliveries. The 64 trials in a block were then summed and the summed data collapsed into 500-ms frames (referred to hereafter as a data file) to increase the signal-to-noise.

Imaging data files were processed and analyzed using V++ software (Digital Optics, Auckland, New Zealand). For each data file, activity for each 500-ms post-stimulus frame was converted to fractional change relative to the 500-ms frame collected immediately prior to stimulus onset on a pixel-by-pixel basis. As expected based on previous findings (Chen-Bee et al., 2007), SWFRs of whisker C2 typically consisted of an imaging signal spanning 10+ s that was triphasic in nature (initial dip below baseline followed by a large overshoot and large undershoot; see Supplementary Presentation 1, middle panel). Within the same subjects, MWFRs were observed to also consist of a triphasic signal; see Supplementary Presentation 1, bottom panel. Detailed analysis of every imaging data file was restricted to the first signal phase (initial dip). The first 500-ms frame containing the maximum areal extent of evoked initial dip activity was processed with a two-pass Gaussian filter (half-width = 5) to remove high-frequency spatial noise. Filtered values were subsequently used for all plotting, quantification, and statistics performed with MATLAB and SYSTAT.

Alpha level was set to 0.05 for all statistical tests performed on the imaging results. For every data file, the location and magnitude of peak activity were obtained from the pixel with the

greatest magnitude within the evoked activity area. Areal extent of the evoked activity area was quantified using a constant threshold of  $-2.5 \times 10^{-4}$  FC, or  $-0.025\%$ , away from 0 (approximately half-max). The peak magnitude and areal extent of the evoked activity area obtained from each MWFR data file was compared to those for single whisker C2 obtained in the same rats using two-tailed paired *t*-tests. For remaining statistics see Table 1.

To permit 2D and 3D plotting of averages (**Fig. 2.3A,B**, respectively), as well as statistical testing, on a pixel-by-pixel basis, filtered data across rats were first aligned in the following manner. Because the spatial scale and neuroaxis were the same for all data files, along with known findings of a single whisker's peak activity co-registering with the appropriate topographical location within barrel cortex (e.g., that whisker's barrel), the whisker C2's peak location identified for each rat was used for aligning data across rats. Whisker C2 peak location was used irrespective of the type of data being aligned (C2, 24- or 4-whiskers) as the field-of-view remained constant across different data files within the same animal. Aligned data were used not only for plotting of average data across rats, but also for various statistical comparisons between stimulation of single whisker C2 (within subjects reference data) vs. 24-whiskers (Table 1, Summary-1) or 4-whiskers (Table 1, Summary-7), or statistical comparisons to modeled data (Table 1, Summaries 4–5 and 10–11).

### *Electrophysiology*

Two groups of rats underwent electrophysiology recordings, analogous to imaging, in which they differed according to the type of MWFR being studied: 24-whiskers ( $n = 12$ ) or 4-whiskers ( $n = 9$ ). In every rat, the SWFR for whisker C2 was also assessed. Craniotomy and dura removal were performed above barrel cortex and surrounding cortical regions, and the cisterna magnum drained of cerebrospinal fluid to minimize edema and brain pulsation. As in

previous studies (Frostig et al., 2008), imaging of whisker C2's SWFR was first performed so that the peak activity location could be used to guide placement of electrodes [imaging peak location overlies C2 barrel (Masino et al., 1993; Brett-Green et al., 2001)]. Subsequently, simultaneous recordings were obtained from eight cortical locations spanning 3.5 mm along the cortical tangential plane with the use of eight Tungsten microelectrodes (~1.5 MΩ impedance; MicroProbe Inc., MD, US; **Fig. 2.2C**). Electrodes were spaced 0.5 mm apart and linearly aligned, and were independently inserted into the cortex perpendicularly to the cortical surface using a micropositioner (EPS, Alpha-Omega, Nazareth, Israel). Recording depth was ~400 μm below the cortical surface corresponding to supragranular layers II/III. Placement of the eight electrodes was optimized according to the type of experiment being pursued, within the constraints of large cortical surface blood vessels. For 24-whiskers stimulation experiments, the second or third electrode was aimed at whisker C2's imaging peak location in order to permit recordings on either side of peak activity while still allowing recordings at far distances away from the peak (toward the medial-caudal direction). For 4-whiskers stimulation experiments, the middle electrodes were aimed at whisker C2's imaging peak location and the eight electrodes aligned parallel to the rostral-caudal axis in order to best detect a shift in peak activity location. Recorded signal was amplified and filtered on-line to allow simultaneous capture of supra-threshold (multi-units; 300–3000 Hz bandpass) and sub-threshold (local field potentials or LFPs; 150 Hz low pass) neuronal activity, and then digitized at 24 KHz rate. Quality and consistency of recordings were monitored throughout the day with real time assessment of multi-unit and LFP signals from every electrode. As with imaging, a block of 64 stimulation trials were collected per stimulation condition, contained within one continuous data trace per electrode and with consecutive stimulus deliveries occurring 21 s apart on average.

All off-line analysis including quantification, plotting, and statistics were performed using

Spike 2 software (CED, Cambridge, England), MATLAB, and SYSTAT. For each block of 64 stimulation trials, the recorded data from each of the 8 electrodes were analyzed in the same manner. The LFP data were averaged across trials and the peak magnitude (first minimum) determined for each of the five whisker deflections comprising a complete stimulus delivery. The peak magnitudes could then be averaged together or separated for subsequent comparisons between whisker stimulation conditions. For the multi-unit data, spiking events were qualified with a threshold criterion ( $\pm 3$  SD away from the mean calculated from the entire data trace excluding outliers), averaged across trials in 5 ms bins, and expressed as firing rate per second per trial before proceeding in the same manner as for the LFP analysis.

Statistical tests are described in Table 1. Alpha level was set to 0.05 for all statistical tests performed on the electrophysiological results.

#### *Modeling Multi-Whisker Functional Representations (MWFRs) Based on Linear Summation of Single Whisker Functional Representations (SWFRs)*

We empirically derived an SWFR with representative properties (topography; peak magnitude; signal decay over distance) based on imaging data collected across several intrinsic signal optical imaging projects including the present study ( $n = 37$  rats). This set of data shared the same surgical and data acquisition protocols for imaging the single whisker C2, and the same data processing up through spatial filtering, as in the present study. Because peak activity of a single whisker co-localizes above that whisker's appropriate anatomical barrel (Masino et al., 1993; Brett-Green et al., 2001; Frostig et al., 2008), the filtered images from the 37 rats were spatially aligned according to peak activity location before averaging across images. The resultant average image served as the representative SWFR with empirically derived representative properties including peak magnitude and signal profile (**Fig. 2.4A,B**). Then,

models of MWFRs were generated by (1) creating the appropriate number of copies of the representative SWFR; (2) spatially aligning those copies according to barrel cortex topography; and (3) linearly summing the aligned copies. For a simplified example of modeling see **Fig. 2.4C**.

#### *Electrophysiology Experiments with Local Silencing of Cortical Activity*

A last set of electrophysiology experiments ( $n = 5$  rats) were conducted to investigate the role played by local cortical activity. These experiments were conducted and analyzed in the same manner as the original set of electrophysiology experiments (see Methods Section “Electrophysiology”) except: (1) multi-whisker stimulation was restricted to the 24-whiskers array; (2) middle electrodes of the 8-electrode array were inserted into the location of peak cortical activity; and (3) data acquisition occurred before and after lidocaine was injected locally into the cortex. 1  $\mu$ L of lidocaine (10%; Sigma) was slowly microinjected over the course of 3 min at 300–450 microns cortical depth between the first and second electrode (thus 1.5 mm distal from the middle electrode corresponding to peak activity location). Lidocaine injection followed a previously used protocol (Frostig et al., 2008) in which the lateral spread of lidocaine injection was deemed less than 1 mm in radius away from the injection site. Three sessions of data collection were collected in every rat, initiated before, few minutes after, and one hour after lidocaine injection.

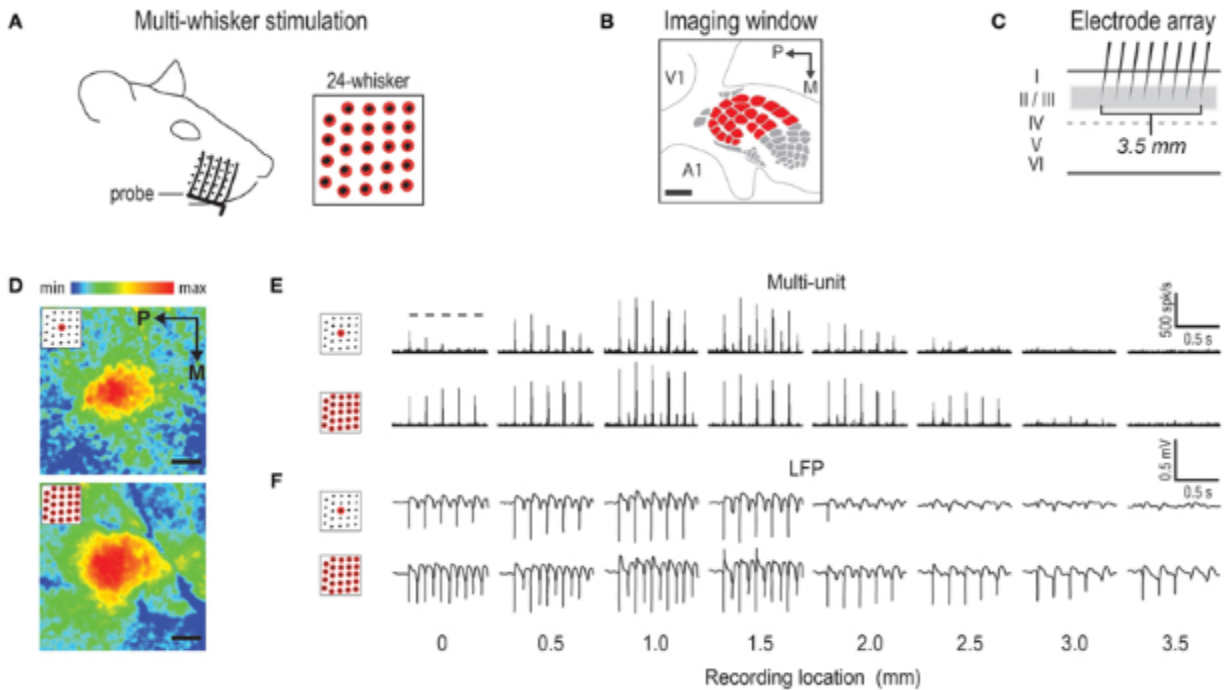


**Figure 2.2. Representative cases of rat barrel cortex response to stimulating an array of 24 whiskers.** (A) 5-prong probe used to achieve multi-whisker stimulation. Stimulated whiskers are indicated in red. (B) 6 × 6 mm intrinsic signal optical imaging field-of-view used when imaging activity simultaneously from the entire barrel cortex plus surrounding regions. V1 = primary visual cortex; A1 = primary auditory cortex. (C) Array of eight independently positioned electrodes, spaced 0.5 mm apart, used to record supra- and sub-threshold neuronal activity from cortical layers II/III. (D) Representative cases of imaging activity for C2 whisker (top) versus 24-whiskers (bottom). Color scale indicates fractional change in poststimulus activity relative to prestimulus activity. (E,F) Representative cases of supra- (E) and sub- (F)threshold neuronal activity for C2 whisker (E,F, top) and 24-whiskers (E,F, bottom). The 5 dashes indicating stimulus delivery in top panel of (E) apply to all supra- and sub-threshold neuronal activity panels. All provided scale bars = 1 mm. Both imaging and neuronal data are aligned according to location of peak activity for whisker C2. Note the similarity in location of peak activity and response magnitude between C2 whisker and 24-whiskers stimulation.

## Results

### *Multi-Whisker Functional Representation (MWFR) of 24 Whiskers Possesses a Single Central Peak*

The MWFR of the 24 largest whiskers (array of neighboring whiskers located in rows

A–E and arcs 1–4, plus the four Greek whiskers; **Fig. 2.1A**) was mapped using intrinsic signal optical imaging ( $n = 10$  rats) with a wide imaging field-of-view (**Fig. 2.2B**). In all rats, the SWFR of whisker C2 was also imaged for reference. Representative and average imaging data are provided in **Fig. 2.2D** and **Fig. 2.3A–C**, respectively.

As expected, on average the SWFR evoked by stimulating whisker C2 consisted of a single activity peak surrounded by a large spread of decaying activity, culminating in a response profile that resembled a single peaked and relatively symmetrical mountain of activity (see black trace in **Fig. 2.3C**). When the number of whiskers being stimulated increased from 1 to 24, the average MWFR for the 24-whiskers still possessed only a single activity peak (**Fig. 2.3A–C**), thereby no longer conveying topographical information about the individual identities of the stimulated whiskers (e.g., 24 local peaks co-registered with the stimulated whisker barrels). This single peak was at a similar location as for whisker C2's activity peak (in **Fig. 2.3C**, compare black trace of C2 whisker to magenta trace of 24-whiskers), meaning that the peak was located centrally within barrel cortex (**Fig. 2.3A**). Note also that this meant the peak location was situated centrally within the collection of the 24 stimulated whiskers' individual SWFRs. Last, compared to whisker C2, there was no increase in the magnitude of peak activity, and the decay of activity away from the peak was more gradual, resulting in an activity mountain with a broader shape (**Fig. 2.3C**). See Table 1, Summary 1, for statistical results obtained from a two-way repeated measure ANOVA performed on the intrinsic signal optical imaging data to compare between the 24-whiskers array's MWFR and whisker C2's SWFR.

The MWFR of the 24-whiskers array, along with whisker C2's SWFR, was also assessed with electrophysiology recordings in each of 12 rats (representative and average data provided in **Fig. 2.2E,F** and **Fig. 2.3D,E**, respectively). Congruent electrophysiology results for the 24-whiskers array were obtained for both sub- and supra-threshold neuronal activity (parent

panels in **Fig. 2.3D,E**, respectively; Table 1, Summaries 2–3, respectively) in which: (1) a single activity peak was still observed; (2) that was in the same location as for whisker C2 and hence located centrally within barrel cortex; (3) with modest (14% for sub-threshold) or no (supra-threshold) increase in magnitude compared to whisker C2; and (4) surrounded by a spread of activity that decayed more gradually away from the peak compared to whisker C2. Additionally, while the sub- and supra-threshold results provided in the parent panels of **Figures 2.3D,E** were for the average response across the five stimulation pulses delivered at 5 Hz rate, we observed the same results when data were subdivided according to stimulation pulse (see insets in **Fig. 2.3D,E**).

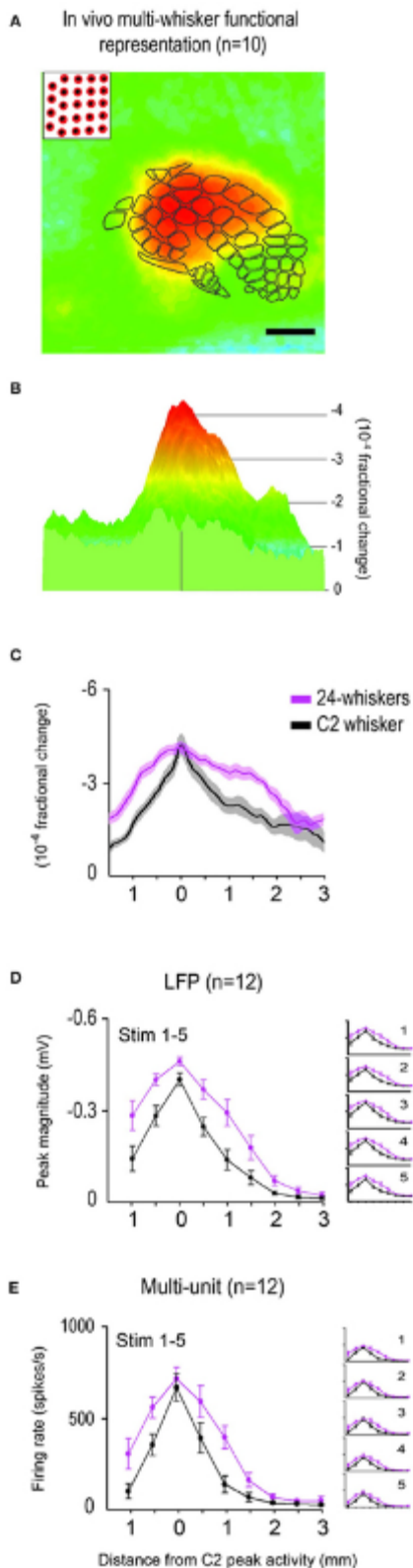


**Figure 2.3. Average *in vivo* data for the 24-whiskers array.** The multi-whisker functional representation (MWFR) for the 24-whiskers array was assessed *in vivo* using intrinsic signal optical imaging ( $n = 10$ ; **A–C**) and supra- and sub-threshold neuronal recordings from an 8-electrode array ( $n = 12$ ; **D,E**). The single whisker functional representation (SWFR) for whisker C2 was also assessed in the same rats for reference. (**A–C**) The average *in vivo*-MWFR for the 24-whiskers as assessed with imaging for the same  $6 \times 6$  mm field-of-view can be plotted in 2D with barrel cortex topography superimposed (**A**) or in 3D (**B**). It can also be plotted as a line plot for the rostral-caudal slice through the center of whisker C2 barrel and hence through the center of the 24-whiskers' MWFR and C2 whisker's SWFR (**C**; mean  $\pm$  SE as solid line and shading, respectively). Scale bar = 1 mm in (**A**); colorscale is the same in (**A,B**). (**D,E**) The average *in vivo*-MWFR as assessed with neuronal recordings. Plotted is the mean  $\pm$  SE of sub- (**D**) and supra- (**E**) threshold neuronal activity of the MWFR for 24-whiskers (magenta trace) vs. the SWFR for whisker C2 (black trace). Whisker stimulation consisted of 5 back-and-forth whisker deflections in the rostral-caudal direction delivered at 5 Hz; parent panels contain data averaged across the five stimulus whisker deflections whereas panel insets contain data separated according to stimulus deflection. For both imaging (**A–C**) and neuronal recording (**D,E**) data, note that the MWFR for the 24-whiskers array consists of a single peak located centrally within a large activation spread, thus resembling a relatively symmetrical activity mountain with one peak. Also note that, compared to the single whisker C2, the 24-whiskers' MWFR exhibited no shift in location of peak activity, no (**C,E**) or modest (14%; **D**) increase in peak magnitude, and relatively moderate increases in the tangential spread of activity and thus a broader shape of the activity mountain.

*Salient Properties of the 24-Whiskers' Multi-Whisker Functional Representation (MWFR) can be Predicted by, and is Dependent on, Interaction Between Single Whisker Functional Representations (SWFRs) of Individual Whiskers*

Based on the well-known topographical and columnar organizational principles of cortical function (**Fig. 2.1**), we could not readily account for the finding of a single activity peak for the 24-whiskers' MWFR (**Fig. 2.3**). Thus, we pursued modeling and pharmacological experiments to determine whether a single whisker's ability to evoke a large cortical activation spread spanning across many barrels (**Fig. 2.4A**) might offer some explanation. As illustrated in **Fig. 2.4B**, the large tangential spread of any given SWFR ensures substantial overlap in the cortical territory occupied by SWFRs of different whiskers even when they are far apart. This overlap should be conducive for SWFRs to interact with one another. We investigated whether interacting SWFRs contributed to the final cortical response evoked by stimulating many whiskers together.

We generated a model of the MWFR for the 24-whiskers array to be expected if cortical activity were indeed dependent on the stereotypical properties of SWFRs and the simplest form of interaction between them (linear summation; **Fig. 2.4C**). The SWFR of whisker C2 as averaged across 37 rats served as the representative SWFR for any large whisker. This representative SWFR possessed empirically derived properties such as a peak magnitude of  $-4 \times 10^{-4}$  fractional change and a specific signal decay function away from the peak. The generated model-MWFR for the 24-whiskers array is shown in **Fig. 2.4D**. We found that modeling based on linear summation of SWFRs was successful in predicting many salient properties of the MWFR observed *in vivo*. Same as for the *in vivo*-MWFR (**Fig. 2.4E**, parent panel), the model-MWFR (**Fig. 2.4D**, parent panel) also possessed only a single activity peak. Also, as observed *in vivo* (**Fig. 2.4E**, insets), the single peak of the model-MWFR was at a similar location to whisker C2's activity peak (**Fig. 2.4D**, lower inset), thus centrally located

within barrel cortex (**Fig. 2.4D**, upper inset) and centrally situated within the collection of the 24 individual SWFRs. After normalizing the model-MWFR to the same peak magnitude as the *in vivo*-MWFR (the entire model-MWFR was divided by a constant term of 12.8), the model-MWFR was observed to be relatively broader in shape as compared to a single whisker (**Fig. 2.4D**, lower inset), which was also observed *in vivo* (**Fig. 2.4E**, lower inset). Indeed, a high goodness-of-fit for the overall mountain profile (including peak location) was found between the model-MWFR and their *in vivo*-MWFR (**Fig. 2.4F**; Table 1, Summary-4). The model accounted for 80% of the *in vivo*-MWFR variance across cortical location, which was greatly reduced to 9% if the model was defined using an incorrect set of SWFRs (Table 1, Summary-5).

Additional experiments were conducted to explicitly verify that the *in vivo*-MWFR and its salient properties such as a single central peak are indeed dependent on interactions between SWFRs. These experiments also addressed whether SWFR interactions responsible for the single-peaked MWFR at the very least occurred at the cortical level, as opposed to subcortical interactions being solely responsible. For example, a single-peaked activity mountain could have already been established subcortically and then passively transmitted to the cortex. Additional 24-whisker MWFR electrophysiological experiments ( $n = 5$  rats) were conducted in which cortical activity was locally silenced by injecting lidocaine into the cortex distal to the MWFR peak location (**Fig. 2.5A**). If the MWFR depends on SWFR interactions that occurred at the cortical level, then the MWFR would alter in ways not easily explained by local silencing of cortical activity. Not only would lidocaine induce the expected decrease in activity at cortical

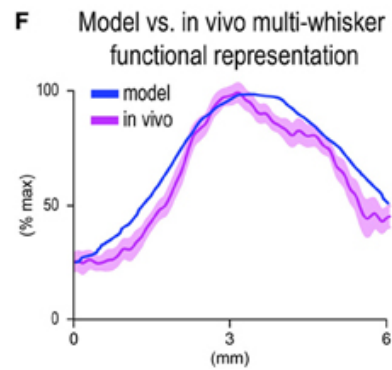
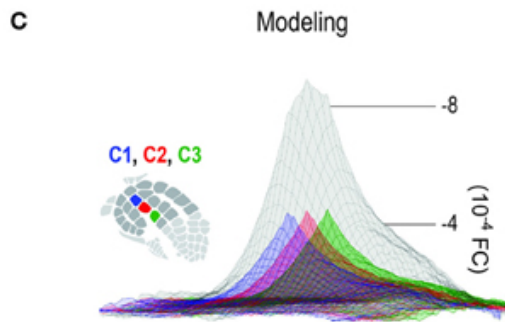
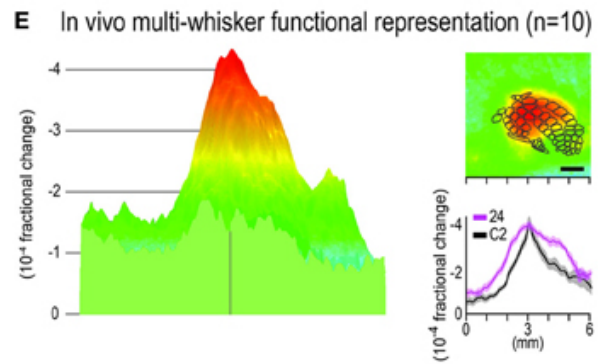
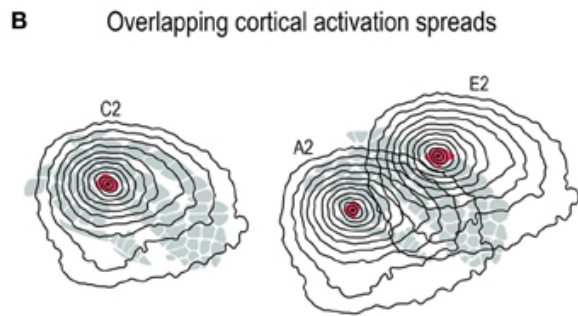
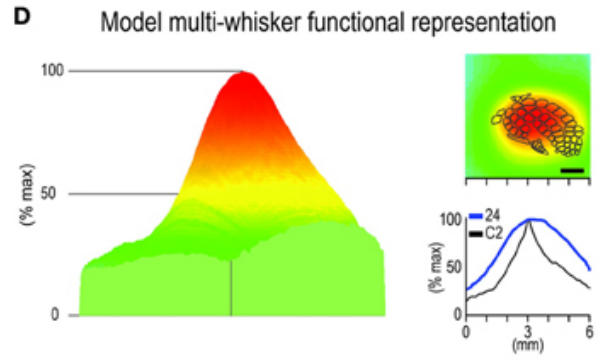
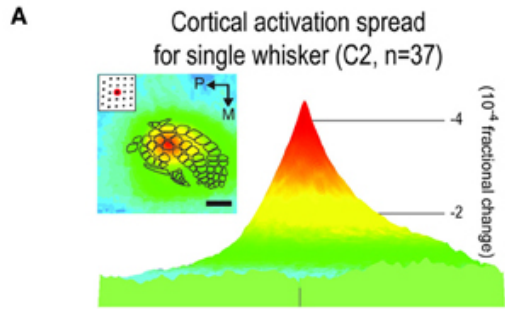


**Figure 2.4. Predicting the *in vivo* multi-whisker functional representation (MWFR) for the 24-whiskers array based on linear summation of single whisker functional representations (SWFRs).** (A) Average activity in barrel cortex evoked by a single whisker plotted in 2D with barrel cortex topography superimposed (inset; scale bar = 1 mm) or in 3D (parent panel), both for the same 6 × 6 mm cortical region. Based on 37 rats assessed with intrinsic signal optical imaging, this example serves as the representative SWFR used in modeling the cortical response to many whiskers. Note the ability of a single whisker to evoke a large spread of cortical activity spanning across many barrels. (B) Contour plots (isolevels spanning from  $-1$  to  $-4 \times 10^{-4}$  fractional change in increments of  $0.25 \times 10^{-4}$ ) of the SWFR for whisker C2 only (left) and whiskers A2 and E2 (right) superimposed on barrel cortex topography. Note the large amount of spatial overlap between cortical activation spreads even for whiskers whose barrels are at opposite borders of barrel cortex. (C) Modeling the MWFR based on linear summation of SWFRs. A simple example is provided here, in which three copies of the representative SWFR are aligned according to C1 (blue), C2 (red), or C3 (green) barrel location before their linear summation to generate the model-MWFR for whiskers C1–C3 (gray). (D–F) Model- vs. *in vivo*-MWFR for the 24-whiskers array. (D) Model-MWFR for 24-whiskers for same 6 × 6 mm field-of-view plotted in 3D (parent panel) or 2D (top inset), or as a line plot for the rostral-caudal slice through the center of C2 whisker barrel (bottom inset), blue trace; black trace is for the representative SWFR in (A). (E) Average *in vivo*-MWFR for 24-whiskers in Figures 3A–C is shown here for easier comparison to the model-MWFR provided in (D). Note that the model-MWFR exhibited many of the salient properties observed for the *in vivo*-MWFR: symmetrical activity mountain with one central peak; peak location aligned with that for whisker C2 and thus located centrally within barrel cortex; a relatively broader mountain shape compared to whisker C2. (F) Response magnitudes for the rostral-caudal slice through the center of whisker C2 barrel are plotted to illustrate the goodness-of-fit between the normalized model- vs. *in vivo*-MWFR.

locations within the infusion site, but it would also disturb SWFR interactions occurring within the infusion site. A new spatial distribution of overlapping activity across SWFRs (as though stimulating only a subset of the 24 whiskers) would be expected, which in turn would lead to a shift in peak location of the MWFR away from the injection site and even an increase in MWFR activity magnitude outside the infusion site (**Fig. 2.5C**). In contrast, if sub-cortical interactions were the sole contributors, this local silencing of cortical activity would not reduce the magnitude of peak activity or shift its location. Instead, a decrease in MWFR activity magnitudes would occur merely at cortical locations within the lidocaine infusion site (**Fig. 2.5B**). As seen in **Figures 2.5D,E**, local silencing of cortical activity succeeded in shifting the location of peak activity away from the injection site and increasing the activity magnitude at locations outside the lidocaine infusion site for both sub- (**Fig. 2.5D**) and supra- (**Fig. 2.5E**) threshold neuronal activity. See Table 1, Summary-6.

#### *Multi-Whisker Functional Representation (MWFR) Findings Extend to a Different Combination of Neighboring Whiskers*

Additional *in vivo* and modeling experiments were conducted to determine whether findings could be extended to a different combination of neighboring whiskers (the four whiskers D3, D4, E3, and E4). Note these four whiskers are located off-center within the 24-whiskers array (refer to **Fig. 2.1A**) and hence the center of their individual SWFRs is located rostral to the center of barrel cortex (refer to **Fig. 2.1B**).

The *in vivo*-MWFR for the 4-whiskers exhibited many properties similar to the 24-whiskers. As assessed with intrinsic signal optical imaging ( $n = 7$  rats), the *in vivo*-MWFR for the 4-whiskers also consisted of a symmetric activity mountain with one central peak (**Fig. 2.6A**, bottom panel). Same as for the 24-whiskers, the 4-whiskers activity peak was situated centrally

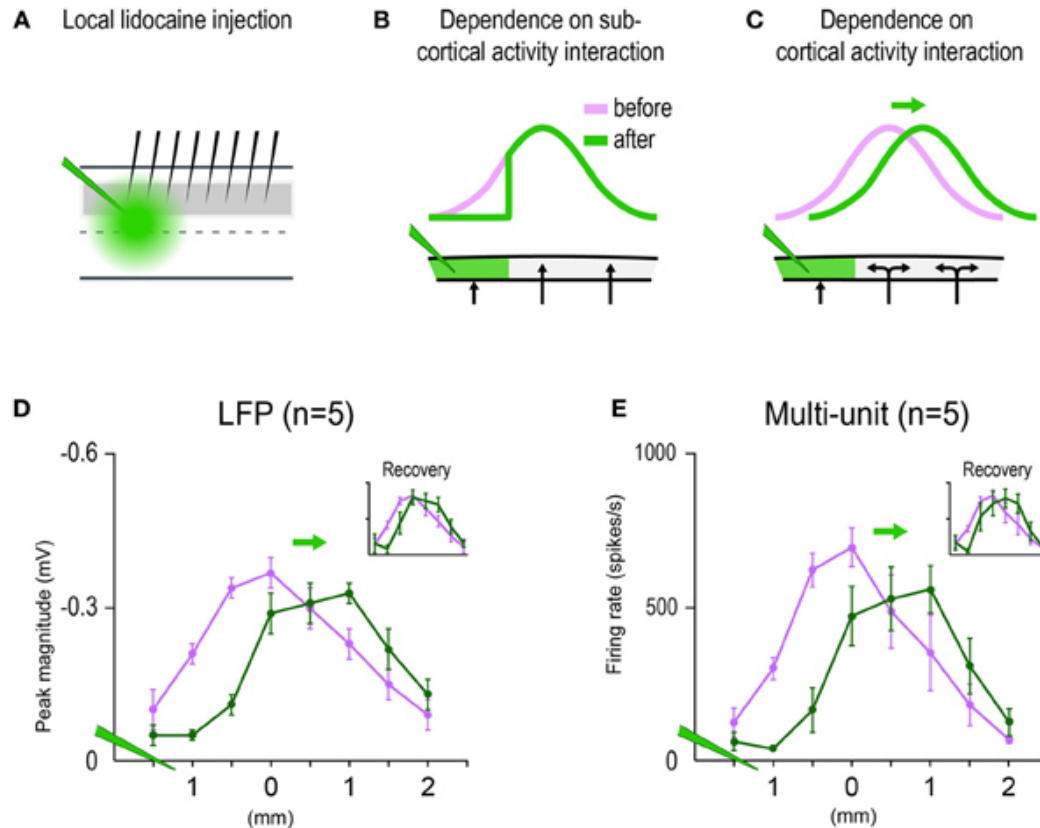


**Figure 2.5. Multi-whisker functional representation (MWFR) for the 24-whiskers array dependent on single whisker functional representation (SWFR) interactions occurring at the cortical level. (A)** Eight electrodes spaced 0.5 mm apart recorded the MWFR for 24-whiskers (middle electrodes aimed at MWFR peak activity location) before and after local lidocaine injection (green) deposited distal (1.5 mm) to the middle electrodes. 1  $\mu$ L of lidocaine (10%; Sigma) was slowly microinjected over the course of 3 min at 300–450  $\mu$ m cortical depth. **(B)** If sub-cortical activity interactions are the sole contributors to the MWFR, then only local silencing of cortical activity within the lidocaine site would occur which, in turn, would lead to a decrease in MWFR response magnitude only within the lidocaine site and thus no shift in MWFR peak activity location nor increases in MWFR response magnitude would occur outside the lidocaine site. **(C)** If SWFR interactions indeed occur at the cortical level (double-headed arrows), then not only the silencing of cortical activity would be induced within the lidocaine site, but also the disruption of SWFR interactions leading to a new spatial distribution of overlapping activity across unaffected SWFRs as though stimulating only a subset of the 24 whiskers. The local silencing of cortical activity should lead to the expected decrease in MWFR response magnitude within the lidocaine site while, importantly, the new SWFR activity overlap should lead to a shift in MWFR peak location away from the lidocaine site and even an increase in MWFR response magnitude outside the lidocaine site. **(D,E)** Results from sub- **(D)** and supra- **(E)** threshold neuronal recordings initiated before versus few minutes after targeted lidocaine injection are congruent with predictions based on SWFR interactions occurring at the cortical level. Recordings initiated 1 h after lidocaine injection revealed recovery of response almost to pre-injection levels (insets).

within the stimulated whiskers' individual SWFRs. Unlike for the 24-whiskers, however, the 4-whiskers activity peak no longer resided in the same location as whisker C2's peak (**Fig. 2.6B**). Rather, it was shifted toward the rostral direction and hence no longer located centrally within barrel cortex (**Fig. 2.6A**, top panel). As for the 24-whiskers, the peak magnitude for the 4-whiskers did not increase compared to whisker C2 (**Fig. 2.6B**). The decay of activity away from the peak, however, was more similar to whisker C2 (**Fig. 2.6B**), which contrasted with the more gradual decay observed for the 24-whiskers (**Fig. 2.3C**). See **Table 2.1**, Summary-7. Last, results from electrophysiology experiments ( $n = 9$  rats; **Fig. 2.6C,D**; **Table 2.1**, Summaries 8–9) once again corroborated the intrinsic signal optical imaging results. With respect to underlying neuronal activity (particularly for supra-threshold), the overall signal decay profile for the 4-whiskers appeared somewhat weaker and less peaked in shape than expected (**Fig. 2.6C,D**, magenta traces) based on intrinsic signal optical imaging results obtained *in vivo* (**Fig. 2.6A,B**). Upon further inspection, the electrophysiology data set from 9 rats was found to consist of two subsets. The peak location was found to have shifted one electrode recording location (0.5 mm) for one set ( $n = 4$  out of 9; **Fig. 2.6E,F**, left plot, magenta traces) and two recording locations (1.0 mm) for the other set ( $n = 5$  out of 9; **Fig. 2.6E,F**, right plot, magenta traces). After their separation, the spatial activity profiles no longer appeared weaker or less peaked compared to single whisker C2's SWFR (**Fig. 2.6E,F**, black traces).

Once again, modeling based on linear summation of SWFRs was successful in predicting many salient properties of the MWFR observed *in vivo*, this time for a different group of neighboring whiskers: (1) single activity peak (**Fig. 2.6G**, middle panel); (2) this single peak was located centrally within the stimulated whiskers' individual SWFRs but rostral to the center of barrel cortex (**Fig. 2.6G**, top panel) and thus rostral to whisker C2's peak location (**Fig. 2.6G**, bottom panel); and (3) shape of activity mountain similar in broadness to whisker C2 (**Fig. 2.6G**,

bottom panel). A high goodness-of-fit for the overall mountain profile was found between the model-MWFR and the *in vivo*-MWFR (**Fig. 2.6H**; Table 2.1, Summary-10), with 79% of the *in vivo*-MWFR variance across cortical location explained by the model that greatly reduced to 26% if the model was defined using an incorrect set of SWFRs (Table 1, Summary-11).

#### *Multi-Whisker Functional Representation (MWFR) Response Properties Obtained in vivo Exhibit Reduction in Variability*

Additional analysis was performed on the *in vivo*-MWFR response properties for the 24- and 4-whiskers, specifically the intrinsic signal optical imaging magnitude at peak activity location and the areal spread of activity quantified using a constant activity threshold (**Fig. 2.7**). For the 24-whiskers, the average peak magnitude was no different (two-tailed paired *t*-test,  $t(9) = 1.21$ ,  $p = 0.26$ ; **Fig. 2.7A**) and the average activity area was 2.6x greater (two-tailed paired *t*-test,  $t(9) = 4.16$ ,  $p = 0.002$ ; **Fig. 2.7C**) compared to those for single whisker C2. Of particular interest was the observed reduction in variability of the *in vivo*-MWFR response properties as measured by the coefficient of variation (ratio between SD and mean)—3.8x reduction for the peak magnitude (**Fig. 2.7A**) and 1.8x reduction for the activity area (**Fig. 2.7C**). For the 4-whiskers, the peak magnitude was found to be significantly but modestly stronger (1.2x; two-tailed paired *t*-test,  $t(6) = 2.72$ ,  $p = 0.03$ ; **Fig. 2.7B**) while the activity area was found not significantly different (two-tailed paired *t*-test,  $t(6) = 1.86$ ,  $p = 0.11$ ; **Fig. 2.7D**) compared to whisker C2. Again, a reduction in variability was observed, 1.5x for the peak magnitude (**Fig. 2.7B**) and 1.9x for the activity area (**Fig. 2.7D**), although it was less pronounced compared to that observed for the 24-whiskers.

As illustrated in **Figures 2.7E,F**, the absolute magnitude values of the *in vivo*-MWFR were much weaker than predicted by modeling based on linear summation of individual SWFRs.

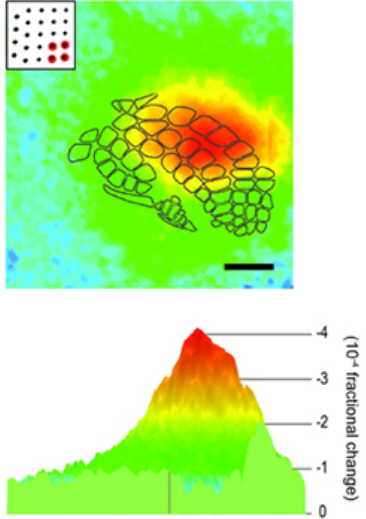
For the 24-whiskers array (**Fig. 2.7E**), the magnitude values obtained *in vivo* were 11.3–16.8x weaker (mean  $\pm$  SD =  $13.7 \pm 1.1$ ), with the location of strongest activity not more or less overestimated by the model compared to elsewhere in barrel cortex. Similarly for the 4-whiskers (**Fig. 2.7F**), the magnitude values obtained *in vivo* was also overestimated by modeling, although differences in magnitude ranged between 2.0–3.6x (mean  $\pm$  SD =  $2.6 \pm 0.4$ ) and therefore were not as striking as for the 24-whiskers array but still occurred relatively uniformly across barrel cortex.

## Discussion

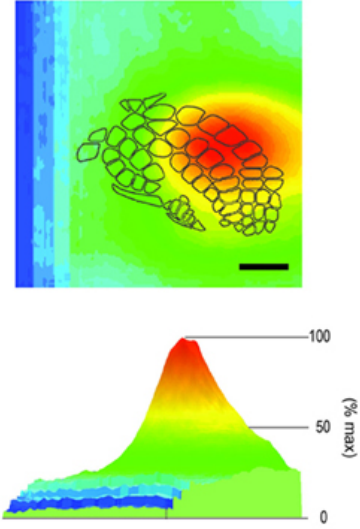
In the present study, both *in vivo* and modeling approaches are used to characterize the rat barrel cortex response to stimulating more than one whisker (MWFR). We find that the MWFR of 24 whiskers possesses only a single peak that is located centrally within a large spread of progressively decaying activity, ultimately resembling a relatively symmetric activity mountain with a single central peak (**Fig. 2.2, 2.3**). By explicitly incorporating SWFRs, which are large in spread and thus highly overlapping, and their interaction with each other (linear summation) into a simple model of MWFRs, we are able to predict salient properties of the 24-whiskers MWFR including the single central peak obtained *in vivo* (**Fig. 2.4**). Furthermore, direct manipulation of cortical activation spreads by locally injecting lidocaine into the cortex distal to the MWFR peak activity leads to results in support of MWFR dependence on SWFR interactions (**Fig. 2.5**). Findings are extended to a different combination of whiskers (subgroup of four neighboring whiskers within the 24-whiskers array; **Fig. 2.6**). Last, we find that *in vivo*-MWFRs exhibit no or relatively modest increase in response magnitude and area but interestingly a reduction in variability of these response properties compared to an SWFR (**Fig. 2.7**).

The finding of the 24-whiskers' MWFR resembling a relatively symmetrical activity mountain with only a single central peak (**Fig. 2.3**) indicates that the cortical response to stimulating many whiskers transcends one-to-one topography to culminate in a single peaked activation spread that no longer conveys information about individual identities of the stimulated whiskers. Our modeling (**Fig. 2.4**) and pharmacological (**Fig. 2.5**) results shed some insight into the mechanism underlying this single peaked cortical response. Once interactions between SWFRs are taken into consideration (**Fig. 2.4A–C**), the single central peak as well as other properties of the 24 whiskers' MWFR obtained *in vivo* (**Fig. 2.4D–F**) can be successfully predicted. Furthermore, the dependence of MWFRs on highly overlapping and hence interacting SWFRs is directly confirmed *in vivo* (**Fig. 2.5**). Our combined modeling and pharmacological findings indicate SWFRs and their interactions play a role in defining salient properties of the cortical response to stimulation of many whiskers. Our pharmacological results (**Fig. 2.5**) also establish that SWFR interactions responsible for single-peaked MWFRs occur at the cortical level (as opposed to single-peaked MWFRs already established subcortically and passively transmitted to the cortex), which is in line with other evidence. Already, it has been demonstrated that the SWFR's large spread of activity occurs intracortically based on cortical transection experiments and anatomical tracer experiments implicating an underlying large spread of long-range intracortical horizontal projections (Frostig et al., 2008). Hence, anatomical infrastructure is in place to support SWFR interactions at the cortical level. Also, the response of cortical neurons have been found to differentiate between stimulation of a single (principal) whisker vs. a group of whiskers comprising the principal whisker plus its adjacent whiskers whereas thalamic neurons do not (Hirata and Castro-Alamancos, 2008). Plus, peripheral

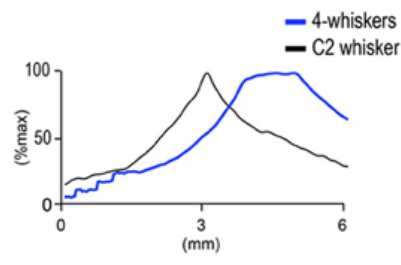
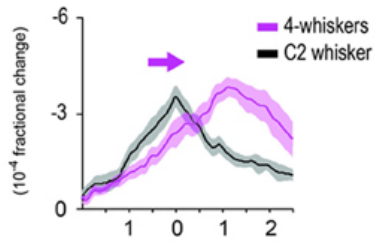
**A** In vivo multi-whisker functional representation (n=7)



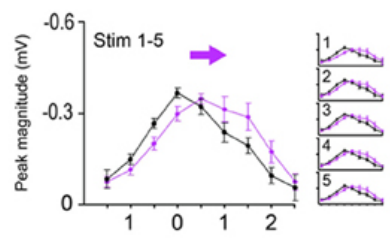
**G** Model multi-whisker functional representation



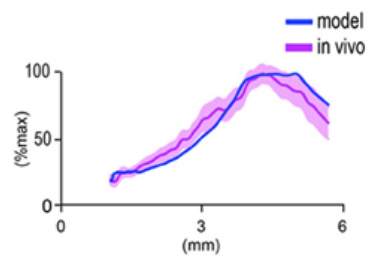
**B**



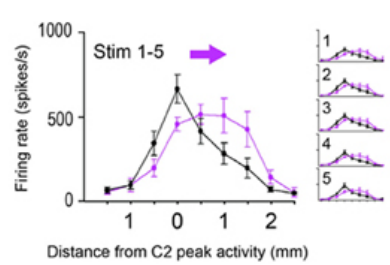
**C** LFP (n=9)



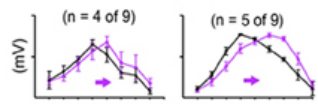
**H** Model vs. in vivo multi-whisker functional representation



**D** Multi-unit (n=9)



**E** LFP (n=9)



**F** Multi-unit (n=9)

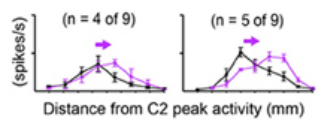


**Figure 2.6. Subset of 4 whiskers also evokes an activity mountain with a single central peak that can be predicted by modeling.** The multi-whisker functional representation (MWFR) for the 4-whiskers array (D3, D4, E3, and E4) was assessed *in vivo* using intrinsic signal optical imaging ( $n = 7$ ; **A–B**) and supra- and sub-threshold neuronal recordings from an 8-electrode array ( $n = 9$ ; **C–F**), and compared to modeling based on linear summation of single whisker functional representations (**G–H**). Details are the same as described in Figures 3–4 except the MWFR is for 4-whiskers instead of 24-whiskers. Note for both imaging (**A,B**) and neuronal recording (**C,D**) data, the MWFR for the 4-whiskers array consisted of a single peak located centrally within a large activation spread, thus resembling a relatively symmetrical activity mountain with one peak. Also, compared to the single whisker C2, the 24-whiskers' MWFR exhibited a shift in location of peak activity (see arrow in **B–D**), similar peak magnitude, and similar tangential spread of activity and thus a similarly broad mountain of activity. Although the activity mountain for the 4-whiskers appeared less peaked compared to C2 whisker, particularly for the supra-threshold activity (**D**), once sub- (**C**) and supra- (**D**) threshold neuronal activity for 4-whiskers were subdivided into two groups according to whether the peak location for 4-whiskers shifted by one ( $n = 4$  out of 9 rats; left panels in **E,F**) or two ( $n = 5$  out of 9 rats; right panels in **E,F**) electrode recording locations, the spatial profile for 4-whiskers no longer appeared less peaked compared to whisker C2. Last, the model-MWFR exhibited many of the salient properties observed for the *in vivo*-MWFR: symmetrical activity mountain with one central peak (**G**, middle panel), peak location shifted away from that for whisker C2 (**G**, bottom panel) and thus located off-centered within barrel cortex (**G**, top panel), a relatively similar broad activity mountain compared to whisker C2 (**G**, bottom panel), ultimately leading to a high goodness-of-fit with data obtained *in vivo* (**H**).

somatosensory neurons exhibit equivalent response patterns for single point vs. multi-point skin stimulation (Gardner and Spencer, 1972a), suggesting minimal interactions between sensory neurons at the peripheral level.

While successful in predicting many MWFR properties, our modeling predictions greatly overestimate the absolute response magnitudes obtained *in vivo* (**Fig. 2.7E,F**). The much lower response magnitudes observed *in vivo* are not artifactual given larger magnitudes are possible (see individual peak magnitude values for single whisker stimulation in **Fig. 2.7A**). The overestimation by the model indicates the cortical response to stimulating many whiskers is dependent on SWFR summation interactions that are specifically sublinear in nature. Indeed, only by normalizing the model with a constant divisive term can we better visualize how well the model fits to the *in vivo* data (**Fig. 2.4F** and **2.6H**). Sublinear summation of SWFRs suggests that at least some interactions between SWFRs must be inhibitory. The normalization of the model using a constant divisive term may even be considered a rudimentary means to model inhibition of activity. Our imaging and electrophysiology (**Fig. 2.3, 2.6, 2.7**) findings of no or modest increases in peak magnitude and area compared to single whisker stimulation also support inhibition of activity. The combined imaging, electrophysiology, and modeling findings would be in line with previous single unit findings on the barrel cortex response to two or few whiskers in support of activity inhibition (for pioneering work see Simons, 1983; Land and Simons, 1985; for review see Fox, 2008), as well as findings obtained at the population level using optical imaging of intrinsic signals (Goldreich et al., 1998) or voltage-sensitive dyes (Kleinfeld and Delaney, 1996; Civillico and Contreras, 2006). Limited studies have been conducted that specifically investigate the simultaneous stimulation of whiskers (Ghazanfar and Nicolelis, 1997; Shimegi et al., 1999; Mirabella et al., 2001; Hirata and Castro-Alamancos, 2008), as is the case in the present study. Our results based on both wide field-of-view imaging of total population response

and electrophysiology recordings of neurons (**Fig. 2.3, 2.6, 2.7**) agree with Mirabella et al. findings of increasing inhibition in cortical activity with increasing number of simultaneously stimulated whiskers.

As the whiskers of awake and behaving rats can be stimulated sequentially as well as simultaneously during active exploration, it would be relevant to determine how our present findings extend to sequential stimulation of the entire whisker array. Based on mapping field potentials (Benison et al., 2006) or single electrode recordings of neuronal responses (Drew and Feldman, 2007) in rat barrel cortex, it already has been shown that the spatial distribution of response properties such as latency (Benison et al., 2006) and peak magnitude (Benison et al., 2006; Drew and Feldman, 2007) can change in a topographical manner depending on the particular parameters of sequential whisker array stimulation. Future imaging studies can be conducted to determine whether sequential stimulation of the entire whisker array can still lead to a large cortical activation spread with a single peak, and if so, whether the location of peak activity can differ in a topographical manner according to sequential stimulation parameters. Also of relevance for future imaging investigation are the possible effects of other stimulation parameters such as frequency (5 Hz used in the present study). We have already shown that the peak magnitude and tangential spread of activity evoked by single whisker stimulation remains the same whether the whisker is deflected 5 times at a rate of 5 Hz (as in the present study) vs. deflected only once (Polley et al., 1999). Given the MWFR dependence on sublinear summation interactions of SWFRs described in the present study, it would be interesting to see whether this constancy in the SWFR despite changes in stimulation parameters lends itself to our MWFR results holding up for at least some stimulation parameters other than those investigated here.

Interestingly, the peak magnitude and area of the single peaked cortical response

obtained in the present study showed marked decrease in variability (**Fig. 2.7**). Interactions between SWFRs occurring at the cortical level provide the opportunity to pool activity from a large population of neurons that could contribute to the improved reliability in cortical response properties to stimulating many whiskers as reported here. Work by Celikel and Sakmann (2007) may point toward a behavioral relevance for such a purpose for SWFR interactions. While able to use a single whisker just as well as the entire whisker array to learn a whisker-dependent gap-crossing task, mice with intact whisker arrays require less time to gather necessary tactile information before successfully crossing the gap. It would be interesting to see whether this faster behavioral response time associated with the use of many whiskers is due to the whiskers initiating interactions between large SWFRs that in turn enable more reliable response properties.

Although no longer conveying one-to-one topographical information about stimulated whiskers, a barrel cortex response to many whiskers possessing a single central peak (**Fig. 2.3**) would be in line with the concept of sensory funneling derived from seminal human psychophysical work by Georg von Békésy. He demonstrated that simultaneous stimulation of several separate and discrete skin sites (i.e., point stimuli) results in perception of a single stimulation site located centrally to the actual stimulation sites (Bekesy, 1967). Important follow-up research by Gardner and colleagues (Gardner and Spencer, 1972a,b; Gardner and Costanzo, 1980a,b; Gardner and Tast, 1981) extended von Békésy's findings by demonstrating that cortical activity itself can exhibit funneling properties (single, central peak of activity) and is predictive of perceptual funneling. Some of these findings have more recently been replicated using evoked potentials (Hashimoto et al., 1999) and functional imaging (Chen et al., 2003).

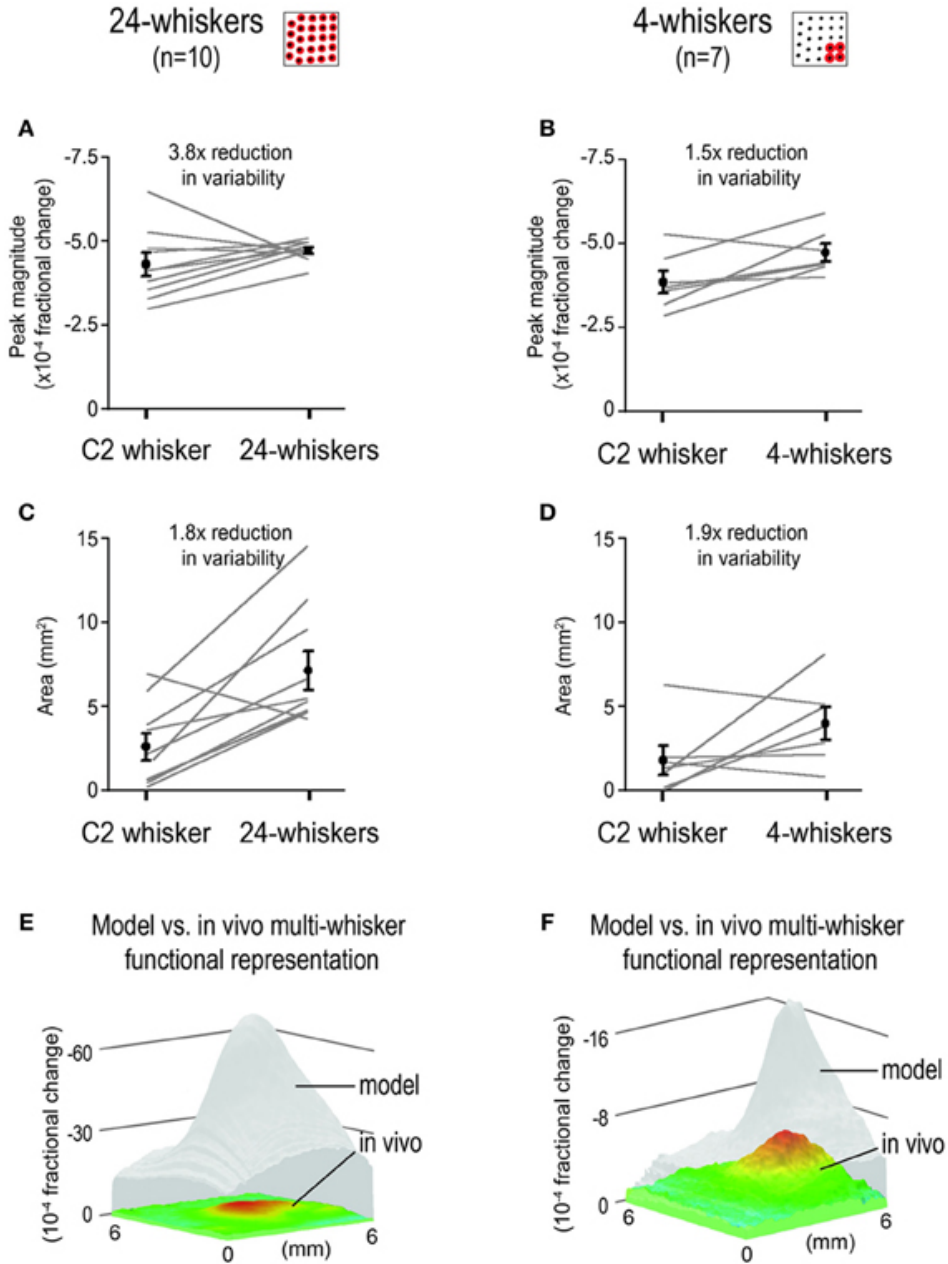


**Figure 2.7. Reduction in variability of response properties for multi-whisker functional representations (MWFRs) compared to single whisker functional representation (SWFR).** Individual and mean  $\pm$  SE values of MWFR peak magnitude (A,B) and area (C,D) for 24-whiskers (A,C) and 4-whiskers (B,D) are provided. For both sets of rats, values for whisker C2 SWFR are obtained within the same animals. Area is quantified using a constant threshold of  $2.5 \times 10^{-4}$  fractional change; peak magnitude is from the pixel location with the peak activity. The coefficient of variation (ratio between mean and variance) is used as a measure of degree in response variability. Note the reduction in response variability for the MWFRs as compared to the SWFR for whisker C2, particularly apparent for the peak magnitude of the 24-whiskers MWFR in panel (A). (E,F) Activity mountains plotted on the same z-scale range to illustrate that the MWFR obtained *in vivo* (color) is much weaker than predicted by modeling based on simple linear summation (transparent gray).

**Table 2.1. Statistics summaries of multi-whisker functional representation (MWFR) and single whisker functional representation (SWFR) data.**

1	See <b>Figure 3C</b> (24-whiskers vs. C2). For the 24-whiskers array, the imaging values were compared between the <i>in vivo</i> -MWFR and whisker C2's <i>in vivo</i> -SWFR obtained within each of 10 rats. Comparison was restricted to the rostral-caudal slice through the center of C2 barrel, corresponding also through the center of the MWFR as well as the SWFR. A two-way repeated measures ANOVA was performed on the imaging values, with the two main variables being Cortical Location (coordinates along the rostral-caudal slice) and Activity Type (MWFR vs. SWFR). Imaging values were first log-transformed to satisfy ANOVA assumptions. The interaction between the two main variables, Cortical Location and Activity Type, was found significant [ $F_{(220, 1980)} = 4.18, p = 9.99 \times 10^{-16}$ ], supporting the observed differences in the relationship between the MWFR and the SWFR magnitudes depending on the cortical location along the rostral-caudal slice (e.g., no difference at the location of peak activity while larger magnitudes for the MWFR at distances away from the peak).
2	See <b>Figure 3D</b> . For the 24-whiskers array, the magnitude of underlying sub-threshold neuronal activity was compared between the MWFR and whisker C2's SWFR obtained within each of 12 rats. Comparison was made for 8 electrodes recording simultaneously from the cortex and spaced 0.5 mm apart along the tangential plane. Electrodes were positioned such that activity could be sampled on opposite sides of the C2 barrel as well as increasing distances away. In support of data observations and congruent with Summary 1 above, a two-way repeated measures ANOVA performed on the log-transformed values found the interaction between Cortical Location and Activity Type significant [ $F_{(6, 66)} = 10.54; p = 3.53 \times 10^{-8}$ ].
3	See <b>Figure 3E</b> . Same as Summary 2 above, except for the magnitude of supra-threshold neuronal activity. A two-way repeated measures ANOVA found the interaction between Cortical Location and Activity Type significant [ $F_{(6, 66)} = 12.65; p = 1.92 \times 10^{-9}$ ].
4	See <b>Figure 4F</b> . For the 24-whiskers array, the goodness-of-fit of the imaging magnitude values was measured between the model-MWFR ( <b>Figure 4D</b> ) and the set of <i>in vivo</i> -MWFRs obtained from 10 rats ( <b>Figure 4E</b> ). The model-MWFR was first normalized to the same peak magnitude as the <i>in vivo</i> -MWFR. Then, reduced chi-squared tests were performed on a pixel-by-pixel basis within a $4.12 \times 2.75$ mm cortical region comprising the barrel cortex associated with the 24 largest whiskers plus nearby surrounding regions. A reduced chi-squared value of 1.125 indicated the best fit possible as achieved by using the mean of the 10 rats. Obtained chi-squared values ranged $1.125\text{--}8.536$ ; mean $\pm$ SD = $1.925 \pm 0.846$ .
5	See <b>Figure 4F</b> . Same as Summary 4 above, except the <i>in vivo</i> -MWFR values were averaged across the 10 rats before comparison to the values of the normalized model-MWFR using a least-squares linear regression. An R-Squared value = 1 indicated that 100% of the variance in the average <i>in vivo</i> values across the $4.12 \times 2.75$ mm cortical region could be explained by the model. Obtained R-Squared value = 0.80. A least-squares linear regression to the model as defined with an incorrect set of SWFRs (specifically the one in <b>Figure 6G</b> ) resulted in an R-Squared value = 0.09.
6	See <b>Figures 5D,E</b> . Two-Way repeated measures ANOVA was performed on the sub-threshold response magnitude values (log-transformed to satisfy ANOVA assumptions), with the two main variables being Cortical Location (8 electrode recordings spaced 0.5 mm apart) and Recording Condition (before vs. after lidocaine injection) (see <b>Figure 5A</b> ). The interaction between Cortical Location and Recording Condition was found significant [ $F_{(7, 28)} = 10.95, p = 1.39 \times 10^{-6}$ ], indicating that differences between recording conditions were dependent on cortical location and supporting the obtained results of decreased response magnitude for cortical locations within the infusion site and increased response magnitude for locations outside the infusion site ( <b>Figure 5D</b> ). Supra-threshold response magnitudes ( <b>Figure 5E</b> ) underwent the same analysis and complementary findings were obtained in which a significant interaction was also found between Cortical Location and Recording Condition [ $F_{(7, 28)} = 9.68, p = 4.48 \times 10^{-6}$ ].
7	See <b>Figure 6B</b> . Same as described for the 24-whiskers array in Summary 1 above, for whiskers D3D4E3E4 the absolute imaging values were compared between the <i>in vivo</i> -MWFR and whisker C2's <i>in vivo</i> -SWFR obtained within each of 7 rats. A Two-Way repeated measures ANOVA performed on the log-transformed values found the interaction between the main variables Cortical Location and Activity Type significant [ $F_{(151, 906)} = 1727.69, p = 9.99 \times 10^{-16}$ ], supporting the observed differences in the relationship between the MWFR and SWFR magnitudes once location along the rostral-caudal slice is taken into consideration (e.g., MWFR is larger at some locations but smaller at other locations).
8	See <b>Figure 6C</b> . Same as described for the 24-whiskers array in Summary 2 above, for whiskers D3D4E3E4 the magnitude of underlying sub-threshold neuronal activity was compared between the MWFR and whisker C2's SWFR obtained within each of 10 rats. Positioning of the 8 electrodes within the cortex was optimized to detect the shift in peak location between the MWFR and the SWFR. In support of data observations and congruent with Summary 7 above, a Two-Way repeated measures ANOVA performed on the log-transformed values found the interaction between Cortical Location and Activity Type significant [ $F_{(6, 48)} = 20.67, p = 8.64 \times 10^{-12}$ ].
9	See <b>Figure 6D</b> . Same as Summary 8 above, except for the magnitude of supra-threshold neuronal activity. A Two-Way repeated measures ANOVA found the interaction between Cortical Location and Activity Type significant [ $F_{(6, 48)} = 6.73, p = 3.00 \times 10^{-5}$ ].
10	See <b>Figure 6H</b> . Same as described for the 24-whiskers array in Summary 4 above, for whiskers D3D4E3E4 the goodness-of-fit was measured between the model- ( <b>Figure 6G</b> ) and the set of <i>in vivo</i> -MWFRs obtained from 7 rats ( <b>Figure 6A</b> ). A reduced chi-squared value of 1.200 indicated the best fit possible, with obtained values ranged $1.200\text{--}4.574$ ; mean $\pm$ SD = $1.629 \pm 0.434$ .
11	See <b>Figure 6H</b> . Same as Summary 10 above, except the <i>in vivo</i> -MWFR values were averaged across the 7 rats before comparison to the model-MWFR normalized values using a least-squares linear regression. Obtained R-Squared value = 0.79. Least-squares linear regression to the model as defined with an incorrect set of SWFRs (specifically the one in <b>Figure 4D</b> ) resulted in an R-Squared value = 0.26.

Here, we extend these findings by showing that a single, central location of peak cortical activity resulting from SWFR interactions can occur in response to stimulating many instead of just a few sites. Interactions between large cortical activation spreads in general could serve as an underlying mechanism of previous funneling reports of cortical activity and their perception. If so, it would be interesting to see whether the awake and behaving rat perceives the stimulation of the 24 whiskers as some integrated perception of a single “broad” whisker located centrally within the array of 24-whiskers rather than a collection of individual stimulated whiskers. Such research pursuits should find useful the findings that when whisker stimulation is delivered in a repetitive manner (e.g., five whisker deflections delivered at 5 Hz rate) just one stimulus occurrence is sufficient for activity to peak at a single central site, even when as little as 4-whiskers are being stimulated (**Fig. 2.3D,E** and **2.6C,D**).

Last, we offer for consideration a more general implication for the functional organization of rat barrel cortex. The existence of SWFRs have already been repeatedly demonstrated with a variety of techniques including intrinsic signal optical imaging, voltage sensitive dye imaging, and traditional electrophysiology techniques (for reviews see Frostig, 2006 and Fox, 2008; for spread observed specifically beyond barrel cortex see Brett-Green et al., 2001; Ferezou et al., 2006, 2007; Frostig et al., 2008; Lim et al., 2012). Furthermore, SWFRs occur for a variety of whiskers and are supported by an existing network of horizontal intracortical projections (Brett-Green et al., 2001; Frostig et al., 2008). With respect to the present findings, the barrel cortex response to stimulating many whiskers has been found dependent on these large SWFRs and their interaction with one another. We posit that large SWFRs and their interaction may even provide an underlying neurophysiological mechanism for previous reports of perceptual and cortical activity funneling. Taken together, our study combined with accumulating evidence support the assertion that large SWFRs (**Fig. 2.4A,B**) be considered alongside topography (**Fig. 2.1B**) and

cortical columns (**Fig. 2.1C**) as a fundamental principle of barrel cortex organization. Interestingly, SWFRs are but one example of large cortical activation spreads evoked by spatially restricted stimulation (e.g., whisker occupies a point on the skin). Large activation spreads evoked by point stimulation appear ubiquitous, having been observed across various sensory modalities and animal species (Grinvald et al., 1994; Bakin et al., 1996; Brett-Green et al., 2001; Ferezou et al., 2006, 2007; Sharon et al., 2007; Frostig et al., 2008; Lim et al., 2012). Future research can be pursued to determine whether large cortical activation spreads following point stimulation can be deemed a fundamental principle of functional organization for not just rat barrel cortex but for the cortex in general.

## **CHAPTER 3: Emergence of spatiotemporal invariance in large neuronal ensembles in rat barrel cortex**

### *Summary*

Invariant sensory coding is the robust coding of some sensory information (e.g. stimulus type) despite major changes in other sensory parameters (e.g. stimulus strength). The contribution of large populations of neurons (ensembles) to invariant sensory coding is not well understood, but could offer distinct advantages over invariance in single cell receptive fields. To test invariant sensory coding in neuronal ensembles evoked by single whisker stimulation as early as primary sensory cortex, we recorded detailed spatiotemporal movies of evoked ensemble activity through the depth of rat barrel cortex using microelectrode arrays. We found that an emergent property of whisker evoked ensemble activity, its spatiotemporal profile, was notably invariant across major changes in stimulus amplitude (up to >200 fold). Such ensemble-based invariance was found for single whisker stimulation as well as for the integrated profile of activity evoked by the more naturalistic stimulation of the entire whisker array. Further, the integrated profile of whisker array evoked ensemble activity and its invariance to stimulus amplitude shares striking similarities to 'funneled' tactile perception in humans. We therefore suggest that ensemble-based invariance could provide a robust neurobiological substrate for invariant sensory coding and integration at an early stage of cortical sensory processing already in primary sensory cortex.

### *Key points*

1. Spatiotemporal profile of ensemble activity could provide robust substrate for invariance

in primary sensory cortex

2. Spatiotemporal profile of single whisker evoked point spreads invariant to stimulus amplitude
3. Spatiotemporal profile of integrated multi-whisker responses also invariant to stimulus amplitude
4. Stereotyped point spreads could serve as reliable “building block” for more complex, integrated responses.

*Reference:*

*Manuscript in submission.* Jacobs, NS, Chen-Bee, CH, Frostig, RD (2015) Emergence of spatiotemporal invariance in large neuronal ensembles in rat barrel cortex. *Frontiers in Neural Circuits*.

## Introduction

Invariance (also known as constancy, tolerance, or robustness) of sensory systems to major changes in sensory parameters is pivotal for survivability in a continuously changing sensory environment. How invariant sensory coding emerges at the neuronal level remains elusive. Neuronal invariance is typically studied in individual cortical neurons (Lueschow et al., 1994; Anderson et al., 2000; MacEvoy and Paradiso, 2001; Quiroga et al., 2005; Li and DiCarlo, 2008; Sadagopan and Wang, 2008). Coordinated activity of neuronal ensembles (Nicoletis and Lebedev, 2009; Quiroga and Panzeri, 2009; Buzsáki, 2010), could offer distinct advantages for invariant coding. For example, neuronal ensembles could mitigate notoriously variable responses in individual cortical neurons (Shadlen and Newsome, 1998). Invariance at the neuronal ensemble level could also rely on emergent response properties, such as spatiotemporal profiles of activity, which would be particularly relevant in topographically organized primary sensory cortices.

Here we analyzed invariance of neuronal ensemble activity and its spatiotemporal characteristics in barrel cortex, a subdivision of primary somatosensory cortex in rodents. Observed from a mesoscopic vantage point, ensemble activity in barrel cortex is highly spatially organized. Single whisker evoke large 'point spreads' of (mostly subthreshold) activity peaking over the appropriate barrel (Frostig et al. 2008), and following simultaneous multi-whisker stimulation unique, single peak integrated spatial patterns of activity emerge resulting from sublinear summation of simultaneously evoked point spreads (Chen-Bee et al. 2012; see schematics in **Fig. 3.1C**). The aim of the current study was to assess the potential for spatiotemporal invariance of such neuronal ensembles following single whisker and whisker array stimulation by testing their potential for invariance to major changes in the amplitude of

whisker stimuli (up to >200 fold changes; **Fig. 3.1**), as rats use and are sensitive to a wide range of whisker deflection amplitudes (Carvell and Simons, 1990) including very small amplitudes on the order of tens of microns (Simons, 1978; Jadhav et al., 2009). Movies of whisker evoked neuronal ensemble activity across a mesoscopic section of barrel cortex including most cortical layers were created from simultaneous multi-site recordings of subthreshold and suprathreshold activity (**Fig. 3.2**). Spatiotemporal profiles of evoked activity were then continuously monitored and quantified with <1 ms temporal resolution, revealing a remarkable degree of ensemble-based spatiotemporal invariance for both single whisker (whisker C2) and whisker array that includes all 24 large whiskers (vibrissae) evoked activity across the major changes in stimulus amplitude. These findings demonstrate invariant, spatially organized ensemble coding for both simple ‘point’ stimuli (i.e., single whisker) as well as for more complex stimuli (i.e., whisker array) that involve integrated patterns of activity. Finally, we discuss how these findings could serve as the underlying neuronal correlate of simultaneous multi-site tactile perception in humans known as ‘funneling’, which is also amplitude-invariant (Békésy, 1967).

## **Materials and Methods**

### *Subjects and surgical preparation*

Seven adult male Sprague–Dawley rats 2-3 months old were used in the study. All procedures were in compliance with the National Institutes of Health guidelines and reviewed and approved by the University of California Irvine Animal Care and Use Committee. Rats were induced with sodium pentobarbital (55 mg/kg b.w.) and maintained with supplemental injections. Fast intrinsic signal optical imaging (Chen-Bee et al., 2010) of the C2 whisker barrel through an 8 x 8 mm region of thinned skull guided placement of electrodes. A small section of thinned skull and dura mater centered over the C2 whisker barrel was removed before insertion of electrode

array. Complete insertion of electrodes was verified visually and with online monitoring of LFP traces. Cytochrome-oxidase staining of post-mortem tissue was used to verify location of electrode bundles within barrel cortex (**Fig. 3.2A**).

### *Whisker stimuli*

Single whisker (whisker C2; **Fig. 3.1A**, left) and whisker array (24 whiskers in rows A–E and arcs 1–4 plus all four Greek whiskers; **Fig. 3.1A**, middle) stimulation was restricted to the right snout. Whiskers were deflected by 0.035°, 0.2°, 1.25°, or 7.5° using a single (for single whisker) or multiple (for whisker array) copper probe(s) mounted to a single arm controlled by a programmable stepping motor (Applied Motion Products, Watsonville, CA) and Master8 pulse generator (AMPI, Jerusalem, Israel). For each trial 5 whisker deflections were delivered at 5 Hz. For each condition, 100 trials were collected at 5 sec intervals. Stimulus conditions were delivered pseudo-randomly such that all single whisker or whisker array conditions were completed before switching whisker probes. All subjects received all 8 whisker stimulus conditions (2 whisker stimulus types x 4 stimulus amplitudes) except one subject that only received whisker array conditions due to surgical complications which terminated the experiment early.

### *Electrophysiology*

Multi-site, extracellular recordings were acquired using 32-channel arrays with an 8x4 design consisting of 8 recording locations each of which had 4 depths targeting layers 1, 2/3, 4, and 5 (**Fig. 3.2A**, middle). Electrode arrays were made from insulated 35  $\mu$ m tungsten wire (California Fine Wire, Grover Beach, CA; insulated with HML and VG bond coating) that were blunt cut and threaded in groups of four through polyimide guide tubes spaced 0.5 mm apart.

Mean impedance of electrodes was  $153 \text{ k}\Omega \pm 55$  (measured with IMP-2, Bak electronics, Sanford, FL). Raw signals starting 1 sec before and ending 1 sec after stimulus onset (total of 3 sec per trial) were amplified and digitized at a 22 kHz sample rate (SnR system, Alpha Omega, Nazareth, Israel).

Analyses were done using custom MATLAB scripts. Raw traces were band-pass filtered for local field potentials (LFP, 1-300 Hz) or multi-unit potentials (MUP, 300-3k Hz) using a two-pole Butterworth function. LFP and MUP were averaged across trials. Trial averages of non-rectified, spike filtered traces have previously been interpreted as population firing synchrony (Temereanca and Simons, 2003). Trials with electrical noise (5.32% of trials) were excluded from trial averages. For the few bad channels in arrays (5.36% of channels overall, equivalent to 1.6 channels per array), trial averages from adjacent channels at the same cortical depth were averaged. In trial averages, mean baseline values 50 ms to 0 ms before stimulus onset were subtracted. A Gaussian filter was used to smooth out electrical noise near 60 Hz in MUP data. For group analyses, trial averaged data was down-sampled to a 10 kHz sample rate. To spatially align data for group analyses, single whisker and whisker array data sets for each subject were shifted horizontally to align peak LFP responses in layers 2/3 and 4 for the strongest stimulus amplitude ( $7.5^\circ$ ). For suprathreshold responses, PSTHs of spike times were consistent with main findings but were not preferred for analysis due to an abundance of overlapping spike waveforms that made these data uninterpretable (see **Appendix A**; Bar-Gad et al., 2001; Temereanca et al., 2008).

### *Spatiotemporal analyses*

Electrophysiology data was analyzed at the mesoscopic level (i.e. data from all electrodes were analyzed concurrently). Frames of activity were normalized by dividing by the

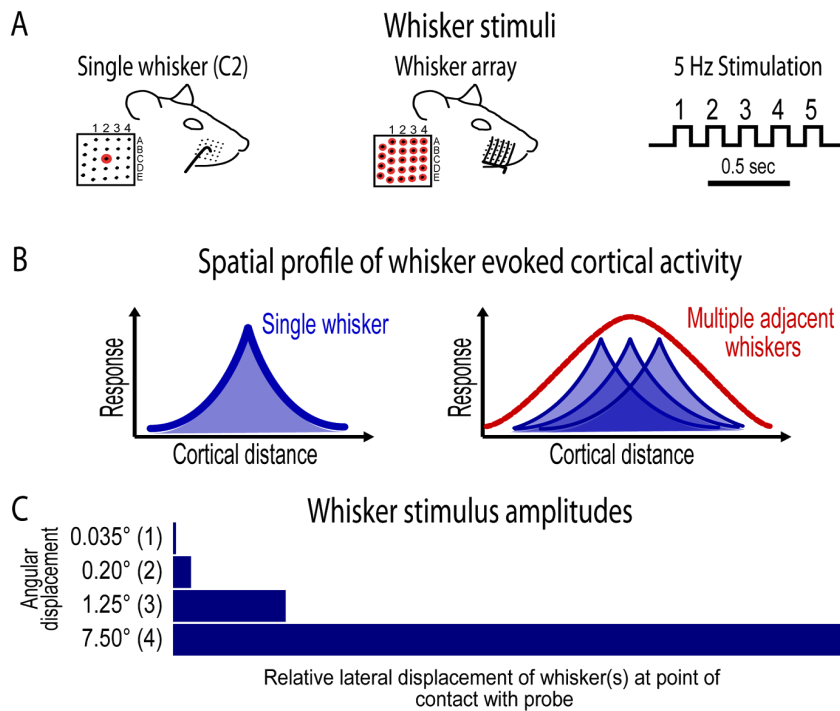


**Figure 3.1. Whisker stimuli and spatial profile of whisker evoked ensemble activity in barrel cortex.** (A) Ensemble-based invariance was investigated for two types of whisker stimuli- a single central whisker located at the center of the whisker pad (whisker 'C2,' left) and the whisker array including all 24 large mistacial whiskers (middle). Whisker stimuli were delivered at a 5 Hz rate and consisted of 5 deflections per trial (right). (B) Schematics of previously reported spatial profiles of single whisker and whisker array evoked activity in barrel cortex (Chen-Bee et al., 2012). Note the large, overlapping profiles for single whisker and the single, central peak in the profile for whisker array. (C) Ensemble-based invariance was tested across logarithmic (base 6) changes in whisker stimulus amplitude that ranged from a barely visible movement of the whisker(s) at 0.035° to the relatively large stimulus amplitude of 7.5°.

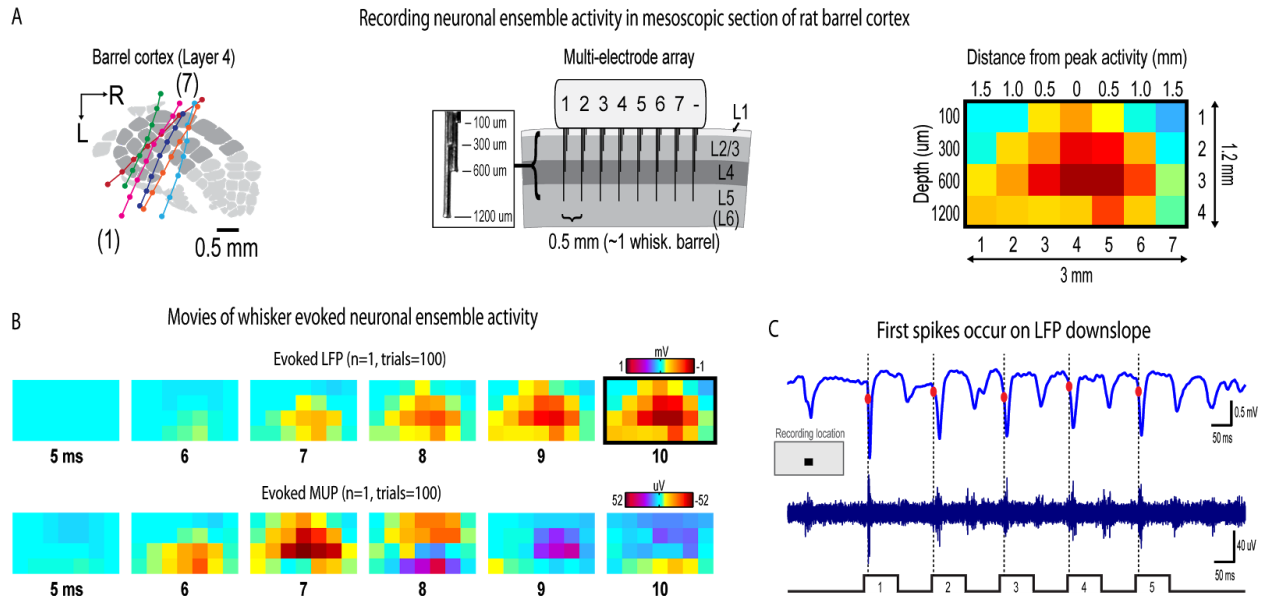


**Figure 3.2. Recording movies of continuous ensemble activity in barrel cortex.** (A) High fidelity 7x4 electrode arrays were used to acquire “snapshots” of ongoing activity across a mesoscopic section of cortex extending beyond the boundaries of rat barrel cortex and penetrating through most cortical layers (left and middle). (B) Representative movies of evoked local field potentials (LFP, top) and multi-unit potentials (MUP, bottom). The last frame of evoked LFP with dark border is same as in (A). (C) It was initially surprising to see very early, small amplitude MUP signals occurring *before* LFP in (B). However, when LFP (top) and MUP (bottom) filtered traces were compared during individual trials, the peak negative deflection of the first detected spike waveform occurred *during* LFP downslopes. The apparent discrepancy is resolved by noting the very early, small amplitude signals in trial averaged MUP (see ‘onset responses’ in Fig. 3.4d and 3.6d) that begin *before* the peak negative deflection of a single spike which are much more visible in individual traces.

maximum value across all recording locations within 50 ms of stimulus onset (data for each deflection was normalized separately). Onset frames of activity were the first frames with a maximum value greater than the 99% confidence interval for pre-stimulus data 10 to 0 ms before stimulus onset. Peak frames of activity were frames with the maximum value within 50 ms of stimulus onset.

Principal component analysis (PCA) was performed on normalized data. Each frame of activity for each subject and condition (stimulus amplitudes 1-4) was vectorized and treated as a single observation without centering about the mean. Loadings for each principal component corresponded to how similar each frame of activity was to that particular principal component. Note that unlike correlations such loadings are sensitive to absolute magnitude, for example the weaker magnitudes in a frame of activity before peak responses would result in a reduced loading even if it had an identical relative profile of activity.

Pearson's correlations were calculated separately for each subject and group averages reported (mixed-model). Confidence intervals for pre-stimulus  $r^2$  values were calculated from all stimulus amplitude comparisons using a pre-stimulus time window (-10 to 0 ms for analysis of 25 ms window in **Fig. 3.3-6E** and -200 to 0 ms for analysis of 1.4 sec window in **Fig. 3.8**). Quartile-quartile plots of data at pre-stimulus, onset, and peak responses revealed no major deviations from a normal distribution. All spatiotemporal analyses were done within subjects and group statistics reported.

### *Statistical analyses*

All parametric statistics (repeated measures ANOVA, paired t-tests) were performed in SYSTAT version 11. For grand means, multiple values for each subject were first averaged before grand mean and s.e.m. calculations.

## Results

The current project assessed invariance in spatiotemporal profiles of whisker evoked ensemble activity in rat barrel cortex across major changes in stimulus amplitude. Two types of whisker stimulation were used, single whisker (C2) and whisker array (all 24 large whiskers), and were delivered at a naturalistic 5 Hz rate for a total of five whisker deflections per trial (**Fig. 3.1A**). For both whisker stimuli, ensemble activity was assessed across logarithmic (base 6) changes in whisker stimulus amplitude (**Fig. 3.1C**). The smallest stimulus amplitude ( $0.035^\circ$ ) was barely perceptible to the eye and the largest stimulus amplitude ( $7.5^\circ$ ) was comparable to our previous studies (Frostig et al., 2008; Chen-Bee et al., 2012). Movies of whisker evoked activity were recorded across a mesoscopic section of cortex that extended through and beyond barrel cortex and penetrated through most cortical layers (**Fig. 3.2**). The exact positioning of electrode arrays was constrained by blood vessel patterns in each subject producing some variability across subjects, however all spatiotemporal analyses were performed within subjects eliminating any between-subjects differences. For suprathreshold responses, trial averaged multi-unit potentials (referred to hereafter as 'MUP'; see methods for details) were preferred over PSTHs because of an abundance of overlapping spike waveforms that made spike counts uninterpretable (**Appendix A**). Spatial profiles of evoked activity were continuously monitored with high temporal resolution ( $< 1$  ms) and compared across major changes in stimulus amplitude (up to  $>200$  fold). Results for the first of five whisker deflections, analogous to a single deflection of a whisker or the whisker array, are presented in **Fig. 3.3-3.7**. Results for repeated single whisker or whisker array deflections, analogous to repetitive whisking behaviors, are presented in **Fig. 3.8-3.9**.

### *Invariance in single whisker evoked LFP for the first deflection*

Movies of single whisker (C2) evoked local field potentials (LFP) for the first of five deflections and their quantification are shown in **Figure 3.3**. For the first deflection, movies are shown from 1-25 ms post-stimulus onset. The same analyses used in this section are repeated in following sections. As discussed in detail below, major changes in stimulus amplitude (up to > 200 fold) affected the magnitude but *not* the spatiotemporal profile of single whisker evoked MUP for the first deflection.

Mean single whisker evoked LFP (n=6) for each of the four stimulus amplitudes (0.035°, 0.2°, 1.25°, 7.5°) is shown in **Figure 3.3A**. Single whisker evoked LFP for each stimulus amplitudes spread vertically and laterally across the field of view within the 25 ms time window. Despite differences in absolute magnitude, a similarly broad lateral profile of evoked LFP for each stimulus amplitude was observed by normalizing each movie to the peak negative value across all frames within the 25 ms window (**Fig. 3.3B**). Further support for the large spatial profile of evoked LFP was that each stimulus amplitude engaged a similarly large region of cortex including all recording locations within the field of view, all of which had evoked LFP within the 25 ms window at least 3 standard deviations above pre-stimulus data (**Fig. 3.10A**). Thus, initial qualitative assessment revealed notably similar spatiotemporal profiles of single whisker evoked LFP for the first deflection.

Spatiotemporal profiles of single whisker evoked LFP for the first deflection were quantified and compared across stimulus amplitudes (**Fig. 3.3C-D**). The spatial profile of evoked LFP at each time point was quantified using principle component analysis (PCA) of normalized data (**Fig. 3.3C**). The first principal component (PC1; **Fig. 3.3C**, top, inset) explained 82% of the variance in frames of evoked LFP, with PC2 and PC3 explaining only 6% and 4% of the variance, respectively. PC1 loadings were then plotted over time for each stimulus amplitude

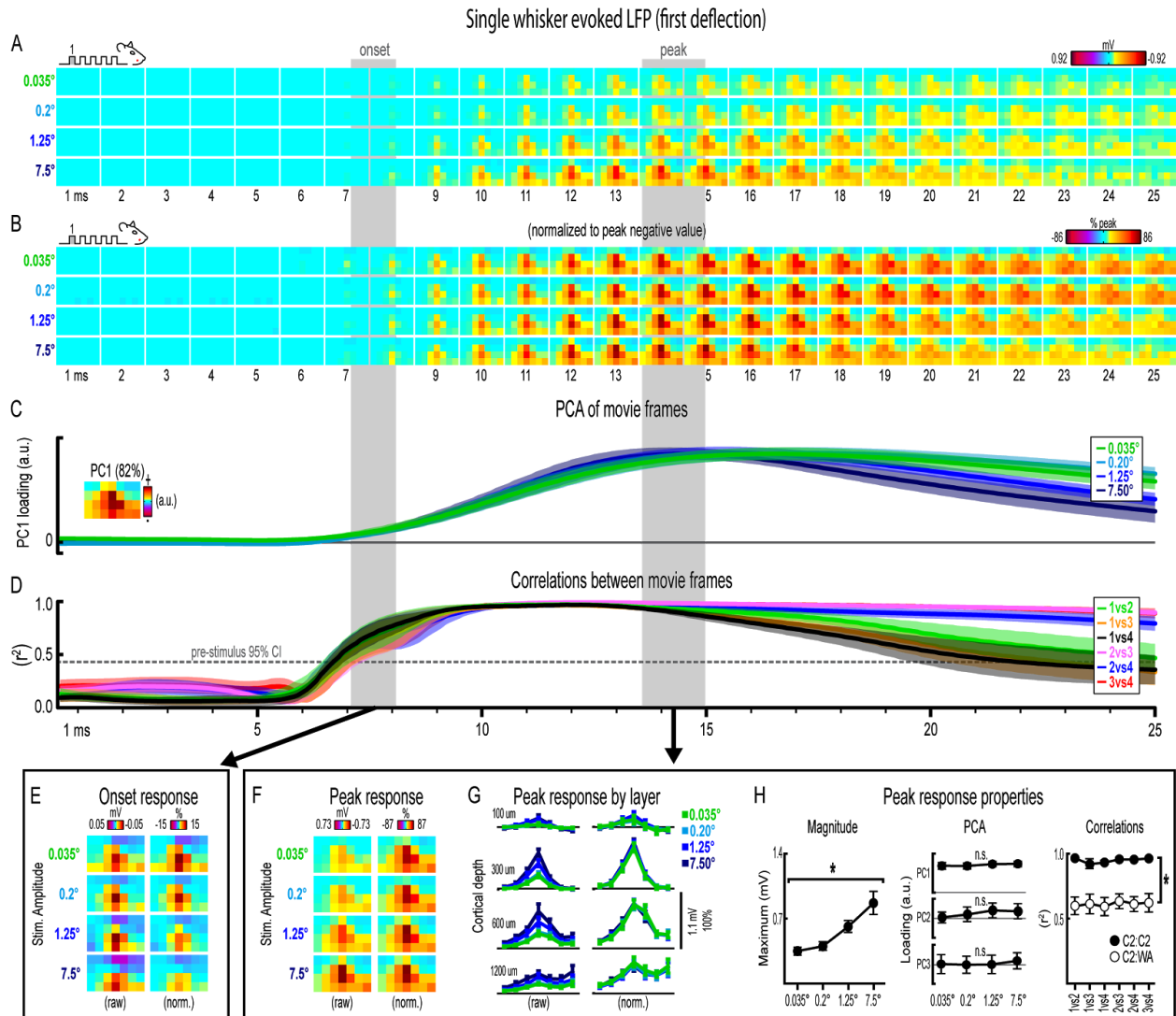


**Figure 3.3. Single whisker evoked LFP for the first deflection.** (A) Movies of averaged ( $n=6$ ) single whisker evoked LFP for the first deflection at each of the four stimulus amplitudes ( $0.035^\circ$ ,  $0.2^\circ$ ,  $1.25^\circ$ , and  $7.5^\circ$ ). Note the laminar and lateral spread of evoked LFP. (B) The relative spatial profile of evoked LFP spread can be compared across stimulus amplitudes by normalizing each movie to the maximum value across all pixels and time points. (C-D) Continuous quantification of spatial profiles with PCA loadings (C) and similarity between spatial profiles with correlations (D). Traces are mean  $\pm$  s.e.m. Gray shaded regions indicate mean onset and peak latencies ( $\pm$  s.e.m.). (E) Raw and normalized mean onset frames. (F-H) Raw and normalized mean peak frames (F), broken down by layer (G), and quantification of peak response properties (H).

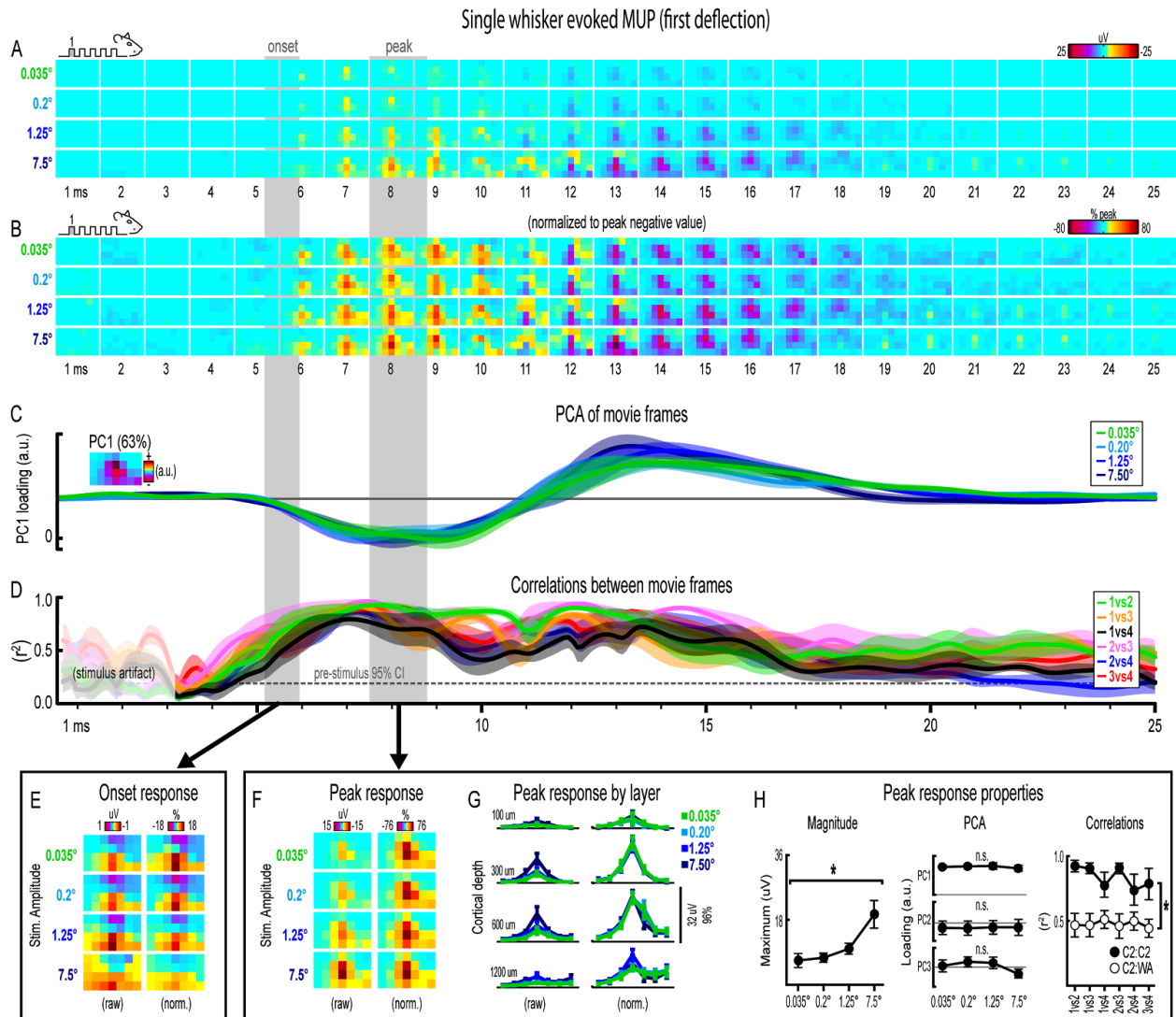


**Figure 3.4. Single whisker evoked MUP for the first deflection.** (A-B) Raw (A) and peak-normalized (B) movies of averaged ( $n=6$ ) single whisker evoked MUP for the first deflection. (C-D) Continuous quantification of spatial profiles with PCA loadings (D) and similarity between spatial profiles with correlations (E). Traces are mean  $\pm$  s.e.m. Gray shaded regions indicate mean onset and peak latencies ( $\pm$  s.e.m). (E-F-H) Raw and normalized mean onset frames (E), broken down by layer (G), and quantification of peak response properties (H).

(**Fig. 3.3C**, top). Note that identical spatiotemporal profiles would result in identical (i.e., completely overlapping) traces of PC1 loadings. Traces of PC1 loadings for each stimulus amplitude were highly overlapping from the onset of responses (left shaded region in **Fig. 3.3C**) through peak responses (right shaded region in **Fig. 3.3C**). PCA results therefore matched initial findings of similar spatiotemporal profiles of single whisker evoked LFP for the first deflection.

Similarity between frames of single whisker evoked LFP for the first deflection was quantified with correlations between all possible stimulus amplitude pairs (1vs2, 1vs3, 1vs4, 2vs3, 2vs4, and 3vs4) at each time point within the 25 ms window (**Fig. 3.3D**). Note that the '1vs4' comparison (black traces in **Fig. 3.3D**) between the smallest (0.035°) and largest (7.5°) stimulus amplitude represented a ~215 fold difference in stimulus amplitude. At ~7 ms post-stimulus onset, mean coefficients of determination ( $r^2$  values) rose above a 95% confidence interval (gray dotted line in **Fig. 3.3D**) calculated from pre-stimulus data for all stimulus amplitude comparisons. Mean  $r^2$  values for all comparisons appeared to reach a maximum at ~10 ms and then slowly tapered off after peak. These data further substantiated the similarity in spatiotemporal profiles of evoked LFP observed in peak-normalized movies (see **Fig. 3.3B**). Together, continuous qualitative and quantitative measures suggested highly similar spatiotemporal profiles of single whisker evoked LFP were maintained despite major changes in stimulus amplitude.

Lastly, onset and peak frames of single whisker evoked LFP for the first deflection warranted closer inspection. Mean onset and peak latencies were 7.6 $\pm$ 0.4 ms and 14.2 $\pm$ 0.6 ms, respectively (shaded regions in **Fig. 3.3A-D**; grand mean of subject and stimulus amplitude  $\pm$  s.e.m.; see **Table 3.1** for details). Onset responses were difficult to see in **Figure 3.3A** due to their small magnitude. Therefore, onset frames of evoked LFP were aligned, averaged, and plotted with a "zoomed in" color scale that was ~ 20 times more sensitive (**Fig. 3.3E**). The more

sensitive color scale revealed a consistent pattern of positive or neutral voltages at the most superficial depth targeted at layer 1 (top row of pixels in each image) and negative voltages in the two deepest depths targeted at layers 4 and 5 (bottom two rows of pixels in each image) for all stimulus amplitudes. Similar patterns were found for all onset frames of evoked LFP and MUP (see relevant sections below), and were likely produced by fast, synchronous activity in thalamocortical afferents (Kandel and Buzsáki, 1997).

Peak frames of single whisker evoked LFP for the first deflection were aligned and averaged (**Fig. 3.3F**). The same data was also broken down by recording depth to allow closer inspection of laminar responses (**Fig. 3.3G**). Similar to before, response magnitudes increased with increasing stimulus amplitude but had nearly indistinguishable spatial profiles. Supporting the observed change in response magnitude, the maximum value in peak frames was significantly different across stimulus amplitudes ( $F(3,15)=16.12$ ,  $p<0.001$ ; **Fig. 3.3H**, left). Supporting the similarity of spatial profiles, PC1, PC2, and PC3 loadings for peak normalized frames were not significantly different across stimulus amplitudes ( $PC1$ ,  $F(3,15)=0.36$ ,  $p=0.780$ ;  $PC2$ ,  $F(3,15)=2.44$ ,  $p=0.105$ ;  $PC3$ ,  $F(3,15)=2.09$ ,  $p=0.145$ ; **Fig. 3.3H**, middle).

Further supporting the similarity of spatial profiles, peak frames were also highly correlated with each other (mean  $r^2 = 0.95 \pm <0.01$ ; grand mean of comparison and subject; **Fig. 3.3H**, right, closed circles). A simple internal control was used to test the sensitivity of correlations by comparing single whisker to whisker array responses, which are both characterized by the same basic shape (a single, central peak of activity; see schematics in **Fig. 3.2B**). Importantly, this control comparison resulted in significantly lower  $r^2$  values (**Fig. 3.3H**, right, open circles; grand mean  $r^2 = 0.62 \pm 0.06$ ;  $F(1,5)=107.86$ ,  $p<0.001$ ; for peak frames of whisker array evoked LFP see **Fig. 3.5F**), indicating that correlations were highly sensitive to even subtle changes in the profile of evoked activity.

Results for single whisker evoked LFP for the first deflection suggested that large changes in stimulus amplitude (up to > 200 fold) affected the magnitude but *not* the spatiotemporal profile of activity.

#### *Invariance in single whisker evoked MUP for the first deflection*

Movies of single whisker evoked multi-unit potentials (MUP) for the first of five deflections and their quantification are shown in **Figure 4A**. The exact same analyses used before were repeated and are summarized briefly below. Note that MUP responses had an early negative and a late positive peak within the 25 ms post-stimulus time window. All analyses of peak MUP responses focused on the earlier negative peak. Similar to before, major changes in stimulus amplitude (up to > 200 fold) again affected the magnitude but *not* the spatiotemporal profile of single whisker evoked MUP for the first deflection.

Mean single whisker evoked MUP (n=6) for the first deflection increased in magnitude with increasing stimulus amplitude (**Fig. 3.4A**), had notably similar spatiotemporal profiles as revealed by normalizing to peak values (**Fig. 3.4B**), and included evoked activity >3 standard deviations above pre-stimulus data across the entire field of view (**Fig. 3.10B**). Continuous quantitative measures further supported the finding of similar spatiotemporal profiles across stimulus amplitudes. For PCA (**Fig. 3.4C**), PC1 explained 63% of the variance with PC2 and PC3 explaining only 12% and 7%, respectively. Traces of mean PC1 loadings for each stimulus amplitude were again highly overlapping, even during transitions between negative and positive MUP phases. For correlations between frames of evoked MUP (**Fig. 3.4D**), mean  $r^2$  values for all stimulus amplitude comparisons rose above the 95% pre-stimulus confidence interval at 4-5 ms post-stimulus onset, appeared to reach a maximum by 7 ms, and were highest during peak negative and peak positive responses. Together, continuous qualitative and quantitative

measures suggested highly similar spatiotemporal profiles of single whisker evoked MUP were maintained despite major changes in stimulus amplitude.

Onset and peak frames of single whisker evoked MUP for the first deflection were again inspected more closely. Onset and peak latencies were  $5.6 \pm 0.4$  ms and  $8.1 \pm 0.5$  ms on average (shaded regions in **Fig. 3.4**; see **Table 3.1** for details). Onset frames of evoked MUP (**Fig. 3.4E**) again had positive or neutral voltages in the most superficial depth and negative voltages in the two deepest depths for each stimulus amplitude. Peak frames of evoked MUP (**Fig. 3.4F-H**) again demonstrated changes in response magnitude but not spatial profile. Supporting the observed change in response magnitude, the maximum value within peak frames was significantly different across stimulus amplitudes ( $F(3,15)=4.47$ ,  $p=0.02$ ; **Fig. 3.4H**, left). Supporting the similarity of spatial profiles, PC1, PC2, and PC3 loadings for peak frames were not significantly different across stimulus amplitudes ( $PC1$ ,  $F(3,15)=0.33$ ,  $p=0.805$ ;  $PC2$ ,  $F(3,15)=0.64$ ,  $p=0.602$ ;  $PC3$ ,  $F(3,15)=2.01$ ,  $p=0.156$ ; **Fig. 3.4H**, middle). Further supporting the similarity of spatial profiles, peak frames were also highly correlated with each other (**Fig. 3.4H**, right, closed circles; grand mean  $r^2 = 0.94 \pm 0.01$ ). Importantly, peak frames of single whisker evoked MUP were significantly less correlated with peak frames of *whisker array* evoked MUP (**Fig. 3.4H**, right, open circles; grand mean  $r^2 = 0.51 \pm 0.06$ ;  $F(1,5)=12.09$ ,  $p=0.018$ ; for peak frames of whisker array evoked MUP see **Fig. 3.6F**), again indicating that correlations were sensitive to even subtle changes in profiles of activity.

Together, results for single whisker evoked MUP and LFP for the first deflection suggested that large changes in stimulus amplitude (up to > 200 fold) affected the magnitude but *not* the spatiotemporal profile of neuronal ensemble activity.

*Invariance in whisker array evoked LFP for the first deflection*

Movies of whisker array evoked LFP for the first of five deflections and their quantification are shown in **Figure 3.5**. The exact same analyses used before were repeated and are summarized briefly below. Similar to before, major changes in stimulus amplitude (up to > 200 fold) again affected the magnitude but *not* the spatiotemporal profile of whisker array evoked LFP for the first deflection.

Mean whisker array evoked LFP (n=7) for the first deflection increased in magnitude with increasing stimulus amplitude (**Fig. 3.5A**), had notably similar spatiotemporal profiles as revealed by normalizing to peak values (**Fig. 3.5B**), and included evoked activity >3 standard deviations above pre-stimulus data across the entire field of view (**Fig. 3.10E**). Continuous quantitative measures further supported the finding of similar spatiotemporal profiles across stimulus amplitudes. For PCA (**Fig. 3.5C**), PC1 explained 85% of the variance with PC2 and PC3 both explaining only ~4% of the variance. Traces of mean PC1 loadings for each stimulus amplitude were again highly overlapping. For correlations between frames of evoked LFP (**Fig. 3.5D**), mean  $r^2$  values for all stimulus amplitude comparisons rose above the 95% confidence interval for pre-stimulus data at ~6 ms, reached a maximum by ~8 ms before slowly tapering off. Together, continuous qualitative and quantitative measures suggested highly similar spatiotemporal profiles of whisker array evoked LFP for the first deflection were maintained despite major changes in stimulus amplitude.

Onset and peak frames of whisker array evoked LFP for the first deflection were again inspected more closely. Onset and peak latencies were 6.0±0.4 ms and 12.3±0.6 ms on average (shaded regions in **Fig. 3.5**; see **Table 3.1** for details). Onset frames of evoked LFP (**Fig. 3.5E**) had positive or neutral voltages in the two most superficial depths and negative voltages in the two deepest depths for each stimulus amplitude. Peak frames of evoked LFP (**Fig. 3.5F-H**) again demonstrated changes in response magnitude but not spatial profile. In

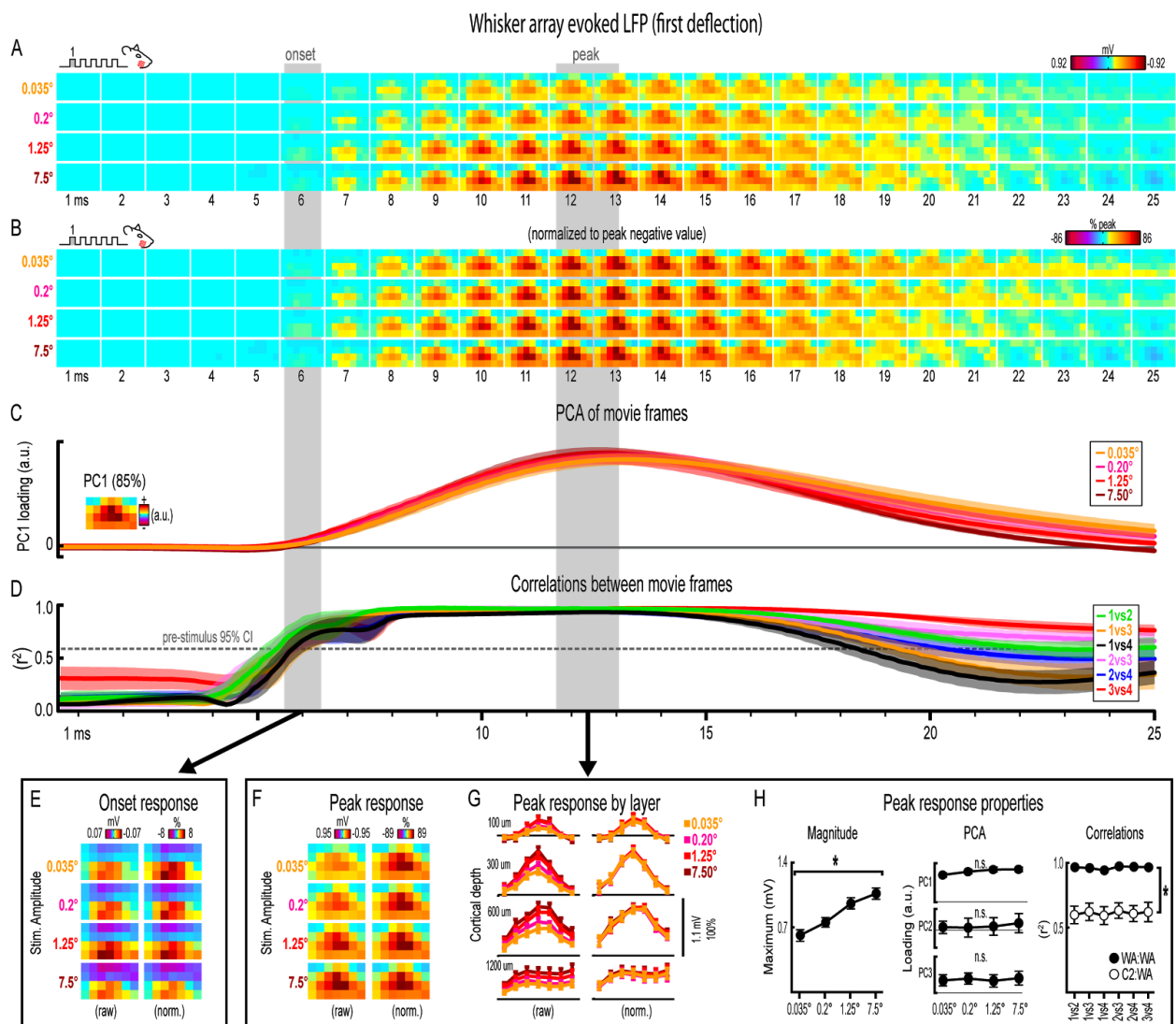


**Figure 3.5. Whisker array evoked LFP for the first deflection. (A-B)** Raw (A) and peak-normalized (B) movies of averaged ( $n=7$ ) whisker array evoked LFP for the first deflection. **(C-D)** Continuous quantification of spatial profiles with PCA loadings (D) and similarity between spatial profiles with correlations (E). Traces are mean  $\pm$  s.e.m. Gray shaded regions indicate mean onset and peak latencies ( $\pm$  s.e.m). **(E)** Raw and normalized mean onset frames. **(F-H)** Raw and normalized mean peak frames (F), broken down by layer (G), and quantification of peak response properties (H).

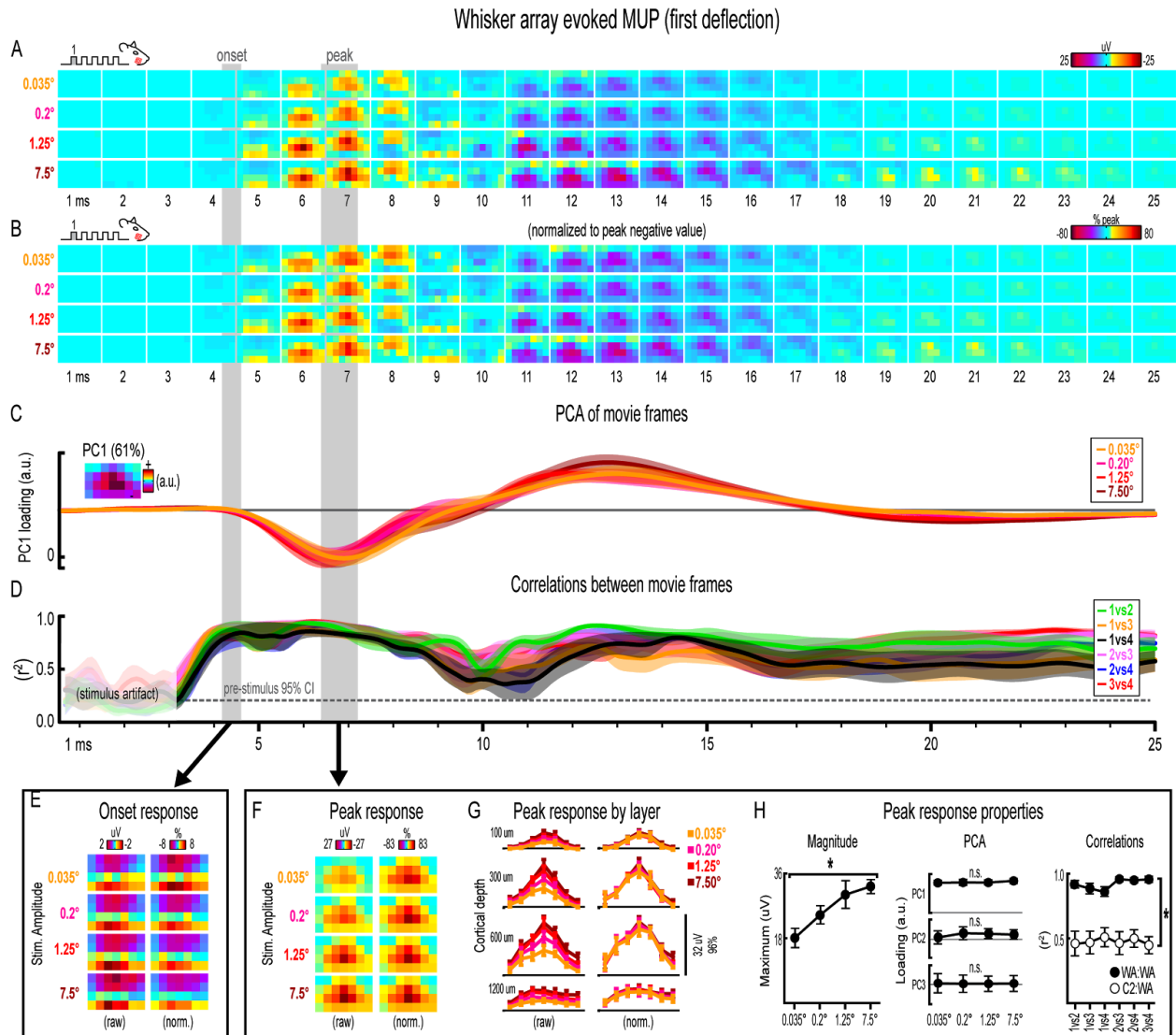


**Figure 3.6. Whisker array evoked MUP for the first deflection.** (A-B) Raw (A) and peak-normalized (B) movies of averaged ( $n=7$ ) whisker array evoked MUP for the first deflection. (C-D) Continuous quantification of spatial profiles with PCA loadings (D) and similarity between spatial profiles with correlations (E). Traces are mean  $\pm$  s.e.m. Gray shaded regions indicate mean onset and peak latencies ( $\pm$  s.e.m). (E) Raw and normalized mean onset frames. (F-H) Raw and normalized mean peak frames (F), broken down by layer (G), and quantification of peak response properties (H).

**Figure 3.5G**, note the single, central peaks of activity at all recording depths except the deepest targeted at layer 5. Supporting the observed change in response magnitude, the maximum value within peak frames was significantly different across stimulus amplitudes ( $F(3,18)=14.75$ ,  $p<0.001$ ; **Fig. 3.5H**, left). Supporting the similarity of spatial profiles, PC1, PC2, and PC3 loadings for peak frames were not significantly different across stimulus amplitudes ( $PC1$ ,  $F(3,18)=2.80$ ,  $p=0.069$ ;  $PC2$ ,  $F(3,18)=0.35$ ,  $p=0.793$ ;  $PC3$ ,  $F(3,18)=0.63$ ,  $p=0.608$ ; **Fig. 3.5H**, middle). Further supporting the similarity of spatial profiles, peak frames were also highly correlated with each other (**Fig. 3.5H**, right, closed circles; grand mean  $r^2 = 0.96 \pm <0.01$ ). Importantly, peak frames of whisker array evoked LFP were significantly less correlated with peak frames of *single whisker* evoked LFP (**Fig. 3.5H**, right, open circles; grand mean  $r^2 = 0.62 \pm 0.06$ ;  $F(1,5)=3,447.61$ ,  $p<0.001$ ; for peak frames of single whisker evoked LFP see **Fig. 3.3F**), again indicating that correlations were sensitive to even subtle changes in profiles of activity.

Results for whisker array evoked LFP for the first deflection again suggested that major changes in stimulus amplitude (up to > 200 fold) affected the magnitude but not the spatiotemporal profile of neuronal ensemble activity, but this time for the more complex whisker array stimulation involving all 24 large whiskers evoking a distinct pattern of sensory integration.

#### *Invariance in whisker array evoked MUP for the first deflection*

Movies of whisker array evoked MUP for the first of five deflections and their quantification are shown in **Figure 3.6**. The exact same analyses used before were repeated and are summarized briefly below. Note again the tendency of spatial profiles to be characterized by a single, central peak of activity at superficial recording depths targeted at layers 1, 2/3, and 4 but not the deepest targeted at layer 5. All analyses of peak MUP responses again focused on the earlier negative peak. Similar to before, major changes in stimulus

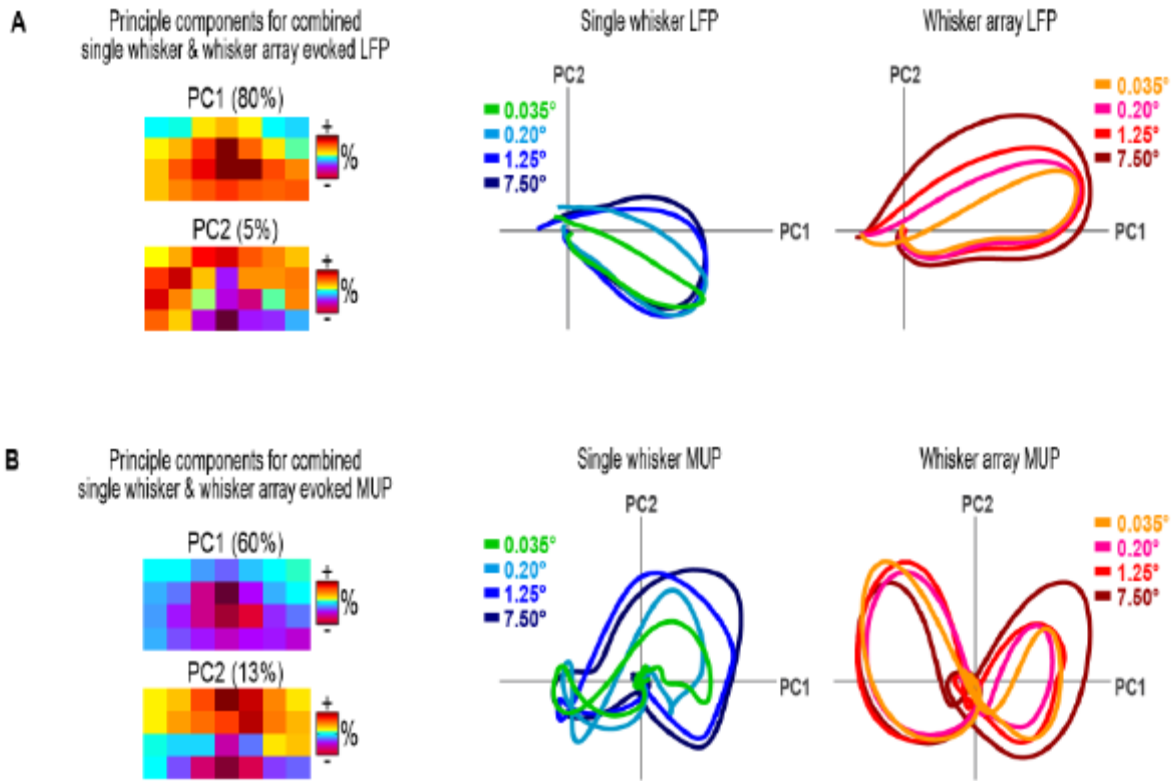


**Figure 3.7. PCA visualizes differences between single whisker and whisker array evoked activity.** PCA was performed on a combined data set with both single whisker and whisker array evoked LFP (A) and MUP (B). Mean PC loadings (n=6), connected in chronological order for each condition, are plotted. In each data set, note that paths for single whisker vs whisker array conditions showed characteristic differences (e.g., in B peanut shaped path only occurs for whisker array conditions). For each data set, the exact same axes are used for single whisker and whisker array results which were separated for the sake of clarity.

amplitude (up to > 200 fold) again affected the magnitude but *not* the spatiotemporal profile of whisker array evoked MUP.

Mean whisker array evoked MUP (n=7) for the first deflection increased in magnitude with increasing stimulus amplitude (**Fig. 3.6A**), had notably similar spatiotemporal profiles as revealed by normalizing to peak values (**Fig. 3.6B**), and included evoked activity >3 standard deviations above pre-stimulus data across the entire field of view (**Fig. 3.10F**). Continuous

quantitative measures further supported the finding of similar spatiotemporal profiles across stimulus amplitudes. For PCA (**Fig. 3.6C**), PC1 explained 61% of the variance with PC2 and PC3 explaining only 16% and 7%, respectively. Traces of mean PC1 loadings for each stimulus amplitude were again highly overlapping, even during transitions between negative and positive MUP phases. For correlations between frames of evoked MUP (**Fig. 3.6D**), mean  $r^2$  values for all stimulus amplitude comparisons rose above the 95% pre-stimulus confidence interval just before onset latencies and were highest during peak negative and peak positive responses. Together, continuous qualitative and quantitative measures suggested highly similar spatiotemporal profiles of whisker array evoked MUP for the first deflection were maintained despite major changes in stimulus amplitude.

Onset and peak frames of whisker array evoked MUP for the first deflection were again inspected more closely. Onset and peak latencies were  $4.4 \pm 0.2$  ms and  $6.8 \pm 0.4$  ms on average (shaded regions in **Fig. 3.6**; see **Table 3.1** for details). Onset frames of evoked MUP (**Fig. 3.6E**) had strongly positive voltages in the two most superficial depths and neutral or negative voltages in the two deepest depths for each stimulus amplitude. Peak frames of evoked MUP (**Fig. 3.6F-H**) again demonstrated changes in response magnitude but not spatial profile. In **Figure 3.6G**, again note the single, central peaks of activity at all recording depths except the deepest targeted at layer 5. Supporting the observed change in response magnitude, the maximum value within peak frames was significantly different across stimulus amplitudes ( $F(3,18)=11.74$ ,  $p<0.001$ ; **Fig. 3.6H**, left). Supporting the similarity of spatial profiles, PC1, PC2, and PC3 loadings were not significantly different across stimulus amplitudes ( $PC1$ ,  $F(3,18)=1.36$ ,  $p=0.287$ ;  $PC2$ ,  $F(3,18)=0.68$ ,  $p=0.579$ ;  $PC3$ ,  $F(3,18)=0.25$ ,  $p=0.859$ ; **Fig. 3.6H**, middle). Further supporting the similarity of spatial profiles, peak frames of whisker array evoked MUP were also highly correlated with each other (**Fig. 3.6H**, right, closed circles; grand mean  $r^2$

=  $0.92 \pm 0.02$ ). Importantly, peak frames of whisker array evoked MUP were significantly less correlated with peak frames of *single whisker* evoked MUP (**Fig. 3.6H**, right, open circles; grand mean  $r^2 = 0.51 \pm 0.06$ ;  $F(1,5) = 65.84$ ,  $p = 0.001$ ; for peak frames of single whisker evoked MUP see **Fig. 3.4F**), again indicating that correlations were sensitive to even subtle changes in profiles of activity.

Together, results for the first single whisker and whisker array deflection suggest that major changes in whisker stimulus amplitude (up to > 200 fold) had a significant effect on the magnitude but not spatiotemporal profile of evoked activity. This finding held for the relatively simple deflection of a single, central whisker (C2) and for the more complex whisker array stimulation involving simultaneous stimulation of all 24 large whiskers. The similarity in profiles of activity was supported by highly sensitive quantitative measures that despite failing to detect differences across stimulus amplitudes could detect differences between two similar whisker stimuli- namely single whisker and whisker array responses both characterized by a single, central peak of activity. Correlation results consistently passed this sensitivity test. PCA also seemed to pass this sensitivity test when performed on a combined data set including both single whisker and whisker array responses (**Fig. 3.7**). Overall, results for the first single whisker and whisker array deflection suggested that major changes in stimulus amplitude systematically affected the magnitude of evoked activity but did not produce any substantial changes in the profile of evoked activity.

#### *Invariance during repeated whisker deflections*

Rodents explore their environment with repetitive, simultaneous movement of their

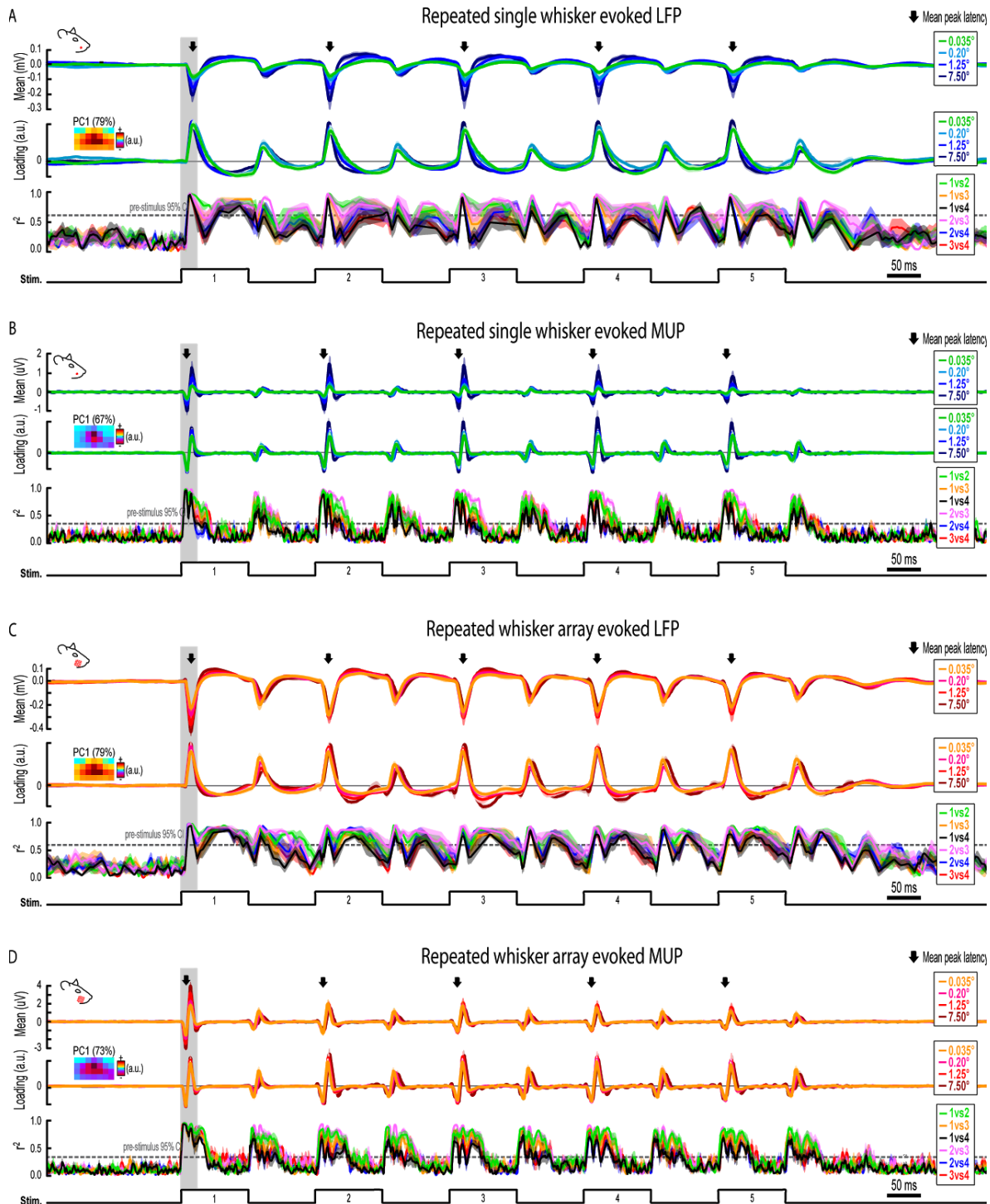


**Figure 3.8. Continuous quantification of evoked LFP and MUP for repeated whisker deflections. (A)** Continuous quantification of the magnitude (top panel), spatial profile (middle panel), and similarity of spatial profiles (bottom panel) for single whisker evoked LFP. **(B-D)** Same data as (A) but for single whisker evoked MUP (B), whisker array evoked LFP (C), and whisker array evoked MUP (D). Note the much larger time window (~2 sec) compared to previous figures. *Arrows indicate mean latencies of peak frames of evoked activity which are further analyzed in Figure 8. All traces indicate mean +/- s.e.m.*

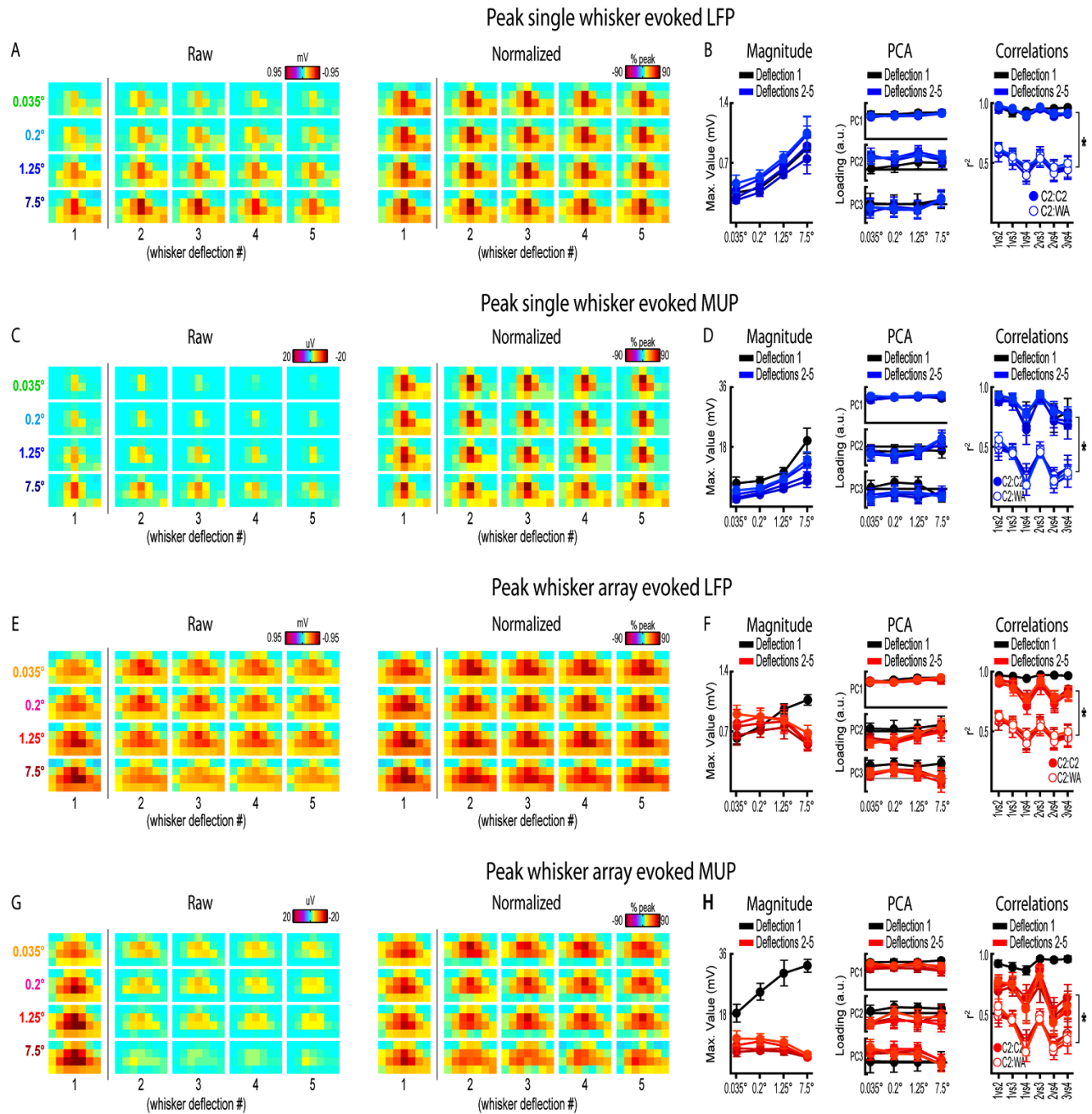


**Figure 3.9. Peak frames of activity for repeated whisker deflections.** Mean peak frames and quantification of peak response properties for single whisker evoked LFP (A,B), single whisker evoked MUP (C,D), whisker array evoked LFP (E,F), and whisker array evoked MUP (G,H) for repeated whisker deflections. *Results from the first deflection are plotted for comparison.*

whiskers. It was therefore important to determine if results from the first deflection, analogous to a single deflection of the whisker(s), extended to repeated whisker deflections 2-5. A similar set of analyses were performed on results during repeated whisker deflections with a few important differences. Now, a larger time window (-0.2 sec to 1.2 sec post-stimulus onset) was used that included all 5 whisker deflections of the 5 Hz stimulation. For each movie, the mean magnitude within each frame of activity was calculated and continuously plotted (**Fig. 3.8A-D**, top panels). Similar to before, mean PC1 loadings and mean  $r^2$  values for all possible stimulus amplitude comparisons were continuously plotted (**Fig. 3.8A-D**, middle and bottom panels, respectively). The gray shaded regions in **Figure 3.8** correspond to the 25 ms time window used for analysis of the first deflection (see **Fig. 3.3-3.6**). Arrows in **Figure 3.8** indicate time of peak responses (mean negative peak latency within 50 ms of stimulus onset for each deflection; see **Table 3.1** for details). All further analyses focused on peak frames of evoked activity (**Fig. 3.8**).

Repeated single whisker deflections 2-5 continued to evoke LFP and MUP that increased in magnitude with increasing stimulus amplitude but did not have major changes in its spatiotemporal profile (**Fig. 3.9A-D**). The maximum value within peak frames was significantly different across stimulus amplitudes (*LFP*, **Fig. 3.9B**, left,  $F(3,15)=8.43$ ,  $p=0.002$ ; *MUP*, **Fig. 3.9D**, left,  $F(3,15)=8.29$ ,  $p=0.002$ ). The spatial profile of peak frames did not change noticeably across stimulus amplitudes (**Fig. 3.9A,C**, right). For PCA results, PC1 explained a majority of variance (79% for LFP and 67% for MUP), with PC2 and PC3 again explaining much less of the variance (between 5-11%). No significant differences in PC1, PC2, or PC3 loadings for LFP or MUP data were found across stimulus amplitudes *except* for PC3 for LFP which explained only 5% of the variance ( $F(3,15)=23.21$ ,  $p<0.001$ ; **Fig. 3.9B**, 'PC3' in middle panel) and PC2 for MUP which explained only 11% of the variance ( $F(3,15)=3.53$ ,  $p=0.041$ ; **Fig. 3.9D**, 'PC2' in middle panel), and overall no major differences in spatial profiles were noticeable (see **Fig. 3.9A** and

**3.9C**, right). Peak frames were well correlated with each other (LFP,  $r^2 = 0.94 \pm 0.01$ ; MUP,  $r^2 = 0.82 \pm 0.03$ ; grand mean of comparisons, deflections, and subjects) and were significantly less correlated with peak frames of *whisker array* evoked activity (LFP,  $r^2 = 0.51 \pm 0.05$ ,  $F(1,5)=132.05$ ,  $p<0.001$ , **Fig. 3.9B**, right; MUP,  $r^2 = 0.36 \pm 0.04$ ,  $F(1,5)=142.00$ ,  $p<0.001$ , **Fig. 3.9D**, right). These data suggest that stimulus amplitude continued to affect the magnitude but not the spatiotemporal profile of evoked LFP and MUP for repeated single whisker deflections.

In contrast to all previous results, repeated whisker array deflections evoked LFP and MUP that did not increase in magnitude despite major increases in stimulus amplitude (up to >200 fold; **Fig. 3.9E,G**, left). There were still some significant differences in the maximum value within peak frames (LFP, **Fig. 3.9F**, left,  $F(3,18)=3.33$ ,  $p<0.043$ ; MUP, **Fig. 3.9H**, left,  $F(3,18)=4.47$ ,  $p=0.016$ ), however all post-hoc tests were not significant (*all*  $F(1,6)<15$ , *all*  $p>0.008$ , *Bonferroni correction for 6 comparisons*). If anything, the *largest* stimulus amplitude appeared to evoke the *weakest* response magnitudes (**Fig. 3.9F-H**, left, red lines). Similar to previous results, the spatial profile of peak frames did not show any major changes across stimulus amplitudes (**Fig. 3.9E,G**, right). For PCA results, PC1 again explained the majority of variance (79% for LFP and 73% for MUP) with PC2 and PC3 again explaining much less of the variance (between 4-8%). No significant differences in PC1, PC2, or PC3 loadings for LFP or MUP data were found across stimulus amplitudes *except* for PC2 for LFP which explained only 6% of variance ( $F(3,18)=5.76$ ,  $p=0.006$ ; **Fig. 3.9F**, 'PC2' in middle panel) and PC3 for MUP which explained only 6% of variance ( $F(3,18)=5.28$ ,  $p=0.009$ ; **Fig. 3.9H**, 'PC3' in middle panel), and overall no major differences in spatial profiles were noticeable (see **Fig. 3.9E** and **9G**, right). Peak frames were well correlated with each other (LFP,  $r^2 = 0.84 \pm 0.04$ ; MUP,  $r^2 = 0.65 \pm 0.05$ ; grand mean of comparisons, deflections, and subjects) and were significantly less correlated with peak frames of *single whisker* evoked activity (LFP,  $r^2 = 0.51 \pm 0.05$ ,  $F(1,5)=60.07$ ,

$p=0.001$ , **Fig. 3.9F**, right; MUP,  $r^2 = 0.36 \pm 0.04$ ,  $F(1,5)=46.98$ ,  $p=0.001$ , **Fig. 3.9H**). These data suggest that the spatiotemporal profile of whisker array evoked LFP and MUP continued to be relatively invariant to even major changes in stimulus amplitude during repeated deflections. Further, in contrast to all previous results, these data also suggest that the absolute magnitude of whisker array evoked LFP and MUP may also become invariant to stimulus amplitude for repeated deflections.

Results from repeated whisker deflections indicate that the spatiotemporal profile of neuronal ensemble activity in rat barrel cortex continued to be notably invariant to even major changes in stimulus amplitude (up to >200 fold). The absolute magnitude of responses, however, consistently increased with increasing stimulus amplitude except, notably, for the more naturalistic repeated deflections of the whisker array.

#### *Whisker array responses faster, less variable across subjects*

Two main differences between single whisker and whisker array responses were observed. First, whisker array responses were faster than single whisker responses. LFP onset latencies were significantly faster for whisker array compared to single whisker conditions (*paired t-test of mean onset latencies for all stimulus amplitudes*,  $t(5)=5.76$ ,  $p=0.002$ ; see **Supp. Table 1** for all latency values). LFP peak latencies were faster for whisker array compared to single whisker but not significantly so (*paired t-test of mean peak latencies for all stimulus amplitudes*,  $t(5)=2.37$ ,  $p=0.064$ ). MUP onset and peak latencies were both significantly faster for whisker array compared to single whisker (*paired t-tests of mean onset and peak latencies; MUP onset latency*,  $t(5)=5.61$ ,  $p=0.003$ ; *MUP peak latency*,  $t(5)=4.59$ ,  $p=0.006$ ).

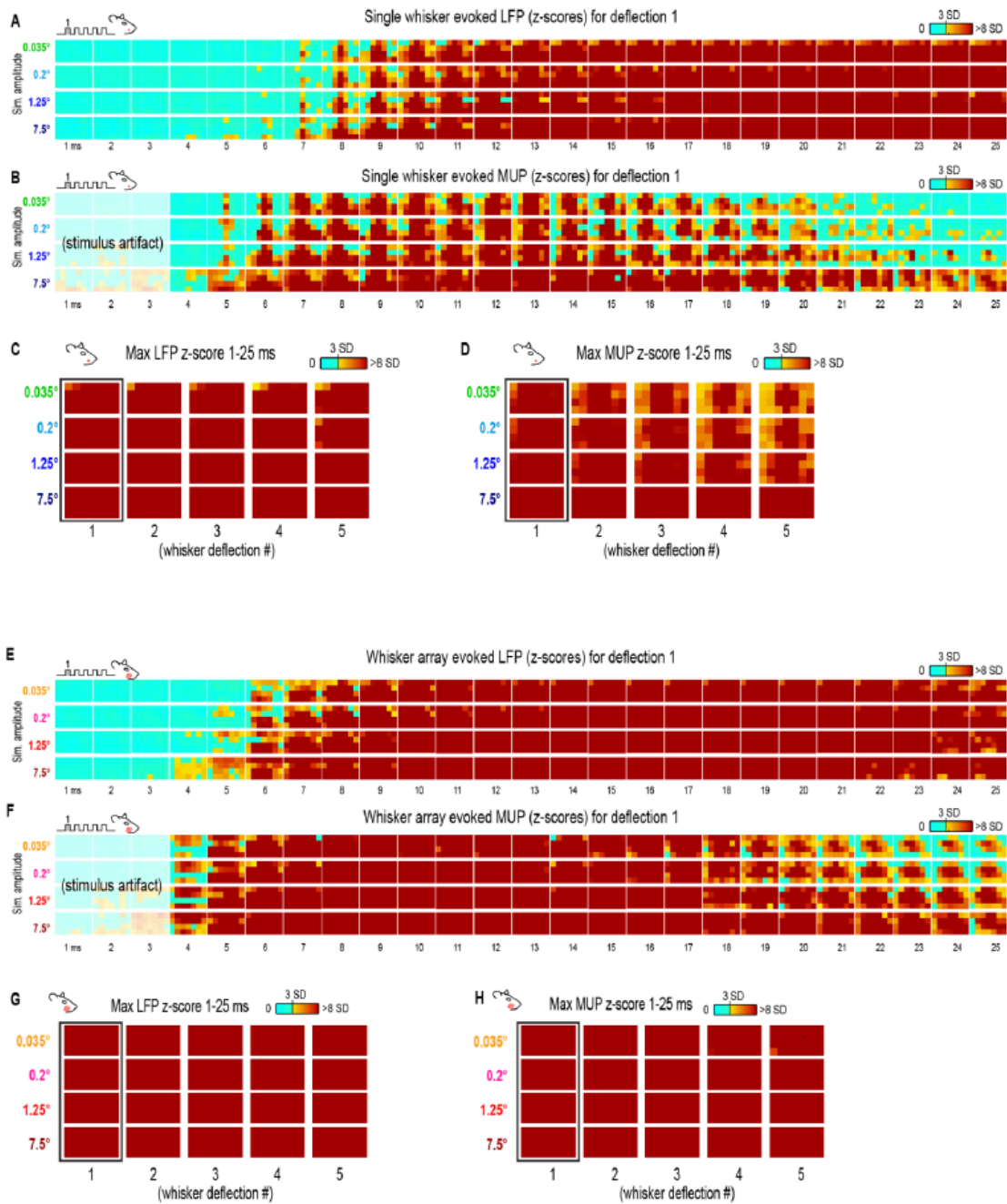


**Figure 3.10. Whisker stimulation engages entire mesoscopic field of view for each stimulus amplitude.** (A, B) Z-scores were calculated for raw single whisker evoked LFP and MUP at each recording location by dividing by the standard deviation of voltages during the 50 ms period before stimulus onset. Note that evoked LFP and MUP can be detected (> 3 standard deviations above pre-stimulus data, warm colors in images) throughout the entire mesoscopic field of view. (C, D) For each recording location, the maximum z-score within the 25 ms of stimulus onset (50 ms for deflections 2-5 since peak latencies tended to be delayed slightly) was calculated. Results for deflection 1, detailed in (A,B), are framed. (E-H) Same as (A-D) but for whisker array data.

In general, the onset latencies for trial averaged MUP data were consistent but at the low end of previously reported latencies in barrel cortex using spike timestamps (e.g., Armstrong-James et al., 1992). The shorter latencies in trial averaged MUP could be explained by increased sensitivity to small amplitude signals which are necessarily excluded in thresholded data used for spike detection. Contributions from small amplitude signals could originate from: the rising phase of action potentials, action potentials from smaller cells such as spiny stellate cells, and synchronized activation of thalamocortical afferents (Kandel and Buzsáki, 1997; for detailed review of origins of extra-cellular currents see Buzsaki et al., 2012).

The second main difference between single whisker and whisker array responses was that maximum response magnitudes were less variable across subjects for the first whisker array deflection. The coefficient of variance (COV, standard deviation divided by mean) for whisker array evoked LFP for the first deflection was 0.19 (mean COV for all stimulus amplitudes), 34% lower than the COV for single whisker evoked LFP for the first deflection which was 0.29. The COV for whisker array evoked MUP for the first deflection was 0.28, 45% lower than the COV for single whisker evoked MUP for the first deflection which was 0.51. For repeated deflections, COVs were not consistently different between single whisker and whisker array conditions.

## **Discussion**

The current research investigated invariance in large, spatially organized neuronal ensembles of rat barrel cortex. Several methods used here (e.g., combined analysis of continuous multi-site recordings) enabled direct comparison of spatial profiles of evoked activity with high temporal resolution over relatively long periods of time. We found that neuronal ensemble activity has a remarkable capacity for spatiotemporal invariance. Such

ensemble-based spatiotemporal invariance was found for a single whisker stimulus as well as for a more complex whisker array stimulus involving many whiskers and a distinct pattern of sensory integration.

### *Emerging invariance in neuronal ensembles*

Neuronal invariance is typically studied at the level of single neurons, which in “higher” sensory cortices can invariantly respond to abstract sensory information such as objects or items (Sáry et al., 1993; Lueschow et al., 1994; Li and DiCarlo, 2008; Rust and DiCarlo, 2010). In primary sensory cortices invariance has been observed in more nuanced aspects of individual neuron responses such as the width of tuning curves (Anderson et al., 2000; Sadagopan and Wang, 2008), yet very little is known about invariance at the neuronal ensemble level in primary sensory cortex.

Here we analyzed a special case of neuronal ensemble: the ‘point spread’, which describes the rapid lateral spread of evoked activity following point sensory stimulation (e.g., whisker). Point spreads are ubiquitous in sensory cortex (somatosensory, auditory, and visual) ranging from mice and rats to cats and monkeys and are found in both anesthetized and awake behaving animals (Grinvald et al., 1994; Barth et al., 1995; Das and Gilbert, 1995; Bakin et al., 1996; Binguier et al., 1999; Brett-Green et al., 2001; Kaur et al., 2005; Roland et al., 2006; Ferezou et al., 2006, 2007; Sharon et al., 2007; Frostig et al., 2008; Chen-Bee et al., 2012; Mohajerani et al., 2013). Interestingly, multiple simultaneous point spreads propagating through presumably overlapping neuronal ensembles have been shown to summate (Chen-Bee et al., 2012; Gao et al., 2012). A potential criticism of studying point spreads in the anesthetized preparation is that anesthesia may result in unnaturally large point spreads. However, this does not seem to be the case as single whisker evoked point spreads in barrel cortex are equally as

large or larger in awake versus anesthetized rodents (Ferezou et al., 2006). Point spreads in the rat barrel cortex are supported by an underlying system of long-range horizontal projections (e.g., Frostig et al. 2008; Stheberg et al. 2014). Why are point-spreads so ubiquitous, especially in light of the expensive metabolic support that cortex has to invest in order to maintain them?

We have previously shown, using stimulus amplitude comparable to the largest stimulus amplitude in the current study, that single whiskers stimulation evokes point spreads that have a considerable degree of spatial overlap even for topographically distant whiskers (Chen-Bee et al., 2012). Importantly, summation of these overlapping point spread accurately predicts a single peak of evoked activity following simultaneous stimulation of all 24 large whiskers (Chen-Bee et al., 2012); and therefore point spreads could be described as a “building block” of integrated cortical activity. Here we expand the importance of point spreads by demonstrating their spatiotemporal invariance. Specifically, spatiotemporal profiles of single whisker evoked activity were notably invariant despite major changes in whisker stimulus amplitude that exceeded 200 fold differences. Further, we reasoned that if point-spreads are indeed building blocks of cortical integrated activity, then this spatiotemporal invariance should also extend to the patterns of multi-point integration they construct. Indeed, a similar degree of spatiotemporal invariance was also found for whisker array evoked neuronal ensemble activity across the same major changes in stimulus amplitude. These findings therefore seem to generalize the critical role of interactions among single whisker evoked point spreads across a wide range of ethologically relevant whisker stimulus amplitudes. Taken together, the building block function and its invariance suggest that point spreads should be considered as important players in cortical functional organization.

The ensemble-based invariance reported here also demonstrates how emergent properties of large neuronal ensembles (e.g., the relative profile of activity across constituent

neurons in the ensemble) can be independent of absolute response magnitude. Sensory coding independent of response magnitude may allow simultaneous coding of stimulus intensity (e.g., stimulus amplitude) and other more nuanced stimulus features (e.g., texture). Such simultaneous sensory coding could help explain why stimulus intensity often does not affect recognition of specific objects or items.

We further suggest that in primary sensory cortices ensemble-based invariance may be more biologically relevant than invariance at the individual neuron level (**Appendix B**). Invariant response features do exist at the individual neuron level in primary sensory cortex (e.g. the tuning curve widths mentioned earlier), but require comparing responses occurring at different times and to different stimuli thus raising important questions about how exactly this information could be used in real time (Quiroga and Panzeri, 2009). In contrast, the ensemble-based invariance described here relies on emergent response features (e.g. the relative profile of activity) that can be used in real-time presumably by so called “reader” cells in downstream cortical areas (Buzsáki, 2010). Combined with the current findings, these observations strongly suggest that neuronal ensembles are not only capable of a remarkable degree of invariance but, given their emergent response properties which allow for continuous, magnitude-independent sensory coding, appear better designed to perform this function than individual neurons.

#### *Habituation during repeated whisker array deflections*

Interestingly it seems that for the more naturalistic stimulation, repeated deflections of the entire whisker array, an additional level of neuronal invariance may occur in the absolute magnitude of responses. In a study of single unit responses in barrel cortex, it was reported that increasing the *frequency* of repeated whisker array deflections increases response magnitude (Mowery et al., 2011). Surprisingly, the current results suggest that this is not the case for

stimulus amplitude. We found that repeated whisker array deflections (ie, beyond the first stimulation) seemed to equilibrate absolute response magnitudes for each stimulus amplitude. The same equilibration of response magnitudes was not observed for repeated single whisker deflections, suggesting that the underlying mechanism may be specific to simultaneous stimulation of many whiskers. These findings, together with noticeable differences in response latencies between the first and repeated deflections (see **Table 3.1**) and known adaptation of responses in the rodent somatosensory system (Chung et al., 2002; Katz et al., 2006; Temereanca et al., 2008), suggest distinct differences in sensory coding for repeated whisker array deflections.

#### *Relevance to funneled tactile perception*

It has been previously established that the spread of subthreshold evoked activity in the anesthetized sensory cortex could serve as a correlate of perceptual phenomenon (Jancke et al., 2004). Could our findings also relate to tactile perception?

The single, central peak of evoked cortical activity observed after simultaneous stimulation of two or more adjacent points in the periphery has been suggested as the underlying neuronal correlate of ‘funneled’ tactile perception (Chen et al., 2003; Chen-Bee et al., 2012) originally described by Georg von Békésy (Békésy, 1957, 1958, 1959, 1967). Békésy and colleagues demonstrated that multiple oscillating tactile stimuli applied simultaneously at several discrete skin sites are perceived as a *single* central stimulus, rather than as multiple points, leading him to describe the altered spatial profile of the perceived stimulus as being ‘funneled’ into the central stimulus location.

The current findings show that a similarly ‘funneled’ spatial profile of evoked activity in barrel cortex is invariant across a wide range of ethologically relevant whisker stimulus

amplitudes, matching original observations that funneled tactile perception is amplitude-invariant (Békésy, 1959). These results further strengthen our previous suggestion that the integrated, spatial profile of evoked cortical activity following simultaneous multi-point stimulation could serve as the underlying neuronal correlate of funneled tactile perception. The current study replicates funneled profiles of cortical activity in superficial cortical layers (targeted at layers 1-4). However, funneled responses were not observed in deeper cortical layers (targeted at layer 5), possibly due to differences in the spatial organization of whisker evoked activity in infragranular layers of barrel cortex as compared to the other cortical layers (Armstrong-James, 1992; Sakata and Harris, 2009).

Similar to funneled tactile perception in humans which improves response latencies (Hashimoto et al., 1999), it is possible that simultaneous stimulation of multiple adjacent whiskers in the rat is perceived as a single highly responsive “super whisker” facilitating neuronal and behavioral responses that are faster, more reliable, and less variable. Consistent with this notion, improved tactile discrimination accuracy and faster behavioral response latencies have been associated with simultaneous multi-whisker stimulation in rodents (Celikel and Sakmann, 2007). Furthermore, decreased variability in neuronal responses in barrel cortex has also been associated with whisker array stimulation (Chen-Bee et al., 2012). Here we also report that neuronal responses in barrel cortex were also significantly faster for whisker array stimulation.

Summarizing the relationship to funneled tactile perception, evoked cortical activity in barrel cortex has a matching spatial profile, has similar latency and variability improvements compared to single point stimuli, and is also invariant to stimulus amplitude at the neuronal ensemble level. Further research can now be pursued to determine whether the emergence of invariance within large, spatially organized neuronal ensembles can be generalized to other

stimulus parameters and other sensory cortical areas.

**Table 3.1. Onset and peak latencies of whisker evoked LFP and MUP.** Mean latencies ( $\pm$  s.e.m) for each stimulus amplitude, whisker stimulus type, and whisker deflection number. Grand means across stimulus amplitudes are bolded.

Single whisker response latencies						
	Onset Latency <i>Deflection 1</i> (ms)	<i>Deflection 1</i> (ms)	<i>Deflection 2</i> (ms)	Peak Latency <i>Deflection 3</i> (ms)	<i>Deflection 4</i> (ms)	<i>Deflection 5</i> (ms)
LFP						
<b>Mean</b>	<b>7.6 <math>\pm</math> 0.4</b>	<b>14.2 <math>\pm</math> 0.6</b>	<b>19.2 <math>\pm</math> 0.9</b>	<b>19.7 <math>\pm</math> 0.9</b>	<b>19.6 <math>\pm</math> 0.9</b>	<b>19.7 <math>\pm</math> 1.0</b>
0.035°	8.0 $\pm$ 0.7	14.4 $\pm$ 1.0	20.5 $\pm$ 1.4	20.5 $\pm$ 1.4	20.3 $\pm$ 1.3	20.3 $\pm$ 1.5
0.2°	7.9 $\pm$ 0.5	14.6 $\pm$ 0.7	19.7 $\pm$ 1.0	20.1 $\pm$ 1.0	20.0 $\pm$ 1.0	20.1 $\pm$ 1.1
1.25°	7.4 $\pm$ 0.3	14.1 $\pm$ 0.5	19.5 $\pm$ 1.1	20.0 $\pm$ 1.1	19.8 $\pm$ 1.0	19.9 $\pm$ 1.1
7.5°	7.2 $\pm$ 0.4	13.6 $\pm$ 0.6	17.8 $\pm$ 0.6	18.4 $\pm$ 0.5	18.4 $\pm$ 0.6	18.5 $\pm$ 0.7
MUP						
<b>Mean</b>	<b>5.6 <math>\pm</math> 0.4</b>	<b>8.1 <math>\pm</math> 0.5</b>	<b>13.6 <math>\pm</math> 0.5</b>	<b>14.0 <math>\pm</math> 0.5</b>	<b>14.0 <math>\pm</math> 0.5</b>	<b>13.7 <math>\pm</math> 0.6</b>
0.035°	5.9 $\pm$ 0.4	8.0 $\pm$ 0.2	13.6 $\pm$ 0.7	13.8 $\pm$ 0.9	14.0 $\pm$ 0.8	13.8 $\pm$ 0.8
0.2°	5.7 $\pm$ 0.4	8.2 $\pm$ 0.3	13.7 $\pm$ 0.6	14.2 $\pm$ 0.5	14.0 $\pm$ 0.6	13.8 $\pm$ 0.6
1.25°	5.6 $\pm$ 0.3	7.7 $\pm$ 0.2	13.8 $\pm$ 0.5	14.4 $\pm$ 0.6	14.2 $\pm$ 0.5	13.7 $\pm$ 0.7
7.5°	5.1 $\pm$ 0.4	8.4 $\pm$ 0.2	13.3 $\pm$ 0.4	13.7 $\pm$ 0.4	13.7 $\pm$ 0.4	13.5 $\pm$ 0.5

Whisker array response latencies						
	Onset Latency <i>Deflection 1</i> (ms)	<i>Deflection 1</i> (ms)	<i>Deflection 2</i> (ms)	Peak Latency <i>Deflection 3</i> (ms)	<i>Deflection 4</i> (ms)	<i>Deflection 5</i> (ms)
LFP						
<b>Mean</b>	<b>6.0 <math>\pm</math> 0.4</b>	<b>12.3 <math>\pm</math> 0.6</b>	<b>18.0 <math>\pm</math> 0.7</b>	<b>18.2 <math>\pm</math> 0.7</b>	<b>18.1 <math>\pm</math> 0.7</b>	<b>17.7 <math>\pm</math> 1.0</b>
0.035°	6.4 $\pm$ 0.4	12.9 $\pm$ 0.8	17.4 $\pm$ 0.9	17.8 $\pm$ 0.7	18.0 $\pm$ 0.7	17.8 $\pm$ 0.8
0.2°	6.1 $\pm$ 0.3	12.3 $\pm$ 0.7	17.2 $\pm$ 0.8	17.9 $\pm$ 0.8	17.7 $\pm$ 0.9	17.3 $\pm$ 1.0
1.25°	5.9 $\pm$ 0.3	12.2 $\pm$ 0.6	17.5 $\pm$ 0.8	18.0 $\pm$ 0.9	18.1 $\pm$ 0.9	17.5 $\pm$ 1.2
7.5°	5.8 $\pm$ 0.5	11.9 $\pm$ 0.5	20.1 $\pm$ 0.7	19.1 $\pm$ 0.6	18.8 $\pm$ 0.8	18.4 $\pm$ 1.2
MUP						
<b>Mean</b>	<b>4.4 <math>\pm</math> 0.2</b>	<b>6.8 <math>\pm</math> 0.4</b>	<b>12.2 <math>\pm</math> 0.3</b>	<b>12.5 <math>\pm</math> 0.4</b>	<b>12.3 <math>\pm</math> 0.4</b>	<b>12.1 <math>\pm</math> 0.4</b>
0.035°	4.7 $\pm$ 0.3	6.9 $\pm$ 0.2	12.1 $\pm$ 0.6	12.3 $\pm$ 0.5	12.2 $\pm$ 0.5	12.1 $\pm$ 0.4
0.2°	4.6 $\pm$ 0.3	6.9 $\pm$ 0.1	11.5 $\pm$ 0.6	12.2 $\pm$ 0.6	11.9 $\pm$ 0.7	11.9 $\pm$ 0.6
1.25°	4.2 $\pm$ 0.1	6.7 $\pm$ 0.1	11.8 $\pm$ 0.3	12.4 $\pm$ 0.6	12.1 $\pm$ 0.6	12.1 $\pm$ 0.5
7.5°	4.2 $\pm$ 0.1	6.9 $\pm$ 0.1	13.2 $\pm$ 0.6	13.3 $\pm$ 0.4	12.8 $\pm$ 0.5	12.4 $\pm$ 0.4

## **CHAPTER 4: Blocking the spread of evoked activity constrains pattern of sensory induced protection from ischemic attack**

### *Summary*

Previous research has shown that tactile or auditory stimulation started within 2 hours of permanent MCA occlusion (pMCAO) in rats increases collateral blood flow, re-establishes cortical function, and prevents any tissue infarction from developing within MCA territory (for review see Frostig et al., 2013). Importantly, complete sensory-induced protection occurs even for discrete stimuli which, under traditional dogma, only activate spatially restricted cortical regions. How can stimulation of a specific area confer protection to the entire ischemic MCA territory? One hypothesis is that spatially restricted cortical activation broadly increases collateral blood flow within the larger MCA territory and is sufficient for complete protection. An alternative hypothesis is that the lateral spread of sensory-evoked activity, which extends throughout MCA territory via intracortical projection fibers, is also necessary for protection. To test these two hypotheses we used gray matter transection to dissociate the effects of collateral blood flow and evoked activity spread. We found that cortical regions beyond the transection and thus not activated by evoked activity spread suffered functional losses not present in cortical regions before the transection. These results suggest that cortical activation and its substantial lateral spread through cortex is directly involved in the mechanism of sensory induced protection from ischemic stroke.

### *Key points*

1. Sensory stimulation completely protects cortex from impending ischemic stroke.
2. Blocking spread of evoked cortical activity (but leaving collateral blood flow intact)

removes sensory-induced protection from areas without evoked cortical activity.

3. Neuronal activity itself may play a direct role in mechanism of sensory-induced protection from ischemic stroke.

*Reference:*

*Manuscript in preparation.* Lay\*, C, Jacobs\*, NS, Davis, MF, Frostig, RD (2015) Blocking the spread of evoked activity constrains pattern of sensory induced protection from ischemic attack.

\*both authors contributed equally to this work.

## Introduction

Previous research in our lab using a rodent model of ischemic stroke (permanent middle cerebral artery occlusion; pMCAO), has shown that tactile or auditory stimulation, can initiate reperfusion through collateral vessels and can confer complete protection from impending stroke (Lay et al., 2010, Davis et al., 2011, Lay et al., 2011, 2012). In this model, the cortical areas protected from infarct included somatosensory and parts of motor and auditory cortex. All of these cortical areas are within MCA territory and it seems reasonable that the blood flow return, which feeds all of the listed areas, would be responsible for the observed protection. Presented in this dissertation, however, is also evidence that cortical activity resulting from stimulation treatment like that described above, plays a role in protection independent of initiating blood flow return. The clinical literature also offers evidence that blood flow return, while clearly necessary for protection from stroke, may not be sufficient for complete protection (van Mook et al., 2005, Pan et al., 2007, De Rango, 2012, Lieb et al., 2012, Chimowitz, 2013, Caplan, 2009). There is therefore sufficient reason to suppose that blood flow is not the only protective agent in sensory induced protection from ischemic stroke.

Importantly, complete sensory-induced protection occurs even for discrete stimuli which, under traditional dogma, only activate spatially restricted cortical regions. How can stimulation of a specific area confer protection to the entire ischemic MCA territory? One hypothesis is that spatially restricted cortical activation broadly increases collateral blood flow within the larger MCA territory and is sufficient for complete protection. An opposing hypothesis is that the lateral spread of sensory-evoked activity, which extends throughout MCA territory via intracortical projection fibers, is also necessary for protection.

We tested which hypothesis was correct by blocking the spread of auditory-evoked cortical activity in Oh auditory stim animals. Surgical transection of the gray matter between

primary auditory, and primary somatosensory cortices was used to prevent spread of subthreshold activity via long range cortical connections. Cortices were mapped using intrinsic signal optical imaging prior to transection and loss of activity spread was confirmed using electrophysiological recording. Animals were assessed for protection from pMCAO using intrinsic signal optical imaging, extracellular recording, and histological assessment with TTC. Blood flow at baseline and on the following day was also assessed. All animals were compared to sham controls that underwent all of the same surgical and other procedures aside from the occlusion of MCA.

The above results support our hypothesis that long range spread of auditory activity is necessary for protection from damage in the somatosensory cortex. Further, blood flow results from these experiments support our prediction that reperfusion is necessary but not always sufficient for protection from impending stroke damage. This information could be used to direct further research and may have translational potential for augmenting current reperfusion treatment in human stroke patients.

## **Materials and Methods**

All procedures were in compliance with NIH guidelines and approved by University of California Irvine Animal Care and Use Committee.

### *Subjects and surgical preparation*

Experimental subjects (295–400 g male Sprague Dawley rats) were individually housed in standard cages. At the beginning of each experiment, animals were injected intraperitoneally with a Nembutal bolus [55 mg/kg body weight (b.w.)]. Supplemental injections of Nembutal (27.5 mg/kg b.w.) were given as necessary. After resection of soft tissue, an  $\sim 6.5 \times \sim 8$  mm imaging

area of the skull over the left and right primary somatosensory cortex (rostromedial corner positioned ~1 mm caudal and 2 mm lateral from bregma) was thinned to ~150 µm using a dental drill. Five percent dextrose (3 ml) and atropine (0.05 mg/kg b.w.) were administered at the beginning of the experiment and every 6 h after until the experiment was complete. Body temperature was measured via a rectal probe, and maintained at 37°C by a self-regulating thermal blanket.

*Experimental groups:*

Auditory 0h stimulation animals (no transection): This experimental group underwent pMCAO *without* any transection of gray matter. Immediately following pMCAO, these animals received auditory stimulation. This protocol resulted in complete protection from infarct.

Unstimulated controls: This control group underwent pMCAO but never received stimulation treatment and had no transection of gray matter.

Auditory 0h stimulation transection animals: This experimental group underwent pMCAO and a transection of the gray matter between primary auditory and somatosensory cortices. (Determination of the location of these cortices was based on intrinsic signal optical imaging). Immediately following pMCAO and transection, these animals received auditory stimulation previously shown to be protective in pMCAO models when delivered at the same timepoint.

Sham pMCAO / transection animals: This control group underwent a sham pMCAO (a surgical window was opened over MCA and sutures were passed beneath the vessel but never tightened to occlude it. These animals underwent a transection of the gray matter between primary auditory and somatosensory cortices and received protective auditory stimulation immediately following sham-occlusion and transection.

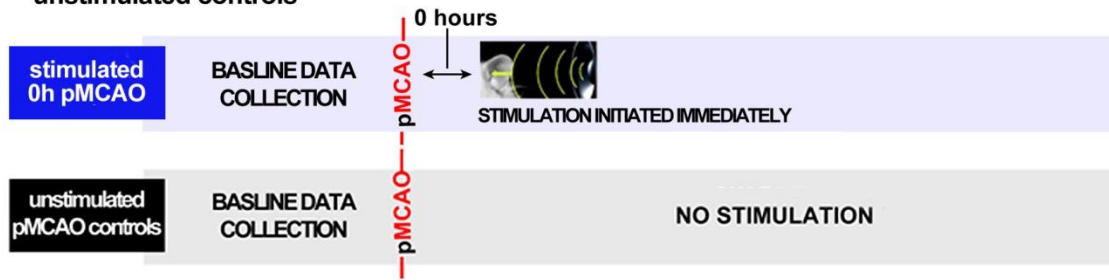
### *Permanent middle cerebral artery occlusion (pMCAO)*

Ischemic conditions were achieved via surgical occlusion and transection of the M1 segment (just distal to lenticulostriate branching) of the left middle cerebral artery such that only MCA cortical branches were affected and thus only cortical infarct (no subcortical damage) was expected (Tamura et al., 1981, Brint et al., 1988, Wang-Fischer, 2009). The skull and dura were carefully removed from a 2 × 2 mm surgical window just anterior and lateral to the imaging window (over the occlusion location) and a half-curve reverse cutting suture needle and thread (4-0 silk) was passed through the pial layer of the meninges, below MCA and above the cortical surface. A double ligature was tied and tightened around MCA and the vessel was then transected (completely severed) between the two knots. Experiments were terminated if there was any sign of bleeding from MCA or if there were obvious arterial abnormalities or malformations (Fox et al., 1993, Niuro et al., 1996, Davis MF, 2013).

### *Gray matter transection*

Gray matter transections were performed between whisker and auditory functional representations (determined via functional imaging). A 26-gauge hypodermic needle (3.4 x 1.7mm, length and depth) was marked from tip to 1.65mm from tip such that the first 1.65mm of the needle was colored. The needle was then bent at the 1.65mm point and used to transect the gray matter by inserting the needle into the cortex up to the 1.65mm point (corresponding to the depth of the cortex) and cutting a line between the cortices. If larger vasculature was encountered, the needle was removed and inserted again on the other side of the vessel to avoid bleeding problems. Very minimal bleeding occurred in a small subset of animals. Transection location and depth was confirmed during histological assessment.

**A Schematic of experimental design for 0h pMCAO auditory stimulation animals and unstimulated controls**



**B Auditory stimulation delivered immediately post-pMCAO protects from infarct seen in unstimulated controls**

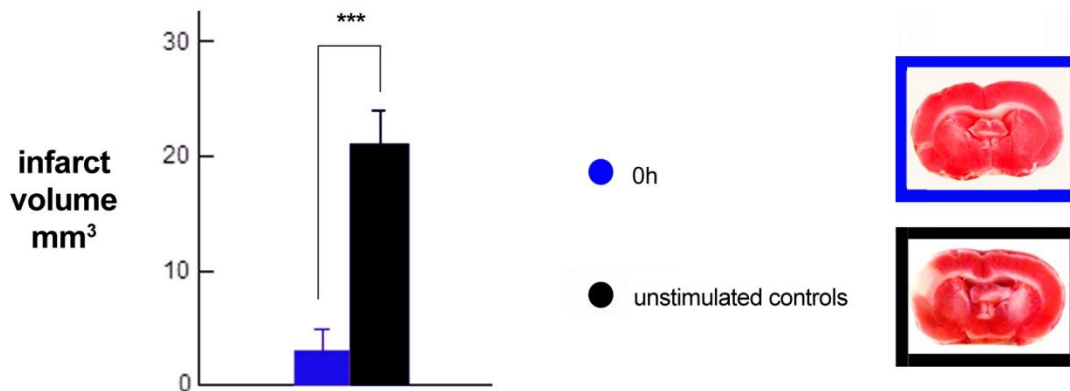


**Figure 4.1. Auditory stimulation protects MCA territory from impending stroke damage.** A. Schematic of experimental design for 0h auditory stimulated animals and unstimulated controls. B. (Left, graph) Quantification of infarct observed in animals that undergo pMCAO but never receive stimulation (unstimulated controls; black; n =9; mean =21.1±2.7mm<sup>3</sup>) and animals that undergo pMCAO but receive auditory stimulation immediately following the occlusion (0h auditory stim animals; blue; n= 7; mean=1.4±1.0mm<sup>3</sup>) Unstimulated animals sustain significantly larger infarct(Mann–Whitney U < 0.00001, n1 =9 n2 = 7, p = 0.0007). (Right, panels) Representative coronal slices stained with TTC for 0h auditory stim animals (blue, upper panel) and unstimulated controls (black, lower panel). Area devoid of staining in unstimulated control slice is infarcted tissue. *It is worth noting that the infarct observed in the 0h auditory stimulated animals is near the infarct size previously reported as resulting from surgical damage (~0.8mm<sup>3</sup>) in previous study (Lay et al., 2010).*  
*Auditory Stimulation Treatment*

Auditory stimulation consisted of 1 s of 5 Hz  $87.8 \pm 0.1$  dB (sound pressure level) white noise ranging from 0 -100 kHz. This stimulation was intermittently (with random intervals averaging 21 seconds) delivered 256 times, totaling 4.27 minutes of stimulation, over the course of 2 hours. The remaining ~25 minutes of the 2 hour treatment period is taken up by anesthetic administration and assessment of the animal's condition. All subjects remained anesthetized throughout the treatment period. In order to confirm consistency between subjects, auditory stimulation volume was measured immediately prior to, immediately after, and 1 day following auditory stimulation delivery. Throughout experimentation, no significant variation in stimulation volume occurred.

#### *Intrinsic Signal Optical Imaging (ISOI)*

We used the functional imaging technique intrinsic signal optical imaging (ISOI) to assess auditory functional representation (AFR) and whisker functional representation (WFR) prior to pMCAO and 24 hours following pMCAO. ISOI has been used extensively to provide high spatial resolution maps of stimulus evoked hemodynamic-related signals as an indirect means to image the functional organization of the cortex, and examine how these contribute to brain function.(Grinvald et al., 1986, Frostig et al., 1990, Ts'o et al., 1990) Though still debated, the initial dip phase of the WFR is generally associated with evoked neuronal activity and the overshoot phase with blood flow response (Frostig and Chen-Bee, 2009, Chen-Bee et al., 2012).

A detailed description of ISOI (Grinvald et al., 1986, Frostig et al., 1990, Ts'o et al., 1990) data acquisition and analysis can also be found elsewhere (Chen-Bee et al., 2000, Chen-Bee et al., 2007). Briefly, the cortex was illuminated with a red light emitting diode (635 nm maximum wavelength with full width at half height of 15 nm) and a charge coupled device (CCD) camera was used for imaging. During each 15-s trial, 1.5 s of prestimulus data followed by 13.5 s of

post-stimulus onset data were collected, with a  $6\pm 5$  sec random inter-trial interval. Stimulus consisted of either auditory stimulation identical to that described above, or single whisker (whisker C2) being deflected by approximately  $9^\circ$  in the rostral-caudal direction at a rate of 5 Hz for total stimulus duration of 1 second. Data were collected in blocks of 64 stimulation trials over a period of about 30 minutes each. Ratio images were created from calculating fractional change (FC) values as described previously (Chen-Bee et al., 1996). The first phase of AFR and WFR were analyzed; the initial dip. The ratio image containing the maximal areal extent this phase was Gaussian filtered and the areal extent quantified at a threshold level of  $2.5 \times 10^{-4}$  FC away from zero. Peak amplitude was quantified in fractional change units of the peak activity pixel.

### *Electrophysiology*

Peak optical activity evoked by whisker stimulation was determined using intrinsic signal optical imaging (ISOI) in order to guide placement of electrodes for subsequent neuronal recording (Masino et al., 1993, Brett-Green et al., 2001, Frostig et al., 2008). Recordings from a linear array of 8 independently drivable microelectrodes (1–2 M $\Omega$ , tungsten, from Microprobe) were amplified and saved at 24 KHz sampling rate using a multi-channel acquisition system (Alpha Lab Pro, Alpha Omega). Electrodes were inserted perpendicularly to a depth of ~300–400  $\mu$ m below the cortical surface to target supragranular layers. Recording sessions consisted of the same whisker stimulation parameters used during ISOI. Spike2 software was used for all off-line analyses, including extraction of MUA and LFP signals with a 1–300 Hz (LFP) or 300–3000 Hz (MUA) band pass filter. LFP waveforms and peri-stimulus time histograms (PSTHs) with 1 ms time bins were generated in Spike2. Peak LFP and MU responses were calculated as the biggest value within the first stimulus pulse minus mean

baseline activity obtained from 1 second duration of pre-stimulus data.

### *Laser speckle imaging of blood flow*

A detailed description of LSI data acquisition and analysis can be found previously (Dunn et al., 2001, Choi et al., 2006; Lay et al., 2010). Briefly, a 632.8 nm 15 mW HeNe laser was used as the illumination source. The laser beam was first expanded with a 2× lens to illuminate the thinned skull region of  $\sim 25\text{mm}^2$  in a more uniform manner. Care was taken to maintain the same level of illumination intensity over the imaged area of interest within each experiment. The speckle pattern from the  $5.12 \times 5.12\text{mm}$  imaged region was captured as  $512 \times 512$  pixel images by a 16-bit CCD camera (Cascade 512F) equipped with a Navitar zoom lens plus extenders such that speckle size matched camera pixel size. The frame exposure time for each image was 1 ms, and 10 consecutive images spaced 1.5 s apart were collected per time point. Collected images were processed as previously described (Briers, 1995). Briefly, for each time point, the 10 raw speckle images were converted to speckle contrast images by calculating the coefficient of variation (SD/mean) for the center pixel within  $5 \times 5$  pixel sliding windows in each image. The resulting 10 speckle contrast images were then converted to speckle index images by calculating their inverse squares multiplied by the exposure time in seconds, so that larger index values corresponded to faster blood flow. Lastly, the 10 speckle index images of each sampled time point were averaged to improve signal-to-noise ratio. LSI animals underwent the same initial experimental protocol as ISOI animals with data collected before pMCAO and at each of the same four post-pMCAO time points across the 120 min period post-pMCAO. For each data collection time point, 10 raw speckle images were collected at 1 s intervals with 1 ms exposure times and converted to speckle contrast images. The resulting 10 speckle contrast images were then converted to speckle index images, so that larger index values corresponded

to faster blood flow. Last, the 10 speckle index images of each sampled time point were averaged to improve signal-to-noise ratio. To quantify blood flow within specific MCA branches downstream from the occlusion for each sampled time point, we calculated the mean value within a region of interest (ROI) in MCA cortical branches as defined according to several criteria described previously (Lay et al., 2010). To determine noise level values, we also imaged each individual animal at 5 min after the cessation of heart beat and collected data from the non-flowing MCA. Analysis of an MCA ROI was performed for these animals in the same manner as for live animals. Each individual's noise value was subtracted from each flow index value.

#### *Histology (TTC staining for infarct)*

Rats were killed with 3.0 ml of Euthasol at the conclusion of each experiment. Their brains were carefully removed and sectioned into 2mm slices along the coronal plane. The brain slices were then incubated in 2% TTC at 37°C for 20 min in the dark (Bederson et al., 1986). TTC is enzymatically reduced, producing formazan (a bright red byproduct) by dehydrogenases in active mitochondria. Red stain intensity correlates with the number and functional activity of mitochondria, with unstained (white) areas being indicative of infarct (Goldlust et al., 1996, Lavie et al., 2001). The TTC-stained sections were photographed with a digital camera and the total infarct volume was determined by multiplying the infarct area of each slice by the thickness of that slice. An observer blind to experimental condition performed this volume calculation. A small lesion (~1mm in diameter or less) was occasionally apparent at the immediate site of MCA occlusion. This occurred infrequently and equivalently in all experimental groups (1–2 rats per group). The small amount of damage occasionally produced at the surgical site could be readily distinguished from the large ischemic infarct and was excluded from infarct analysis (Tamura et

al., 1981).

### *Statistical analysis*

For statistical analysis, within-subjects repeated-measures ANOVAs were used with an  $\alpha$ -level of significance set at 0.05. Transformed values for infarct volume were used for most analyses unless raw values satisfied the assumptions of the ANOVA. In cases where many individual infarct values within a group were '0', nonparametric analysis was used. For statistical analysis of intrinsic signal optical imaging data, evoked area and amplitude were converted to difference score values (post-occlusion - baseline), with values away from 0 signifying a change from baseline. A constant was added in order to allow for ANOVA, scores were transformed with a natural log function to better satisfy the assumptions of an ANOVA, and inferential statistics were performed on the transformed data.

## **Results**

### *Auditory stimulation completely protects MCA territory following pMCAO*

Following pMCAO, if auditory stimulation (intermittent 85 dB white noise pulsed at 5 Hz every ~20 sec) is delivered from 0-2 hr post-ischemic onset complete sensory induced protection from impending stroke damage is found (**Fig. 4.1**), similar to previous reports using whisker stimulation (Lay et al., 2010; Lay et al., 2011). Infarct is observed in animals that undergo pMCAO but never receive stimulation (unstimulated controls;  $n = 9$ ; mean =  $21.1 \pm 2.7 \text{ mm}^3$ ). Animals that undergo pMCAO but receive auditory stimulation (5 Hz white noise delivered in the same pattern and over the same period as in our previous whisker stimulation model) immediately following the occlusion are protected from this infarct (0h auditory

stim animals;  $n = 7$ ;  $\text{mean} = 1.4 \pm 1.0 \text{ mm}^3$ ) (Mann–Whitney  $U < 0.00001$ ,  $n_1 = 9$   $n_2 = 7$ ,  $p = 0.0007$ ) (Figure 1AB). The infarct observed in these stimulated animals is near the infarct size previously reported as resulting from surgical damage ( $\sim 0.8 \text{ mm}^3$ ; Lay et al., 2010). The somatosensory cortex is among the areas protected by auditory stimulation in the above animals.

#### *Gray matter transection blocks spread of auditory evoked activity*

Auditory-evoked cortical activity, which normally spreads laterally into somatosensory cortex, was blocked by gray matter transection (**Fig. 4.2A,B**). The size of auditory evoked activity spreads was significantly smaller following transection ( $T = 6.46$ ,  $df = 5$ ,  $p = 0.002$ ; area quantification based on thresholded data at  $2.5 \times 10^{-4}$  FC; **Fig. 4.2B**) and did not extend beyond the transection in any subject.

Importantly, gray matter transection does not affect collateral blood flow (**Fig. 4.2C,D**). Representative LSI data before and 1 hr after transection and pMCAO (C) shows collateral flow on both sides of the transection. At 24 hours post-occlusion, blood flow in M2 branches of MCA were not significantly different between transected ( $n = 8$ ;  $\text{mean} = 68.4 \pm 19.9\%$  of baseline) and non-transected ( $n = 6$ ;  $\text{mean} = 62.9 \pm 11.9\%$  of baseline) rats receiving 0h auditory stimulation (*paired t-test*  $t(8) = 0.89$ ;  $p = 0.4$ ).

Together, evoked activity data and blood flow imaging suggest that gray matter transection successfully blocked cortical activity but not collateral blood flow in a subregion of the MCA territory. Thus, any functional losses in this subregion of MCA territory could be attributed to the lack of evoked cortical activity and not any differences in collateral reperfusion.

Finally, gray matter transection by itself did not cause infarct. Infarct volumes for animals that received sham pMCAO and gray matter transection was  $0 \pm 0 \text{ mm}^3$  (ie, no detectable infarct was observed in subjects receiving just transection).

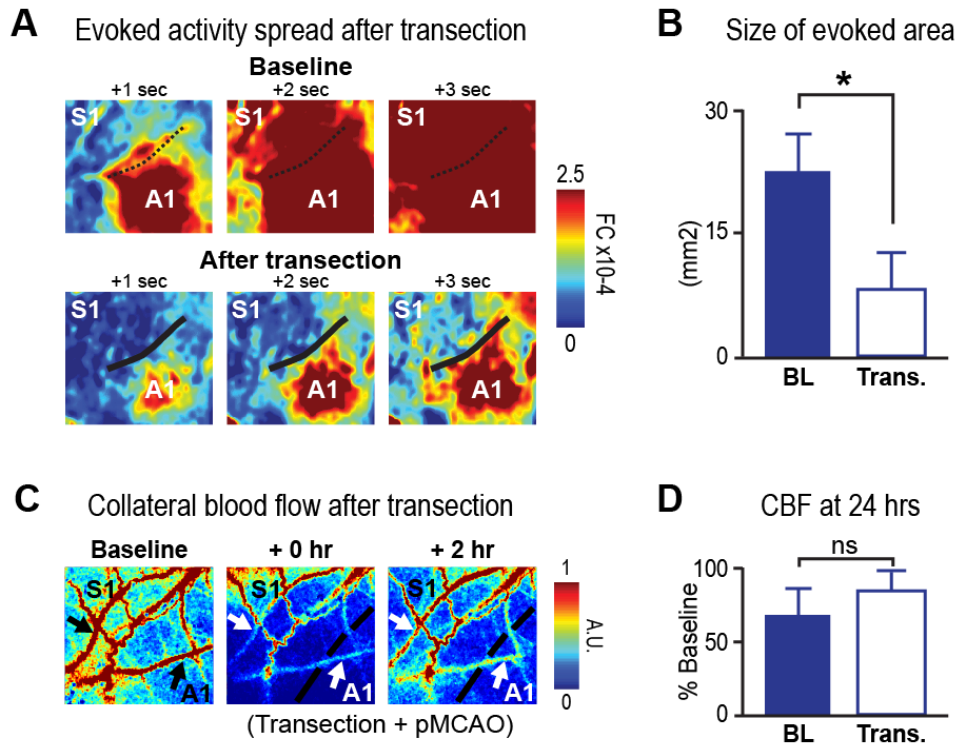


**Figure 4.2. Gray matter transection blocks spread of auditory evoked activity but leaves collateral blood flow intact. (A,B)** Gray matter transection blocks the spread of auditory evoked activity. In (B) representative ISOI data auditory evoked activity spread was extensive at baseline (top) but was constrained by transection (bottom, solid line, dotted line in top panel indicates location of future transection). Quantification of the size of auditory evoked area based on  $2.5 \times 10^{-4}$  FC threshold revealed significantly smaller areas of evoked activity after transection (B). Remaining evoked areas were limited to the near side of the transection. **(C,D)** Importantly, collateral blood flow was not affected by transection. In (C) representative LSI data shows collateral blood flow in subject with pMCAO, transection, and early auditory stimulation (0-2 hr). At the end of auditory stimulation (2 hr post-pMCAO, far right image in C), collateral flow can be seen on both sides of transection. Quantification at 24 hr post-pMCAO revealed no differences in collateral blood flow between transected and non-transected subjects (D). *For (B), values were pooled from sham-pMCAO + transection and pMCAO + transection groups.*

### *Gray matter transection constrains pattern of sensory-induced protection*

0h auditory stim transection animals (n =9; mean=33.1±5.6) have significantly larger infarcts than their non-transected counterparts (0h auditory stim animals; n= 7; mean=1.4±1.0mm<sup>3</sup>) (Mann–Whitney U < 0.00001, n1 =10 n2 = 8, p = 0.0005).

0h auditory stim transection animals have reduced functional response according to intrinsic signal optical imaging at 24 hours post occlusion compared to their own baselines whereas sham-pMCAO transection animals have baseline level response at 24 hours post-sham-occlusion. There was a within subjects difference for area ([F<sub>1,8</sub>=34.1; p=0.00002, ANOVA]) and amplitude of the initial dip ([F<sub>1,8</sub>=17.3; p=0.00009, ANOVA]) (**Fig. 4.3**). These results support the hypothesis that cortical activity plays a critical role in protection from ischemic stroke in this model because blocking the spread of activity blocks the previously observed protection.

0h auditory stim transection animals have reduced spontaneous activity and multiunit and local field potential responses to whisker stimulation the following day compared to sham-pMCAO transection animals. Multiunit activity showed a between groups difference at 24 hours post occlusion or sham occlusion ([F<sub>1,8</sub>=18.2; p=0.003, ANOVA]), as did spontaneous activity ([F<sub>1,8</sub>=7.5; p=0.025, ANOVA]), and local field potential ([F<sub>1,8</sub>=18.6; p=0.003, ANOVA]) (**Fig. 4.3C**). Similar to functional imaging and histology, neuronal recordings support the finding that transection blocks the spread protective activity from auditory cortex, and that spread of activity plays a key role in protecting the cortex from ischemic stroke.

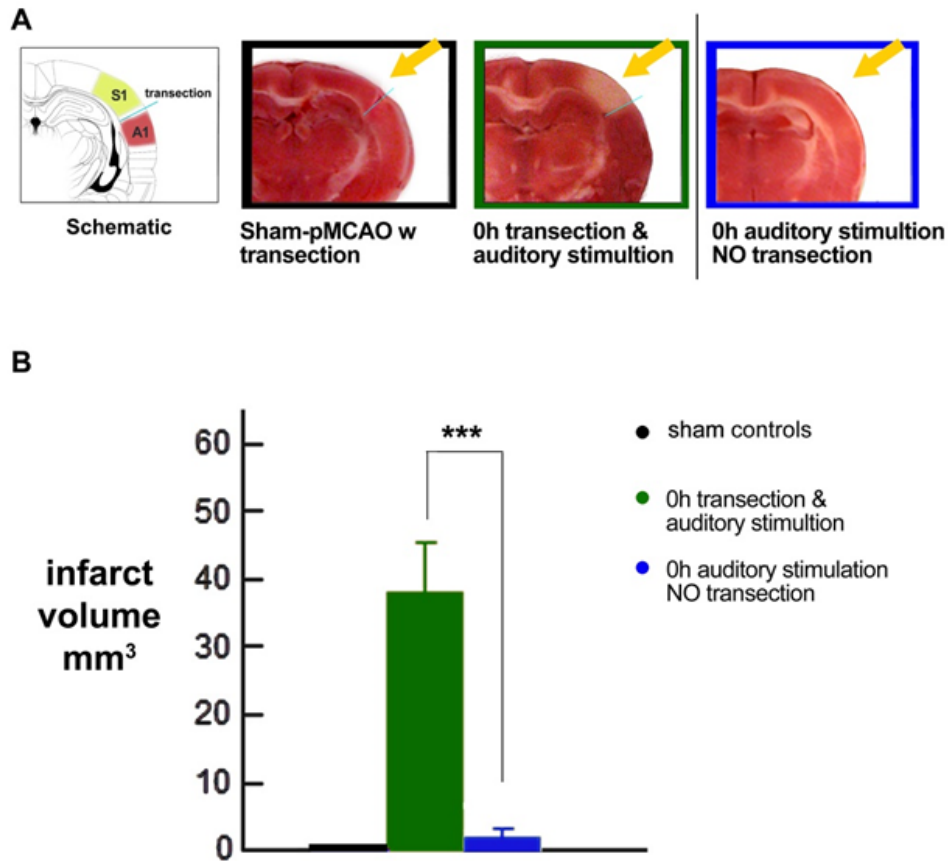


**Figure 4.3. Gray matter transection by itself produces no tissue infarction, but blocks sensory induced protection from ischemic stroke.** A. (Left panel) A schematic of approximate transection between auditory and somatosensory cortices viewed from coronal slice perspective. (Right three panels) Representative coronal sections taken from (left to right) sham pMCAO transection (black), 0h auditory stimulation transection (green), and 0h auditory (no transection)(blue) animals 24 hours after pMCAO using TTC assay for infarct. Note that transection itself did not cause infarct (black, sham pMCAO transection animals n=8). The area devoid of staining (arrow) in the 0h auditory stimulation transection animal's (green) cortex is indicative of ischemic infarct that the transection prevented protection from. This area is protected in 0h auditory animals (blue) that do not have a transection. B. Quantitative analysis of infarct volumes. 0h auditory stimulation transection animals (green; n =9; mean =33.1±5.6mm<sup>3</sup>) sustained significantly more infarct than their non-transected counterparts (blue; n =7; mean =1.4±1.0mm<sup>3</sup>)(Mann-Whitney U < 0.00001, n1 =10 n2 = 8, p = 0.0005). No infarct was observed in animals with transection and sham pMCAO (n =8).

*0h auditory stim transection animals have blood flow return equivalent to protected 0h pMCAO animals without transection*

0h auditory stimulation animals sustain infarct despite the fact that blood flow in MCA is equivalent to protected 0h non-transected animals. By 24 hours post-occlusion blood flow in MCA branches for 0h auditory stimulation transection animals (n =8; mean = 68.4±19.9% of baseline) was equivalent to animals with no occlusion of MCA (n =6; mean =62.9±11.9% of baseline)(paired t-test  $t(8) = 0.89$ ;  $p = 0.4$ ; **Fig. 4.4**). Similarly to previous data, this suggests that reperfusion in the absence of stimulation is not necessarily protective. Further, these data provide evidence that cortical activity plays the same protective role independent of reperfusion in both tMCAO and pMCAO models. The addition of cortical activity to the rapid reperfusion that occurs in tMCAO animals eliminates impending infarct and here we show that removing cortical activity from the gradual collateral based flow resulting from stimulation in pMCAO models eliminates protection.

## **Discussion**

These results indicate that early cortical activity (0-2 hr post-ischemic onset) plays a direct role in protection from impending ischemic stroke. Auditory activation was capable of completely protecting somatosensory cortex from impending stroke damage despite the distance between cortices. 0h auditory stim animals maintained baseline or greater levels of cortical function (evoked and spontaneous neuronal activity and functional responses assessed with intrinsic signal optical imaging) in both auditory and somatosensory cortices and did not sustain infarct. These data demonstrate that alternative sensory stimulation can be as protective as whisker stimulation and solidify the assumption that activating the ischemic cortex is the critical aspect in stimulation induced protection. The spatial range over which cortical

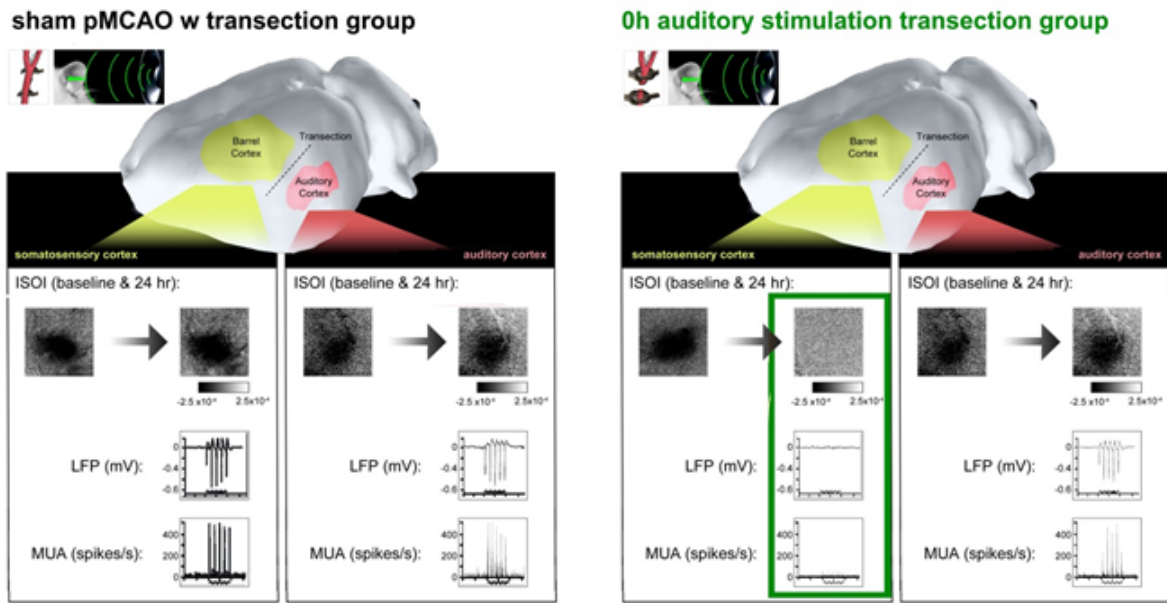
activity was able to protect was surprising. We predicted that this long range extension of protection to surrounding cortices when one sensory cortex was activated might be based on long range intracortical horizontal projections previously described in our lab(Frostig et al., 2008).

We found evidence that the mentioned long range horizontal connections between these cortices were responsible for the extended protection; auditory stimulation was prevented from protecting somatosensory cortex in transected animals by a transection of gray matter between the cortices. This along with evidence from preliminary studies showing that weaker auditory stimulus reduced the anterior extent of auditory stimulation's protection range led us to conclude that activated tissue corresponds to protected tissue in our protected model.

Further, blood flow returned equivalently in transected 0h auditory stim transection animals and non-transected, protected 0h animals. This suggests that cortical activity was the critical aspect – clearly blood flow is necessary for neuronal survival, but does not appear to be sufficient for protection in the absence of cortical activity.

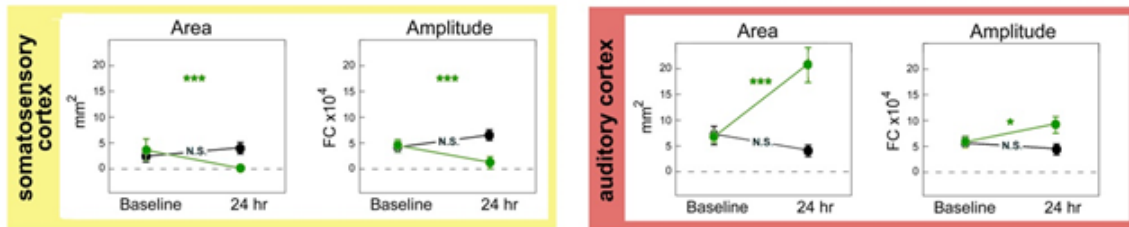
The current experiments provided an opportunity to dissociate the variables of reperfusion and cortical activity in a pMCAO, collateral reperfusion model. Activity spread to somatosensory cortex was prevented by the transection, but blood flow was returned to the entire region via collateral reperfusion induced by activity in auditory cortex. Thus we were able to conclude that collateral based blood flow return in the absence of activated

**A** Representative functional imaging and extracellular recording for sham pMCAO transection animals and 0h auditory stimulation transection animals at baseline and 24 hours. Note that only areas beyond the transection (somatosensory cortex) have lost responses in 0h auditory stimulation transection animals



**B** Functional response according to ISOI is decreased in areas beyond the transection in 0h auditory stimulation transection animals but not sham pMCAO transection animals

- sham pMCAO w transection
- 0h auditory stim transection



**C** Neuronal activity is decreased in areas beyond the transection in 0h auditory stimulation transection animals but not sham pMCAO transection animals

- sham pMCAO w transection
- 0h auditory stim transection

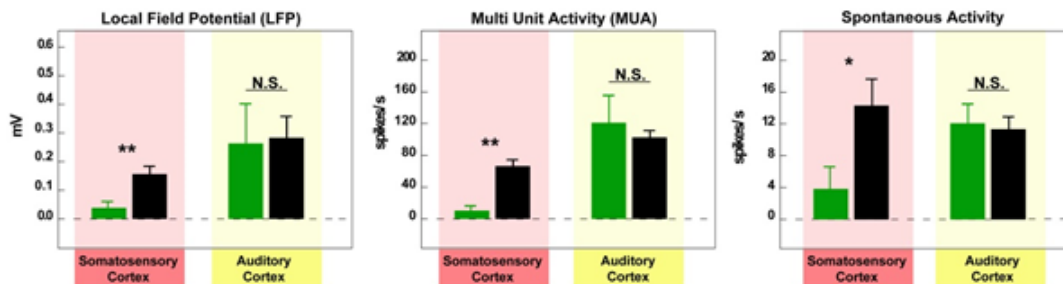


**Figure 4.4. Beyond transection, somatosensory cortex suffers loss of function.** Animals that are transected, but do not undergo pMCAO do not suffer any loss of function. **(A)** Representative cases functional imaging, LFP, MUA, and blood flow data collected from experimental subjects (green) and sham pMCAO animals (black) from the somatosensory (left for each), and auditory (right for each) cortices. 24 hours following protective auditory stimulation, experimental animals maintain normal function within the auditory cortex, but not in the somatosensory cortex. **(B)** Baseline and 24hr assessment of functional response according to ISOI is quantified for experimental and control groups. 0h auditory stim transection animals have reduced functional response according to intrinsic signal optical imaging at 24 hours post occlusion compared to their own baselines whereas sham-pMCAO transection animals have baseline level response at 24 hours post-sham-occlusion. There was a within subjects difference for area ( $[F_{1,8}=34.1; p=0.00002, \text{ANOVA}]$ ) and amplitude of the initial dip ( $[F_{1,8}=17.3; p=0.00009, \text{ANOVA}]$ ). Means and standard errors are provided for the area and amplitude of the somatosensory and auditory cortices. Asterisks indicate a significant difference from baseline, while 'N.S.' indicates no change from baseline. **(C)** LFP (left), MUA (middle), and spontaneous activity (right) recorded from the auditory and somatosensory cortices are quantified in control (black) and experimental animals (green). 0h auditory stim transection animals have reduced spontaneous activity and multiunit and local field potential responses to whisker stimulation the following day compared to sham-pMCAO transection animals. Multiunit activity showed a between groups difference at 24 hours post occlusion or sham occlusion ( $[F_{1,8}=18.2; p=0.003, \text{ANOVA}]$ ), as did spontaneous activity ( $[F_{1,8}=7.5; p=0.025, \text{ANOVA}]$ ), and local field potential ( $[F_{1,8}=18.6; p=0.003, \text{ANOVA}]$ ). Means and standard errors are provided, and asterisks indicate a significant difference between groups (\* $p<0.05$ ; \*\* $p<0.01$ ; N.S. indicates no significance). Similar to functional imaging and histology, neuronal recordings support the finding that transection blocks the spread protective activity from auditory cortex, and that spread of activity plays a key role in protecting the cortex from ischemic stroke.

cortex resulted in infarct in the somatosensory cortex. (Only 24 hour blood flow data was compared however, so an assessment of acute blood flow return in transection animals is warranted to confirm matching during-treatment reperfusion between 0h and 0h transection animals strengthen this conclusion).

Also interesting to note, and relevant to the above conclusion, is that no difference between flow in arterial branches crossing auditory versus somatosensory cortex in the 0h auditory stim transection group was observed (data not shown). This suggests two things: 1) That while blood flow to an ischemic region is obviously necessary for protection from ischemia, it is not sufficient for protection – somatosensory cortex received blood flow return equivalently to auditory cortex, but was not protected in the absence of the spread of activity from auditory cortex and 2) That stimulation induced collateral reperfusion is not specific to the stimulated region, but rather reperfuses MCA branches indiscriminately. The latter even more strongly suggests that localized induction of blood flow return cannot account for protection and that activating ischemic tissue is critical.

A final important note is that the current experimental approach cannot resolve potential protective effects of cortical activity itself versus activity induced changes in hyper-local perfusion states such as blood flow in small arterioles and capillaries. Therefore future research may be required before conclusions can be drawn, for example, about interactions between intracellular signalling cascades associated with neuronal activity and ischemic intracellular molecular cascades.

To summarize, protection occurred specifically within the auditory cortex where activity was initiated - up to the line of transection between auditory and somatosensory cortices. The somatosensory cortex, usually protected in this paradigm, was deprived of activity spread from auditory cortex by the transection, and sustained infarct. Importantly, the transection itself did

not cause any infarct or loss of function. Thus, regions outside the bounds of the spread of activity remained vulnerable to ischemic stroke damage. Blood flow was equivalent in all areas in all animals and therefore cannot be responsible for differences observed on either side of the transection or between groups. Thus, while sensory-evoked blood flow redistribution is a necessary prerequisite for protection, the spread of evoked activity is also critical for complete protection following pMCAO in this model.

## CHAPTER 5: Experimental summary & conclusions

A thesis is a single idea that is put forward with supporting evidence for a reader to judge. What is the thesis of this document? The thesis presented and argued here is that emergent, spatially organized patterns of activity are a fundamental aspect of whisker coding in barrel cortex.

This thesis was tested by focusing on a particular type of emergent, spatially organized activity in barrel cortex- large cortical activity spreads or point spreads. Point spreads are a ubiquitous feature of sensory cortex (Grinvald et al., 1994; Barth et al., 1995; Das and Gilbert, 1995; Bakin et al., 1996; Bringuier et al., 1999; Brett-Green et al., 2001; Kaur et al., 2005; Roland et al., 2006; Ferezou et al., 2006, 2007; Sharon et al., 2007; Frostig et al., 2008; Chen-Bee et al., 2012; Mohajerani et al., 2013). Such large spatial profiles of activity are puzzling given their likely high metabolic cost. What are the functional contributions of point spreads and their potential interactions?

This dissertation identified three distinct functional contributions that make point spreads worth their metabolic cost. First, point spreads provide a mesoscopic substrate for sensory coding that underlies emergent forms of multi-point integration (**Chapter 2**). Second, point spreads provide a novel substrate for invariant sensory coding that is often overlooked at the single neuron level (**Chapter 3**). Finally, point spreads create a broad region of sensory-induced protection from ischemic stroke (**Chapter 4**). Together, these data provide a unique view of barrel cortex based on emergent, spatially organized patterns of activity in large neural networks.

An important aspect of this dissertation is that it approaches sensory coding in barrel cortex from an intermediate (mesoscopic) perspective that is not well represented in our understanding of brain function. Neuroscience has made substantial progress in understanding

brain function at the macroscopic level (e.g., mapping the hierarchy of sensory cortices with fMRI) and at the microscopic level (e.g., identifying the tuning curves of individual neurons). Despite much effort and considerable interest, it continues to be difficult to bridge these two bodies of knowledge with an understanding of brain function at the mesoscopic scale, where large networks of neurons within each brain structure exhibit emergent properties and functions. This leaves a large spatial and temporal gap in our understanding of brain function, specifically at the level of mesoscopic network activity within each brain structure.

In general, there is a concerted effort to better understand brain function at the level of neural networks. This effort can be split into two basic approaches- a top down approach and a bottom up approach. A top down approach measures more global patterns of activity across very large populations of neurons (thousands if not hundreds of thousands) without resolving responses in individual neurons. This “big picture” view of network activity is typically accomplished using functional imaging methods such as intrinsic signal optical imaging (ISOI), fMRI, or voltage sensitive dye imaging (VSDI). Importantly, functional imaging methods implicitly include information about the spatial structure of activity (each image is a snapshot of activity across space). Local field potentials and other slow wave recordings also provide a more localized view of population activity, and if recorded from carefully designed multi-electrode arrays can also offer information about the spatial profile of network activity. Despite implicitly collecting information about the spatial organization of mesoscopic network activity (ie, *within* brain regions), this information is often ignored in favor of macroscopic spatial patterns (ie, *between* brain regions).

A bottom up approach to studying network activity relies on simultaneously measuring activity in up to hundreds of individual neurons. Multi-site recordings and calcium imaging can both be used to simultaneously record suprathreshold (spiking) activity in many single neurons.

Group statistics such as the tuning of individual neurons provide information about the constituents in the network, but do not effectively describe network behavior and emergent functions. A more dynamic view of network activity at the single neuron level comes from analytical techniques such as population codes (sum of spikes from all neurons), decoding algorithms (which ask if response vectors accurately report a stimulus), and information theoretic analysis (which ask how much information spikes from each neuron carry). These techniques allow assessment of network-level information coding in real time, introducing important new substrates for information coding and emergent functions such as robustness. However, similar to top-down approaches this research also tends to favor abstract, non-spatial relationships *between* brain regions rather than spatial relationships *within* a given brain region.

In both top-down and bottom-up approaches to studying network activity, potential contributions from the mesoscopic spatial arrangement of constituent neurons within brain regions is typically ignored. Instead, each brain region or neuron is often treated as an abstract “node” with topological, rather than topographic (spatial), relationships with other nodes. Focusing on abstract (non-spatial) relationships within networks is well supported by the concepts of sparse coding and specific connectivity and has been popularized by analytical approaches such as graph theory. Does focusing on just abstract, specific, and sparsely activated networks produce yet another gap in our understanding of brain function?

Spatially organized networks are common in sensory cortices, which exhibit both topographic organization as well as large point spreads. In such spatially organized networks the spatial profile of network activity is likely to be highly relevant. Spatial organization in large cortical networks is not limited to sensory cortices, though. Spatially organized differences in subthreshold oscillations has been found in the entorhinal cortex (Giocomo et al., 2007), suggesting that at least some degree of spatial organization may be a general property of

cortical networks. It remains to be seen if other non-sensorimotor cortical areas also have a latent spatial organization that has not yet been discovered. This would not be surprising, as it has been suggested that the high metabolic cost of network activity may actually be mitigated by spatial organization where adjacent neurons and cortical regions share common functions (Bullmore and Sporns, 2012).

**Chapters 2-4** of this dissertation detailed several potential functional contributions of spatially organized mesoscopic network activity in barrel cortex. It is possible that many of these findings could extend to other sensory cortices and other spatially organized networks. A final potential contribution of mesoscopic network activity is providing unambiguous sensory coding on single trials. In **Appendix B**, we describe several fundamental ambiguities regarding real time sensory coding at the single neuron level, and how these ambiguities are resolved if the spatial profile of activity is considered. It is important to note that such global, spatially organized population activity could occur without necessarily negating or interfering with activities in smaller, sparser, or more specific cortical networks.

An overarching theme of this dissertation is emergence, the concept that a system is more than the sum of its parts. We know a lot about the individual parts of barrel cortex, the different cell types and their coding properties. This dissertation has taken several important steps to begin understanding how barrel cortex may be more than just the sum of many differently tuned neurons. Several emergent features of the spatially organized networks in barrel cortex were found that could not have easily been predicted from the perspective of individual neurons. Speaking of emergence, Hazen and colleagues in 2009 said: a single grain of sand cannot form a sand dune, a single neuron cannot be conscious, and a single ant cannot perform the complex behaviors of an ant colony. In all of these cases, it is the complex and unpredictable interactions between many constituents (sand grains, neurons, ants) that are

required to produce the emergent property (sand dune, consciousness, colony behavior). To fully understand the nature and function of the rodent barrel cortex, we must continue to pursue its emergent features and the unique sensory functions they support.

## References:

Anderson JS, Lampl I, Gillespie DC, Ferster D (2000) The contribution of noise to contrast invariance of orientation tuning in cat visual cortex. *Science* 290:1968–1972.

Bakin JS, Kwon MC, Masino SA, Weinberger NM, Frostig RD (1996) Suprathreshold auditory cortex activation visualized by intrinsic signal optical imaging. *Cerebral Cortex* 6:120–130.

Bar-Gad I, Ritov Y, Vaadia E, Bergman H (2001) Failure in identification of overlapping spikes from multiple neuron activity causes artificial correlations. *J Neuroscience Methods* 107:1–13.

Barth DS, Goldberg N, Brett B, Di S (1995) The spatiotemporal organization of auditory, visual, and auditory-visual evoked potentials in rat cortex. *Brain Research* 678:177–190.

Bederson JB, Pitts LH, Germano SM, Nishimura MC, Davis RL, Bartkowski HM (1986) Evaluation of 2,3,5-triphenyltetrazolium chloride as a stain for detection and quantification of experimental cerebral infarction in rats. *Stroke* 17:1304-1308.

Békésy GV (1957) Neural Volleys and the Similarity between Some Sensations Produced by Tones and by Skin Vibrations. *Journal of the Acoustical Society of America* 29:1059–1072.

Békésy GV (1958) Funneling in the Nervous System and its Role in Loudness and Sensation Intensity on the Skin. *Journal of the Acoustical Society of America* 30:399–412.

Békésy GV (1959) Neural Funneling along the Skin and between the Inner and Outer Hair Cells of the Cochlea. *Journal of the Acoustical Society of America* 31:1236–1249.

Békésy GV (1967) *Sensory Inhibition*. Princeton, NJ: Princeton University Press.

Benison, A.M., Ard, T.D., Crosby, A.M., and Barth, D.S. (2006). Temporal patterns of field potentials in vibrissa/barrel cortex reveal stimulus orientation and shape. *Journal of Neurophysiology* 95, 2242-2251.

Brett-Green BA, Chen-Bee CH, Frostig RD (2001) Comparing the functional representations of central and border whiskers in rat primary somatosensory cortex. *Journal of Neuroscience* 21:9944–9954.

Briers JD, Webster, S. (1995) Quasi real-time digital version of single-exposure photography for full-field monitoring of velocity or flow-fields. *Optical Communications* 36-42.

Bringuier V, Chavane F, Glaeser L, Frégnac Y (1999) Horizontal propagation of visual activity in the synaptic integration field of area 17 neurons. *Science* 283:695–699.

Brint S, Jacewicz M, Kiessling M, Tanabe J, Pulsinelli W (1988) Focal brain ischemia in the rat: methods for reproducible neocortical infarction using tandem occlusion of the distal middle cerebral and ipsilateral common carotid arteries. *Journal of Cerebral Blood Flow and Metabolism*

8:474-485.

Bullmore, E., & Sporns, O. (2012). The economy of brain network organization. *Nature Reviews Neuroscience*, 13(5), 336-349.

Buzsáki G (2010) Neural syntax: cell assemblies, synapse ensembles, and readers. *Neuron* 68: 362–385.

Camazine, S. (2003). Self-organization in biological systems. Princeton University Press.

Caplan, L. (2009) Caplan's stroke: a clinical approach. Philadelphia: Saunders/Elsevier.

Carmichael, ST (2005) Rodent models of focal stroke: size, mechanism, and purpose. *NeuroRx* 2(3): 396-409.

Carvell GE, Simons DJ (1990) Biometric analyses of vibrissal tactile discrimination in the rat. *Journal of Neuroscience* 10:2638–2648.

Celikel T, Sakmann B (2007) Sensory integration across space and in time for decision making in the somatosensory system of rodents. *PNAS* 104:1395–1400.

Chen-Bee CH, Kwon MC, Masino SA, Frostig RD (1996) Areal extent quantification of functional representations using intrinsic signal optical imaging. *Journal of Neuroscience Methods* 68:27-37.

Chen-Bee, C.H., Polley, D.B., Brett-Green, B., Prakash, N., Kwon, M.C., and Frostig, R.D. (2000). Visualizing and quantifying evoked cortical activity assessed with intrinsic signal imaging. *Journal of Neurosci Methods* 97, 157-173.

Chen-Bee C, Agoncillo T, Lay C, Frostig R (2010) Intrinsic signal optical imaging of brain function using short stimulus delivery intervals. *Journal of neuroscience methods* 187:171–182.

Chen-Bee CH, Zhou Y, Jacobs NS, Lim B, Frostig RD (2012) Whisker array functional representation in rat barrel cortex: transcendence of one-to-one topography and its underlying mechanism. *Frontiers in Neural Circuits* doi: 10.3389/fncir.2012.00093.

Chimowitz MI (2013) Endovascular treatment for acute ischemic stroke--still unproven. *New England Journal of Medicine* 368:952-955.

Choi B, Ramirez-San-Juan JC, Lotfi J, Stuart Nelson J (2006) Linear response range characterization and in vivo application of laser speckle imaging of blood flow dynamics. *Journal of Biomedical Optics* 11:041129.

Chung S, Li X, Nelson SB (2002) Short-term depression at thalamocortical synapses contributes to rapid adaptation of cortical sensory responses in vivo. *Neuron* 34:437–446.

Chen, L.M., Friedman, R.M., and Roe, A.W. (2003). Optical imaging of a tactile illusion in area 3b

- of the primary somatosensory cortex. *Science* 302, 881-885.
- Civillico, E.F., and Contreras, D. (2006). Integration of evoked responses in supragranular cortex studied with optical recordings in vivo. *Journal of Neurophysiology* 96, 336-351.
- Das A, Gilbert CD (1995) Long-range horizontal connections and their role in cortical reorganization revealed by optical recording of cat primary visual cortex. *Nature* 375:780–784.
- Davis MF, Lay CC, Chen-Bee CH, Frostig RD (2011) Stimulation of auditory cortex following permanent MCA occlusion confers complete or near complete protection from ischemic stroke in the adult rat. Neuroscience 2011 Washington DC: Society for Neuroscience.
- Davis MF LC, Frostig RD (2013) Permanent Cerebral Vessel Occlusion Via Double Ligature and Transection. *Journal of Visualized Experiments*.
- De Rango P (2012) Cerebral Hyperperfusion Syndrome: The Dark Side of Carotid Endarterectomy. *European Journal of Vascular and Endovascular Surgery* 43:377.
- Drew, P.J., and Feldman, D.E. (2007). Representation of moving wavefronts of whisker deflection in rat somatosensory cortex. *Journal of Neurophysiology* 98, 1566-1580.
- Dunn AK, Bolay H, Moskowitz MA, Boas DA (2001) Dynamic imaging of cerebral blood flow using laser speckle. *Journal of Cerebral Blood Flow & Metabolism* 21:195-201.
- Feldmeyer D (2012) Excitatory neuronal connectivity in the barrel cortex. *Frontiers in Neuroanatomy* 6:24.
- Ferezou I, Bolea S, Petersen CC (2006) Visualizing the cortical representation of whisker touch: voltage-sensitive dye imaging in freely moving mice. *Neuron* 50:617–629.
- Ferezou I, Haiss F, Gentet LJ, Aronoff R, Weber B, Petersen CC (2007) Spatiotemporal dynamics of cortical sensorimotor integration in behaving mice. *Neuron* 56:907–923.
- Fox G, Gallacher D, Shevde S, Loftus J, Swayne G (1993) Anatomic variation of the middle cerebral artery in the Sprague-Dawley rat. *Stroke* 24:2087-2092.
- Fox, K. (2008). Barrel Cortex. New York: Cambridge University Press.
- Frostig RD, Lieke EE, Ts'o DY, Grinvald A (1990) Cortical functional architecture and local coupling between neuronal activity and the microcirculation revealed by in vivo high-resolution optical imaging of intrinsic signals. *PNAS* 87:6082-6086.
- Frostig, R.D. (2006). Functional organization and plasticity in the adult rat barrel cortex: moving out-of-the-box. *Current Opinion Neurobiology* 16, 445-450.
- Frostig RD, Xiong Y, Chen-Bee CH, Kvasnák E, Stehberg J (2008) Large-scale organization of rat sensorimotor cortex based on a motif of large activation spreads. *Journal of Neuroscience*

28:13274–13284.

Frostig RD, Chen-Bee CH (2009) Visualizing Adult Cortical Plasticity Using Intrinsic Signal Optical Imaging. In: *In Vivo Optical Imaging of Brain Function* (Frostig, R. D., ed), pp 255- 287: CRC Press.

Gardner, E.P., and Costanzo, R.M. (1980a). Spatial integration of multiple-point stimuli in primary somatosensory cortical receptive fields of alert monkeys. *Journal of Neurophysiology* 43, 420-443.

Gardner, E.P., and Costanzo, R.M. (1980b). Temporal integration of multiple-point stimuli in primary somatosensory cortical receptive fields of alert monkeys. *Journal of Neurophysiology* 43, 444-468.

Gardner, E.P., and Spencer, W.A. (1972a). Sensory funneling. I. Psychophysical observations of human subjects and responses of cutaneous mechanoreceptive afferents in the cat to patterned skin stimuli. *Journal of Neurophysiology* 35, 925-953.

Gardner, E.P., and Spencer, W.A. (1972b). Sensory funneling. II. Cortical neuronal representation of patterned cutaneous stimuli. *Journal of Neurophysiology* 35, 954-977.

Gardner, E.P., and Tast, J.M. (1981). Psychophysical measurements of perceived intensity of single point and multiple-point cutaneous stimuli in humans and subhuman primates. *Journal of Neurophysiology* 46, 479-495.

Ghazanfar, A.A., and Nicolelis, M.A. (1997). Nonlinear processing of tactile information in the thalamocortical loop. *Journal of Neurophysiology* 78, 506-510.

Giocomo, L. M., Zilli, E. A., Fransén, E., & Hasselmo, M. E. (2007). Temporal frequency of subthreshold oscillations scales with entorhinal grid cell field spacing. *Science*, 315(5819), 1719-1722.

Grinvald A, Lieke E, Frostig RD, Gilbert CD, Wiesel TN (1986) Functional architecture of cortex revealed by optical imaging of intrinsic signals. *Nature* 324:361-364.

Grinvald A, Lieke EE, Frostig RD (1994) Cortical point-spread function and long-range lateral interactions revealed by real-time optical imaging of macaque monkey primary visual cortex. *Journal of Neuroscience* 14: 2545-2568.

Goldlust EJ, Paczynski RP, He YY, Hsu CY, Goldberg MP (1996) Automated measurement of infarct size with scanned images of triphenyltetrazolium chloride-stained rat brains. *Stroke* 27:1657-1662.

Goldreich, D., Peterson, B.E., and Merzenich, M.M. (1998). Optical imaging and electrophysiology of rat barrel cortex. II. Responses to paired-vibrissa deflections. *Cerebral Cortex* 8, 184-192.

Hashimoto I, Yoshikawa K, Kimura T (1999) Sensory funneling of liminal multiple-point air-puff stimulation produces dramatic reduction in reaction time but relatively invariant P300 somatosensory evoked potential. *Neuroreport* 10:3201–3205.

Hazen, R. M., Griffin, P. L., Carothers, J. M., & Szostak, J. W. (2007). Functional information and the emergence of biocomplexity. *Proceedings of the National Academy of Sciences*, 104(1): 8574-8581.

Hirata, A., and Castro-Alamancos, M.A. (2008). Cortical transformation of wide-field (multiwhisker) sensory responses. *Journal of Neurophysiology* 100, 358-370.

Hubel, D. H., & Wiesel, T. N. (1962). Receptive fields, binocular interaction and functional architecture in the cat's visual cortex. *The Journal of physiology* 160(1), 106-154.

Jacob, V., Le Cam, J., Ego-Stengel, V., and Shulz, D.E. (2008). Emergent properties of tactile scenes selectively activate barrel cortex neurons. *Neuron* 60, 1112-112.

Jadhav S, Wolfe J, Feldman D (2009) Sparse temporal coding of elementary tactile features during active whisker sensation. *Nature neuroscience* 12:792–800.

Jancke D, Chavane F, Naaman S, Grinvald A (2004) Imaging cortical correlates of illusion in early visual cortex. *Nature* 428:423–426.

Katz Y, Heiss JE, Lampl I (2006) Cross-whisker adaptation of neurons in the rat barrel cortex. *Journal of Neuroscience* 26:13363–13372.

Kaur S, Rose HJ, Lazar R, Liang K, Metherate R (2005) Spectral integration in primary auditory cortex: laminar processing of afferent input, in vivo and in vitro. *Neuroscience* 134:1033–1045.

Killackey, Herbert P., and Steven Leshin. "The organization of specific thalamocortical projections to the posteromedial barrel subfield of the rat somatic sensory cortex." *Brain research* 86.3 (1975): 469.

Kleinfeld, D., and Delaney, K.R. (1996). Distributed representation of vibrissa movement in the upper layers of somatosensory cortex revealed with voltage-sensitive dyes. *Journal of Comparative Neurology* 375, 89-108.

Lavie G, Teichner A, Shohami E, Ovadia H, Leker RR (2001) Long term cerebroprotective effects of dexanabinol in a model of focal cerebral ischemia. *Brain Research* 901:195-201.

Lay CC, Davis MF, Chen-Bee CH, Frostig RD (2010) Mild sensory stimulation completely protects the adult rodent cortex from ischemic stroke. *PLoS One* doi: 5:e11270.

Lay CC, Davis MF, Chen-Bee CH, Frostig RD (2011) Mild sensory stimulation reestablishes cortical function during the acute phase of ischemia. *Journal of Neuroscience* 31:11495-11504.

Lay CC, Davis MF, Chen-Bee CH, Frostig RD (2012) Mild sensory stimulation protects the aged

rodent from cortical ischemic stroke following permanent middle cerebral artery occlusion. *Journal of the American Heart Association Cardiovascular and Cerebrovascular Disease* doi: 10.1161/JAHA.112.001255.

Li N, DiCarlo JJ (2008) Unsupervised natural experience rapidly alters invariant object representation in visual cortex. *Science* 321: 1502-1507.

Lieb M, Shah U, Hines GL (2012) Cerebral hyperperfusion syndrome after carotid intervention: a review. *Cardiology Reviews* 20:84-89.

Lueschow A, Miller EK, Desimone R (1994) Inferior temporal mechanisms for invariant object recognition. *Cerebral Cortex* 4:523-531.

MacEvoy SP, Paradiso MA (2001) Lightness constancy in primary visual cortex. *PNAS* 98:8827-8831.

Masino, SA, Kwon, MC, Dory, Y, and Frostig, RD (1993). Characterization of functional organization within rat barrel cortex using intrinsic signal optical imaging through a thinned skull. *PNAS* 90, 9998-10002.

Merzenich, MM, and Kaas, JH (1980) "Principles of organization of sensory-perceptual systems in mammals." *Progress in psychobiology and physiological psychology* 9: 1-42.

Mirabella, G., Battiston, S., and Diamond, M.E. (2001). Integration of multiple-whisker inputs in rat somatosensory cortex. *Cerebral Cortex* 11, 164-170.

Mohajerani MH, Chan AW, Mohsenvand M, Ledue J, Liu R, McVea DA, Boyd JD, Wang YT, Reimers M, Murphy TH (2013) Spontaneous cortical activity alternates between motifs defined by regional axonal projections. *Nature Neuroscience* 16:1426-1435.

Mountcastle, Vernon B (1957) "Modality and topographic properties of single neurons of cat's somatic sensory cortex." *Journal of neurophysiology* 20(4): 408-434.

Mowery TM, Harrold JB, Alloway KD (2011) Repeated whisker stimulation evokes invariant neuronal responses in the dorsolateral striatum of anesthetized rats: a potential correlate of sensorimotor habits. *Journal of Neurophysiology* 105:2225-2238.

Narayanan, R. T., Egger, R., Johnson, A. S., Mansvelder, H. D., Sakmann, B., de Kock, C. P., & Oberlaender, M. (2015). Beyond Columnar Organization: Cell Type-and Target Layer-Specific Principles of Horizontal Axon Projection Patterns in Rat Vibrissal Cortex. *Cerebral Cortex* doi: 10.1093/cercor/bhv053.

Nicolelis M, Lebedev MA (2009) Principles of neural ensemble physiology underlying the operation of brain-machine interfaces. *Nature Reviews Neuroscience* 10: 530-540.

Niuro M, Simon RP, Kadota K, Asakura T (1996) Proximal branching patterns of middle cerebral artery (MCA) in rats and their influence on the infarct size produced by MCA occlusion. *Journal*

*of Neuroscience Methods* 64:19-23.

Pan J, Konstas AA, Bateman B, Ortolano GA, Pile-Spellman J (2007) Reperfusion injury following cerebral ischemia: pathophysiology, MR imaging, and potential therapies. *Neuroradiology* 49:93-102.

Penfield, Wilder, and Herbert Jasper. "Epilepsy and the functional anatomy of the human brain." (1954). Oxford, England: Little, Brown & Co.

Petersen, CCH (2007) The Functional Organization of the Barrel Cortex. *Neuron*. 56: 339-355.

Petersen, RS, Panzeri, S, and Maravall, M (2009). Neural coding and contextual influences in the whisker system. *Biology Cybernetics* 100, 427-446.

Quian Quiroga R, Panzeri S (2009) Extracting information from neuronal populations: information theory and decoding approaches. *Nature Reviews Neuroscience* 10:173–185.

Quiroga RQ, Reddy L, Kreiman G, Koch C, Fried I (2005) Invariant visual representation by single neurons in the human brain. *Nature* 435:1102–1107.

Roland PE, Hanazawa A, Undeman C, Eriksson D, Tompa T, Nakamura H, Valentiniene S, Ahmed B (2006) Cortical feedback depolarization waves: a mechanism of top-down influence on early visual areas. *PNAS* 103:12586–12591.

Rust NC, DiCarlo JJ (2010) Selectivity and tolerance (“invariance”) both increase as visual information propagates from cortical area V4 to IT. *Journal of Neuroscience* 30: 12978-12995.

Sadagopan S, Wang X (2008) Level invariant representation of sounds by populations of neurons in primary auditory cortex. *Journal of Neuroscience* 28: 3415-3426.

Sakata S, Harris KD (2009) Laminar structure of spontaneous and sensory-evoked population activity in auditory cortex. *Neuron* 64:404–418.

Sáry G, Vogels R, Orban GA (1993) Cue-invariant shape selectivity of macaque inferior temporal neurons. *Science* 260:995–997.

Shadlen MN, Newsome WT (1998) The variable discharge of cortical neurons: implications for connectivity, computation, and information coding. *Journal of Neuroscience* 18:3870–3896.

Sharon D, Jancke D, Chavane F, Na’aman S, Grinvald A (2007) Cortical response field dynamics in cat visual cortex. *Cerebral Cortex* 17:2866–2877.

Shimegi, S., Ichikawa, T., Akasaki, T., and Sato, H. (1999). Temporal characteristics of response integration evoked by multiple whisker stimulations in the barrel cortex of rats. *Journal of Neuroscience* 19, 10164-10175.

Simons DJ (1978) Response properties of vibrissa units in rat SI somatosensory neocortex.

*Journal of Neurophysiology* 41:798–820.

Stehberg J, Dang PT, Frostig RD (2014) Unimodal primary sensory cortices are directly connected by long-range horizontal projections in the rat sensory cortex. *Frontiers in Neuroanatomy* doi: 10.3389/fnana.2014.00093.

Tamura A, Graham DI, McCulloch J, Teasdale GM (1981) Focal cerebral ischaemia in the rat: 1. Description of technique and early neuropathological consequences following middle cerebral artery occlusion. *Journal Cerebral Blood Flow and Metabolism* 1:53-60.

Temereanca S, Brown EN, Simons DJ (2008) Rapid changes in thalamic firing synchrony during repetitive whisker stimulation. *Journal of Neuroscience* 28:11153–11164.

Temereanca S, Simons DJ (2003) Local field potentials and the encoding of whisker deflections by population firing synchrony in thalamic barreloids. *Journal of Neurophysiology* 89:2137–2145.

Ts'o DY, Frostig RD, Lieke EE, Grinvald A (1990) Functional organization of primate visual cortex revealed by high resolution optical imaging. *Science* 249:417-420.

van Mook WN, Rennenberg RJ, Schurink GW, van Oostenbrugge RJ, Mess WH, Hofman PA, de Leeuw PW (2005) Cerebral hyperperfusion syndrome. *Lancet Neurology* 4:877-888.

Van Regenmortel, MH (2004). Reductionism and complexity in molecular biology. *EMBO reports* 5(11), 1016-1020.

Wang-Fischer Y (2009) *Manual of Stroke Models in Rats*. pp 17-30, 239-278 Boca Raton: CRC Press.

Woolsey, T.A., Van Der Loos, H. (1970). The structural organization of layer IV in the somatosensory region (SI) of mouse cerebral cortex: The description of a cortical field composed of discrete cytoarchitectonic units. *Brain Research*. 205-238.

## **Appendix A. Coincident spike waveforms confound interpretation of spike counts**

Spontaneous (open arrows) and evoked (closed arrows) multi-unit activity at varying distances from peak responses are plotted for 10 consecutive trials of whisker array stimulation. Note the maximum amplitude of evoked multi-unit potentials which are denoted by dotted red lines in each trace. At 2 mm from peak responses, the amplitudes of evoked and spontaneous spikes are comparable (**Fig. A1A**). Closer to peak responses (1 mm away; **Fig. A1B**) and at the location of peak responses (**Fig. A1C**), the amplitude of evoked spike waveforms are greater than the amplitude of spontaneous spikes. Since the amplitude of action potentials for individual neurons remains relatively constant, the increased spike waveform amplitude indicates contribution from many simultaneously active neurons (Bar-Gad, 2001). In barrel cortex, such coincident, overlapping spike waveforms may be more prevalent due to the acute onset and short time-course of whisker evoked responses.

Coincident spike waveforms confound the interpretation of peri-stimulus time histograms (PSTHs) which assume one action potential per spike. A spike waveform produced by many coincident action potentials, therefore, will be registered only as one action potential. Thus, if coincident spike waveforms are abundant then PSTHs are confounded by a ceiling effect and become very difficult to interpret. One option to get around this issue is to analyze trial averaged traces rather than spike timestamps. Referred to in this document as “multi-unit potentials” or MUP, this measure remains sensitive to the number of action potentials during bursts of high activity. However, MUP may be much less sensitive to low levels of activity or non-synchronized, sparse activity.

In situations where overlapping spike waveforms are infrequent, PSTHs provide the most comprehensive measure of suprathreshold spiking activity. In situations where overlapping, coincident spike waveforms are abundant and significantly confound the

interpretation of PSTHs, MUP offers an alternative solution with the caveat of reduced sensitivity to sparse or de-synchronized suprathreshold activity.

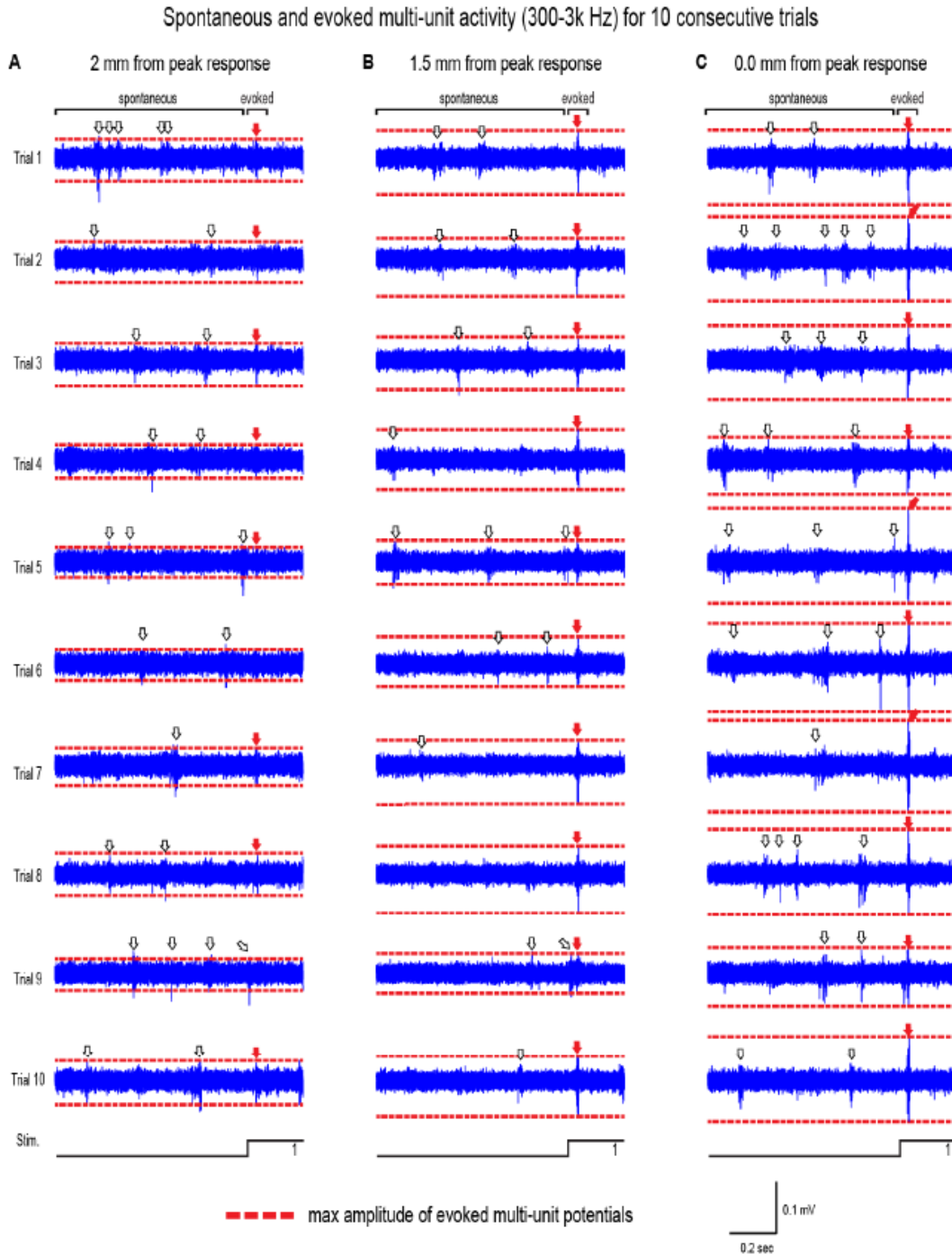


**Figure A1. Coincident spike waveforms near peak responses.** Spontaneous (open arrows) and evoked (closed arrows) spikes at 2 mm (A), 1.5 mm (B), and 0 mm (C) from from peak activity.

## **Appendix B: Spatially organized ensembles provide substrate for real time sensory coding**

Sensory coding is typically studied at the level of single neurons for example by focusing on their tuning properties, or at a macroscopic scale for example in identifying structures within a hierarchy of a sensory system. Thus a major challenge in understanding of sensory coding is the potential contributions of emergent response features in large, spatially organized networks such as the rodent barrel cortex. Another unrelated challenge is understanding how network state and ongoing spontaneous activity may affect sensory coding on individual trials. A third and final challenge is understanding how sensory coding occurs in real time, where robust neural codes must mitigate variable and in some cases ambiguous responses in individual neurons (Shadlen and Newsome, 1998). All of these challenges may actually be related to one another. The variable and sometimes ambiguous responses of single neurons on single trials could potentially be resolved by pooling information from a broader segment of the spatiotemporal profile of evoked network activity.

Sensory coding in primary sensory cortices is very often described in terms of the tuning of single neurons. Tuning curves indicate the preferred stimulus of a particular neuron (**Fig. B1**, top panels), and require multiple trials in which a set of varied stimuli are presented often with systematic changes in a specific stimulus parameter such as whisker identity. The stimulus that evokes the most vigorous response is referred to as a particular neuron's "preferred" stimulus (e.g., the principal whisker).

A complementary substrate for sensory coding is the spatial profile of activity evoked by a single stimulus. Spatial profiles of activity can be observed on single trials by simultaneously recording or imaging activity at multiple *different* spatial locations (**Fig. B1**, bottom panels). The spatial profile of activity evoked by a particular stimulus is often referred to as a functional

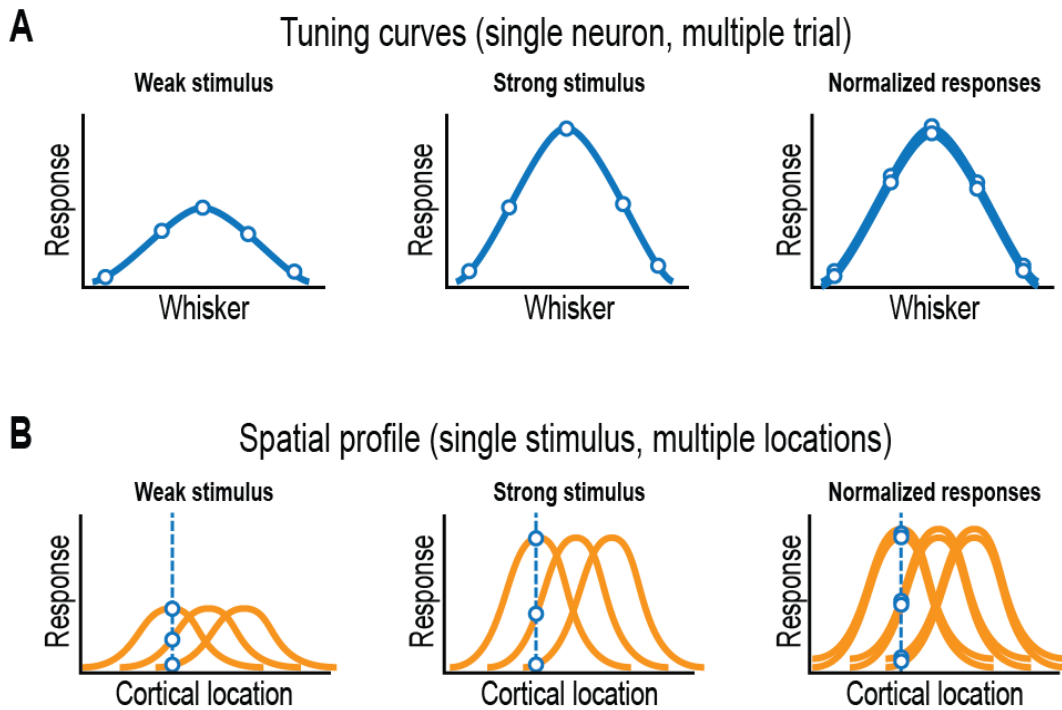


**Figure B1. Relationship between single neuron tuning curves and single whisker evoked point spreads.** **(A)** Single neuron tuning curves are constructed by repeatedly measuring the responses of a neuron to different stimuli. In primary sensory cortices, invariance in the shape (e.g. half width) of tuning curves has been found (see main text). **(B)** The spatial profile of activity is the relative magnitude of responses at different cortical locations. The spatial profile of single whisker evoked point spreads, which propagate into neighboring whisker barrels (see **Chapter 2**), is related to the shape of tuning curves at a specific recording location (blue dotted line).

representation. Whereas tuning curves are composed of responses from single neurons on different trials, functional representations are composed of many responses at different spatial locations.

**Figure B1** illustrates how tuning curves (top panels) can be derived from the spatial profiles of evoked activity spreads (bottom panels) and vice versa. Weaker responses from “inappropriate” whiskers in the tuning curve can be thought of as the evoked activity spread from neighboring whisker barrel(s). The suggested relationship between single neuron tuning curves and evoked point spreads should exist for weak stimuli (schematic in **Fig. B1**, left panels) as well as for strong stimuli (schematic in **Fig. B1**, middle panels), since the spatial profile of single whisker point spreads seems to remain constant across large changes in whisker stimulus amplitude (**Chapter 3**). Further support for this relationship would be if the shape of tuning curves were also invariant in primary sensory cortices (schematic in **Fig. B1**, right panels), which has been reported in primary auditory (Sadagopan and Wang, 2008) and visual (Anderson et al., 2000) cortex. Thus, it is likely that tuning curves and point spreads are simply two different measures of the same underlying neural signal.

An important constraint for determining the plausibility of a neural substrate for sensory coding should be its performance in real-time on single trials. This constraint is supported by the simple observation that many simple sensory functions in animals like stimulus recognition rarely requires multiple trials. For example, a person’s face is immediately recognized without having to stare. This highlights an important difference between tuning curves, which are based on responses to different stimuli on multiple trials, and point spreads, which are based on responses to the same stimulus at different locations. On single trials, a single whisker stimulus evokes a dynamic spatiotemporal profile of activity across barrel cortex. In contrast, tuning curves are not accessible on single trials. This can be countered with the argument that tuning

curves are simply an experimental method of revealing which stimulus a particular neuron is tuned to. Once you know the preferred stimulus of a neuron, its responses or the combined responses from many neurons with the same tuning should provide a reliable sensory code. But do they?

This raises an important question- *does the brain use the preferred stimuli of single neurons or the spatial profile of evoked activity to identify stimuli on single trials?* There are several fundamental reasons why single neuron responses are inherently ambiguous on single trials, regardless of whether their preferred stimulus is known or if you pool responses from many similarly tuned neurons. These same reasons, outlined below, also suggest that these fundamental ambiguities are easily resolved by considering responses at multiple, *different* spatial locations (ie, the spatial profile of activity). As an example, responses in barrel cortex are focused on but the same logic should apply to any spatially organized networks such as other primary sensory cortices.

First, as already mentioned tuning curves are not accessible on single trials. On single trials, only one stimulus can be presented and unlike the experimenter the brain does not have a *priori* information about what that stimulus will be. Given that the tuning of neurons is rarely perfect each neuron will respond to a variety of different stimuli. Without comparing the relative magnitude of these responses across trials, and with no guarantee that the experimenter isn't changing multiple stimulus parameters at once such as whisker identity and stimulus amplitude, how can this information be used to identify a whisker stimulus? The answer is it probably can't, at least not without information from other neurons with *different* tuning properties. This reasoning is explained below.

The second line of reasoning supporting spatial profiles of activity as the neural substrate for sensory coding comes from evaluating what neural information is likely available on single

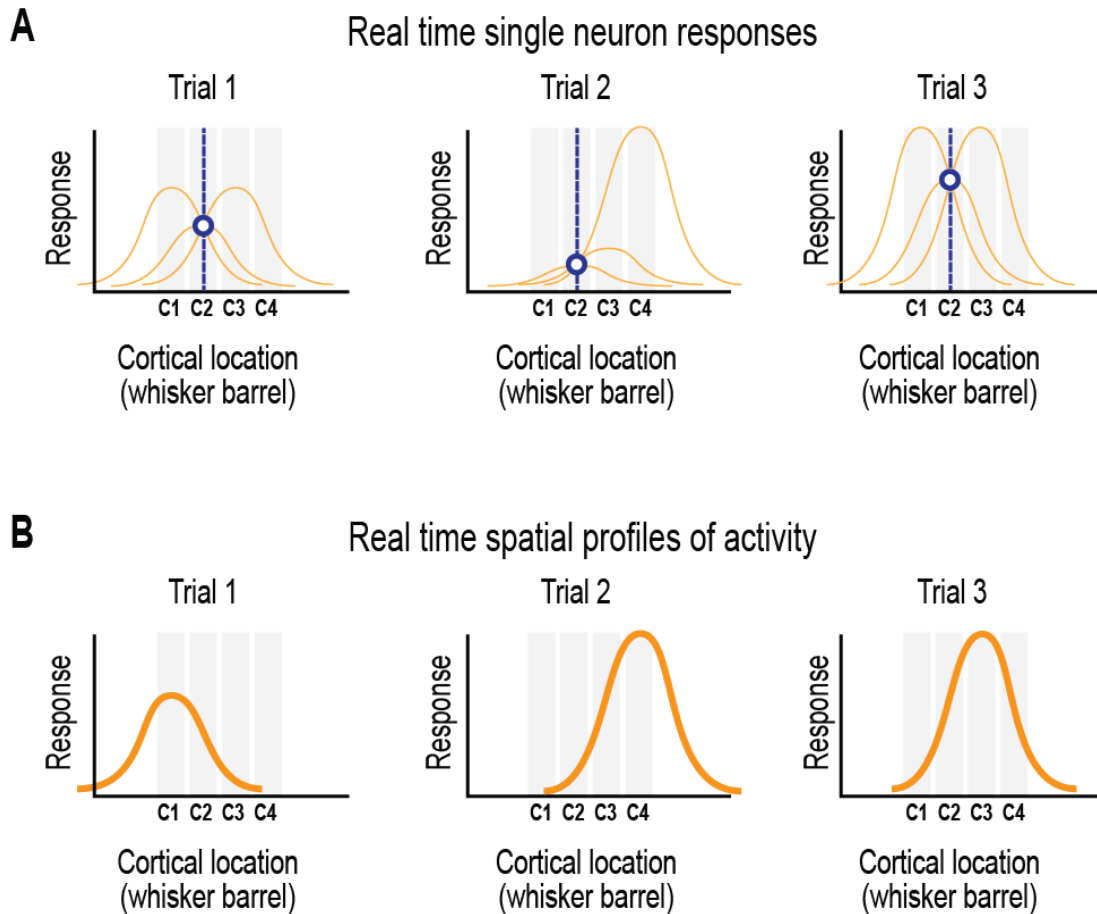


**Figure B2. Spatial profile of activity resolves ambiguity of whisker stimulus identity on single trials.** **(A)** Responses from an individual neuron in the C2 whisker barrel column may not be sufficient to identify the correct whisker stimulus on individual trials. Three hypothetical trials of whisker stimulation are shown. On each trial, the neuronal response (blue dot) could have been produced by stimulating any one of a number of different whiskers at different stimulus intensities. Possible whisker stimuli are indicated by spatial profiles of evoked activity (thin orange lines). For example, on trial 1, the response could be from stimulation of C2 whisker or from stronger stimulation of either C1 or C3 whisker. **(B)** The spatial profile of activity resolves this ambiguity. Combining information from multiple locations removes any ambiguity as to which whisker was stimulated, and provides a sensory code that is invariant to changes in response magnitude (see **Chapter 3** for more details).

trials (**Fig. B2**). On single trials, information from any one individual neuron is inherently ambiguous (**Fig. B2A**). First imagine the most ambiguous scenario possible, in which responses are considered from a neuron without any knowledge about the source of the signal. The responses from this neuron would contain very little information, since the signal could have come from any number of sensory regions or even from a non-sensory region. This extreme ambiguity is decreased, but not eliminated, with information about the neuron's exact spatial location or position within a neural network.

Next imagine that responses are considered from a neuron in the C2 whisker barrel of barrel cortex. Responses from this neuron carry much more information than the first scenario (e.g. probably is result of a somatosensory stimulus and not an auditory stimulus), but some ambiguity still remains. The remaining ambiguity comes from the observation that whisker stimulation engage large numbers of neurons distributed over large cortical areas (see **Chapter 2**). A response from this neuron in the C2 whisker barrel *does not* necessarily indicate that the C2 whisker was stimulated. Very similar responses would be seen for all of the following stimuli: modest stimulation of the C2 whisker, stronger stimulation of the neighboring whisker C3, and even stronger stimulation of the next whisker over C4. Therefore, responses from any one neuron in barrel cortex are unlikely to be able to reliably code for whisker stimulus identity on single trials.

In order to remove ambiguity about whisker stimulus identity on single trials, concurrent information from multiple neurons is required. One possibility is to look at multiple neurons at the same cortical location (ie, within the C2 barrel column). Additional neurons from the C2 barrel column are unlikely to be useful due to the close similarities in their tuning properties. It is possible that subtle differences in latencies across cortical layers could provide enough information to identify the correct whisker stimulus, but this remains to be shown. What can be

shown clearly is that combining information (either response magnitude or latency) from neurons at multiple *different* spatial locations sufficiently resolves ambiguity about whisker stimulus identity (**Fig. B2B**). For example, if responses in the C1 and C3 whisker barrels are weaker than the response in the C2 whisker barrel, it provides clear indication that the C2 whisker was stimulated (and not stronger stimulation of other whiskers). Therefore, the simplest, most biologically plausible way to identify whisker stimulus identity on single trials is with spatial profiles of activity.

This thought experiment focused on the magnitude of responses, but the latency of responses could also be used to solve whisker stimulus identity. Importantly, response latencies would still likely be ambiguous at the single neuron level but again would be resolved by considering responses latencies at multiple, *different* spatial locations. As already mentioned, it's possible that subtle laminar differences in latency could be used to solve whisker identity on single trials, but this remains to be shown. Furthermore, any latency differences would likely be very subtle since intracortical activity spreads seem to maintain the traditional laminar profile of onset latencies with granular layers showing earlier responses than superficial layers even beyond the activated whisker barrel column (see Figure 2 of Frostig, 2008).

A third and final line of reasoning supporting spatial profiles of activity as the neural substrate for sensory coding is illustrated in **Figure B3**. Spatial profiles of whisker evoked activity have been shown to be important in dictating the “funneled” shape of multi-whisker responses that are characterized by a single, central peak in barrel cortex (see **Chapter 2**). If sensory coding based on spatial profiles of activity is relevant on a single trial basis, funneled profiles of activity should be seen in real time and not just on trial averages. This indeed was the case for most trials of a representative subject (**Fig. B3B**).

In summary, knowing the preferred stimuli of individual neurons may not provide

sufficient information even with unique single whisker stimuli and even in a highly spatially organized network such as the barrel cortex. This is due not only to intrinsic variability of single neuron responses but also due to fundamental ambiguities about stimulus identity given large point spreads of evoked activity and potential changes in stimulus amplitude from trial to trial. It should also be noted that the information content of spatial profiles of activity could be further improved by adding the temporal domain which was not focused on here. Considering the spatio-temporal dynamics of ongoing network activity could reveal additional emergent features of network activity in barrel cortex and other spatially organized cortices.

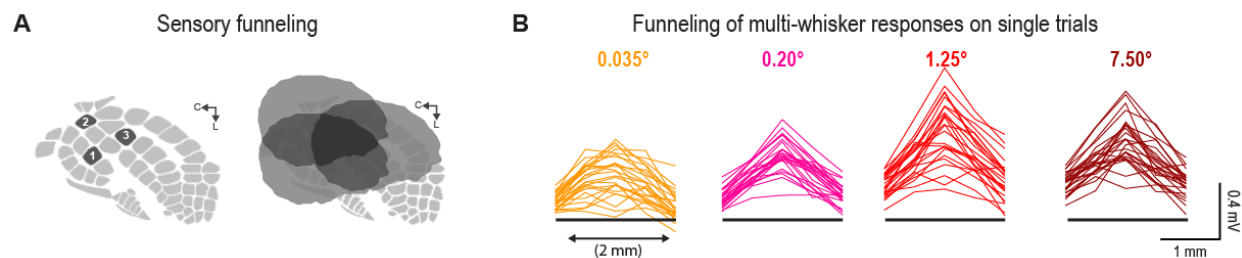


**Figure B3. Funneling of multi-whisker responses occurs on single trials.** (A) Spatial overlap of large single whisker point spreads peaks at a single, central location. Additive sub-linear interactions between these overlapping point spreads are presumed to be the mechanism underlying ‘funneled’ multi-whisker responses characterized by a single, central peak of evoked activity (see **Chapter 2** for details). (B) Profiles of whisker array evoked LFP in layer 4 of barrel cortex for a representative subject. All recording locations shown are within the boundaries of barrel cortex. Each trace corresponds to evoked LFP +10 ms post-stimulus onset at 0.5 mm intervals centered over the C2 whisker barrel. Funneled profiles of activity (single, central peak) are noticeable on most single trials. This is consistent with spatial profiles of activity potentially being used in real time to produce funneled multi-whisker responses.

## Appendix C: Lateral versus vertical functional connectivity in barrel cortex

The spatial organization of whisker evoked activity in barrel cortex was investigated in more detail. A particular focus was to determine if lateral functional connectivity (ie, within cortical layers) was equivalent to vertical functional connectivity (ie, within cortical columns). To do this, cross-correlations were run on single whisker evoked LFP (C2 stimulation at 7.5 degrees, +0-100 ms post-stimulus onset) between pairs of cortical locations within the same 8x4 frames used in **Chapter 3**. In addition to running all possible cross-correlations (fully crossed correlation matrix), time lags at 0-70 ms were also tested. For the sake of clarity, the analysis and results are separated into three steps: 1) *representative cross-correlograms*, 2) *representative seed analysis (correlation map)*, and 3) *selected results from full correlation matrix focusing on lateral and vertical functional connectivity*.

First, representative cross correlograms between pairs of recording locations within the 8x4 array of electrodes are shown (**Fig. C1A**, location of electrode pairs in array indicated by insets on left). Cross-correlograms between electrodes in the field of view can reveal a positive correlation (e.g., activity at locations 1 and 2 increase and decrease together; **Fig. C1A**, green line), a correlation that involves a time lag (e.g., activity at location 1 increases 10 ms after activity at location 2 increases; **Fig. C1A**, blue line), or a negative correlation (e.g., activity at location 1 increases when activity at location 2 decreases; **Fig. C1A**, red line). Thus each cross-correlogram provides details about the functional relationship between the two cortical locations. The maximum absolute correlation coefficient is a general measure of how correlated the activity at two locations is, regardless of the nature of the correlation (positive, negative, or with a time lag).

Second, at each recording location a seed analysis was done by running all possible cross-correlations with the other recording locations. A seed analysis describes the functional

relationship between a single location (the “seed”) and a much larger region as a correlation map. A representative correlation map for a recording location in layer 5 of barrel cortex is shown in **Figure C1B**. This representative correlation map reveals strong correlations to locations within the same cortical column (pixels above and below) as well as to locations within the same cortical layer (pixels to the left and right). This suggests that in addition to exhibiting a prominent vertical connectivity, the cortex also exhibits prominent lateral connectivity. Features such as lateral and vertical functional connectivity can be extracted from each correlation map. Lateral functional connectivity was calculated by averaging correlation coefficients for locations within the same cortical layer (as many as 2 recording locations on either side of seed location for a maximum lateral distance of 1 mm; **Fig. C1B**, bottom left). Likewise, vertical functional connectivity was calculated by averaging correlation coefficients for locations within the same cortical column (all other recording locations within column for a maximum vertical distance from seed location of 0.9 mm; **Fig. C1B**, bottom right). Thus for each seed analysis, average  $r^2$  values could be calculated indicating the degree of lateral and vertical functional connectivity.

Third and last, mean  $r^2$  values for the lateral and vertical functional connectivity were compared using a data set pooled across 28 locations and 2 subjects. Correlation coefficients for both lateral and vertical functional connectivity was high ( $>0.8$ ; **Fig. C1C**). These data indicate that lateral functional connectivity is at the very least equivalent to the vertical functional connectivity of barrel cortex.

Together, these results verify strong vertical functional connectivity in barrel cortex (ie, barrel columns). These results also provide a compelling demonstration of the robust lateral functional connectivity of barrel cortex, the possible functions of which were explored in **Chapter 2**, **Chapter 3**, and **Chapter 4** of this dissertation. In addition these results, pooled across many cortical depths, add to previous work suggesting that large scale horizontal connectivity is not

restricted to specific cortical layers (Frostig et al., 2008).

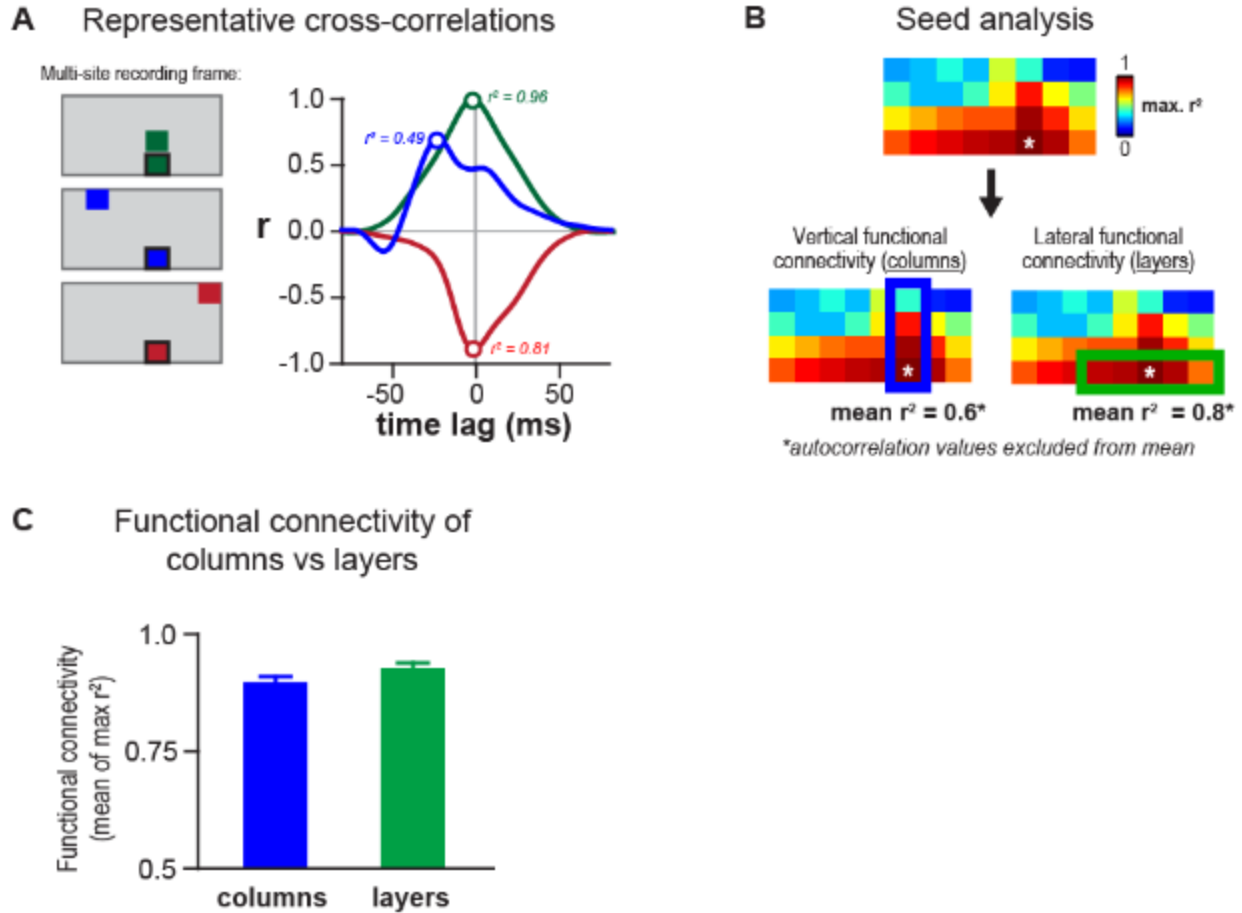


**Figure C1. Cortical activity is more correlated within layers than within columns. (A)**

Cross-correlograms for individual pairs of recording locations. **(B)** Representative seed analysis for the recording location framed in left panels in (A). Within an individual seed analysis, correlation coefficients could be averaged within cortical columns (left) or cortical layers (right). **(C)** Correlation coefficients for comparisons within layers versus within columns for full correlation matrix. *Correlations based on a subset of data from Chapter 3. Results in (C) are means  $\pm$  standard error pooled from 56 recording locations across 2 subjects.*